NANOPHARMACEUTICAL FOR IMPROVED ANTI-HIV THERAPY

By

LI WAN

A Dissertation submitted to the

Graduate School-New Brunswick

Rutgers, The State University of New Jersey

in partial fulfillment of the requirements

for the degree of

Doctor of Philosophy

Graduate Program in Pharmaceutical Science

written under the direction of

Professor Patrick J. Sinko

and approved by

_____

_____

_____

_____

New Brunswick, New Jersey

May, 2007

ABSTRACT OF THE DISSERTATION

NANOPHARMACEUTICAL FOR IMPROVED ANTI-HIV THERAPY

By LI WAN

Dissertation Director:
Professor Patrick J. Sinko

Curing HIV-1 infection has remained elusive due to low and fluctuating drug levels, arising from poor absorption, viral reservoirs and sanctuary sites, toxicity and patient non-adherence. The theme of the current study is to investigate the value of combining AIDS drugs and modifiers of cellular uptake into macromolecular nanocarriers having novel pharmacological properties for improving current anti-HIV therapy. Nanopharmaceuticals were prepared from different combinations of saquinavir (SQV), R.I.CK-Tat9 and the polymeric nanocarrier polyethylene glycol. Anti-HIV activities were measured in MT-2 cells while parallel studies were performed in uninfected cells to determine cellular toxicity. Flow cytometry and confocal microscopy studies suggested that variations in intracellular uptake and intracellular localization, as well as synergistic inhibitory effects of SQV and Tat peptides, contributed to the unexpected and substantial differences in antiviral activity. Our results demonstrate that highly potent multi-drug nanopharmaceuticals with low non-specific toxicity can be produced by combining moieties with anti-HIV agents for different targets onto macromolecules having improved delivery properties.

The present study also addressed the issue of insufficient drug exposure of viral reservoirs in macrophages. Macrophages are a key target and primary cellular reservoir for HIV, and are believed to be responsible for the viral rebound effect observed upon the discontinuation of therapy. In this study, multiple copies of N-formyl-Met-Leu-Phe (fMLF), a known chemo-attractant for macrophages, were conjugated to multifunctional nanocarrier derived from commercially available or novel peptide-based PEGs. The results of uptake studies indicated that appending only two copies of fMLF to the nanocarrier is sufficient for optimal binding and the optimal size of the nanocarrier was about 20 kDa. Further pharmacokinetics and biodistribution studies demonstrated that the attachment of fMLF increased accumulation of PEG nanocarriers in major macrophage-residing tissues such as liver, kidneys and spleen. Taken together, these results demonstrated the feasibility of using macrophage-targeted nanocarriers for enhancing drug uptake in human macrophage-like cells *in vitro* or macrophages residing in tissues *in vivo*. These results indicate great promise for enhancing targeted drug delivery to HIV-infected macrophages, which may eventually improve current anti-HIV therapy by improving therapeutic efficacy, minimizing systemic toxicity and simplifying administration regimens.

DEDICATION

To my loving wife Bin Liu and son Andrew Bochen Wan

Whose love and support give me the strength to fulfill my dreams.

To my loving parents: Jiashou Wan and Shuying Li

Whose inspirations and expectations always encourage me to face challenges in life.

and the many friends, too numerous to count, that have helped me along the way.

ACKNOWLEDGEMENTS

I am deeply grateful to my dissertation advisor, Professor Patrick J. Sinko, for providing a constant source of intellectual stimulation, encouragement and support from this project's inception until its completion, without which this work could not have been completed. His depth of knowledge and dedication to science has inspired me throughout my training. Most importantly, Dr. Sinko has given me the precious opportunity to be involved in some of the most exciting and cutting-edge scientific projects funded by NIH.

I would like to thank Dr. Michael Leibowitz, Dr. Stanley Stein, Dr. Guofeng You for serving as members of my dissertation committee. Dr. Stanley Stein has been a constant source of new ideas. I appreciate his numerous inputs on the design and chemistry. I wish to express my gratitude to Dr. Michael Leibowitz for his advice with many experiments and critical review of my papers and dissertation. I want to thank Dr.You for her kindness and always advice and suggestions on many scientific issues and non-scientific issues.

I would also like to thank the past and present members of the Sinko Research Group for their support, help and friendship. Special thanks are due to: Dr. Xiaoping Zhang for his help on various aspects of research; Dr. Simi Gunaseelan and Dr. Shahriar Pooyan for help in chemical synthesis; Peidi Hu for help on many animal experimental techniques; Peiming Chen and Matthew Palombo for RT-PCR and western blots; Yu Chen for his many advice on chemistry; Amy Grabowski, Marianne Shen and Sharana Taylor for help in all the administrative processes. I would like to extend my thanks to,

Pankaj Parajpe, Seonghee Park, Bee Chao, Sunghack Lee, Yaming Su, Hilliard Kutscher and Sreepriya Anumolu for making Sinko lab a fun place to work.

I would like to thank all the members of Department of Pharmaceutics for their encouragement, stimulating conversation and friendship. Thanks are due to: Dr. Tamara Minko for serving on my NIH proposal committee, Dr. Thomas Cook and Dr. Gregory Knipp for their counsel on various aspects of research; Hui Pung for help in all the administrative processes and final dissertation defense and submission. I would also like to thank many friends at AAPS Rutgers Student Chapter, too many to mention here, for their support when I served as chairman from 2003 to 2005 and making my life at Rutgers a truly fulfilling and memorable experience.

I would like to thank my entire family for their constant love, encouragement and support throughout my graduate education. In particular, to my parents, Jiashou Wan and Shuying Li, who have always been there every step of my life with loving support, encouragement, and faith, which helped immeasurably in reaching my final goal. There are no words adequate to express my thanks. Thanks also to my son, Andrew Bochen Wan, whose smiles offered comfort when needed most.

Finally, I would like to offer my deepest gratitude to my wife, Bin Liu, who has always there with words of encouragement and enthusiasm, love, and support whilst suffering from my frustrations and disappointments. This work would not have been possible if not for her great love, support and sacrifice. I am eternally grateful.

TABLE OF CONTENTS

LIST OF TABLES

LIST OF ILLUSTRATIONS

LIST OF ABBREVIATIONS

AcOEt: ethyl acetate

AIDS: acquired immunodeficiency syndrome

BOP: benxotriazolyl-oxy-tris-(dimethylamino)-phosphoniumhexafluoro phosphate

CCR5: chemokine C-C motif receptor 5

CD4: cluster designation 4

$CDCl_3$: deuterated chloroform; CH_2Cl_2: methylene chloride

CNS: central nervous system

CPP: cell penetrating peptide

CPT: camptothecin

CXCR4: chemokine C-X-C motif receptor 4

Cys: cysteine

DCM: dichloromethane

Dde: 1-(4,4-dimethyl-2,6-dioxocyclohexylidene)ethyl

DIEA: diisopropylethyl amine

DIPC: 1,3-diisopropyl carbodiimide

DMAP: 4-dimethylaminopyridine

DMF: dimethyl formamide

DMSO: dimethyl sulfoxide

DTT: dithiothreitol

EC: effective concentration

EC_{50}: the concentration achieving 50% of maximum protection response

ED: effective dose

ED_{50}: the dose achieving 50% of maximum protection response

EDT: ethanedithiol

ESI-MS: electrospray ionization mass spectrometry

Et_2O: diethyl ether

FBS: fetal bovine serum

fMLF (fMLP): N-formyl-methionyl-leucyl-phenylalanine

Fmoc: fluorenylmethoxylcarbonyl

FPR: N-formyl peptide receptor

FPRL1: N-formyl peptide receptor like-1

FRET: fluorescence resonance energy transfer

Gly: glycine

HAART: highly active anti-retroviral therapy

HIV: human immunodeficiency virus

HOBt: N-hydroxybenzotriazole

LC: lethal concentration

LC_{50}: the concentration achieving 50% of maximum lethal response

LD: lethal dose

LC_{50}: the dose achieving 50% of maximum lethal response

Lys: lysine

MALDI-TOF: matrix-assisted-laser-desorption ionization time of flight

MeOH: methanol

MOI: multiplicity of infection

MTT: 3-(4,5-dimethylthiazol-2-yl)-2,5-diphenyltetrazolium bromide

NHS: N-hydroxy succinimide

NMR: nuclear magnetic resonance

PBS: phosphate buffered saline

PEG: poly(ethylene) glycol

PI: protease inhibitor

PR: protease

R.I.CK-Tat9: retro-inverso-cysteine-lysine-Tat nonapeptide

RP-HPLC: reverse-phase-high-performance-liquid-chromatography

SEC: size exclusion chromatography

SQV: saquinavir

TFA: trifluoroacetic acid

TIS: triisopropyl silane

TMS: tetramethyl silane

TP: 2-thiopyridine

Trt: trityl

CHAPTER 1

INTRODUCTION

The introduction of highly active antiretroviral therapy (HAART) nearly ten years ago revolutionized the treatment of human immunodeficiency virus (HIV) infection (*1-3*). HAART usually consists of a combination of at least three antiretroviral drugs including protease and reverse transcriptase inhibitors that together have shown remarkable efficacy for the treatment of HIV-1 infection in vitro and in the clinic. Clearly, the widespread use of HAART has dramatically changed the clinical course of HIV-1 infection and has led to a dramatic improvement in the morbidity and mortality of HIV disease, and ultimately turned HIV disease from a death sentence to a manageable chronic disease. However, the eradication of HIV infection has never been achieved in clinical practice due to many challenges such as low and fluctuating drug concentrations due to poor drug absorption or patient non-adherence (*4*), the presence of viral reservoirs and sanctuary sites (*5*), and drug toxicity due to the chronic therapy (*6, 7*). For instance, the therapeutic efficacy of saquinavir, the first FDA approved HIV-1 protease inhibitor (PI), was limited by poor aqueous solubility, low and variable bioavailability and poor penetration into the lymphatic and central nervous sytems (CNS) (*8, 9*). Macrophages are infected early but remain productive and noncytopathic, permitting macrophages to serve as long-lived source of HIV production (*10-13*). Therefore, macrophages play a key role in HIV pathogenesis and the dissemination of the virus throughout the immune system

and various organs such as the CNS and lymphatic tissues (*12*). In addition HIV located within macrophages may be protected from the effect of highly active antiretroviral regimens containing protease inhibitors, because the activity of PIs in chronically infected monocytes/macrophages (M/M) is much lower than in plasma, acutely infected M/M and chronically infected lymphocytes (*14*). P-glycoprotein, an efflux transporter, found in macrophage membranes may be responsible for this phenomenon (*15*). These challenges prompted the search for new therapeutic agents and strategies with the aim of achieving: (1) increased anti-HIV potency; (2) lower resistance profiles; (3) better pharmacokinetic properties; (4) lower toxicity; (5) and simpler administration regimens with fewer drug-drug interactions and food restrictions.

Drug delivery technologies using biomaterials have been effectively used in patients to enhance the pharmacological activity of non-AIDS drugs by changing biopharmaceutical properties such as disposition (i.e., body distribution, metabolism or excretion). We hypothesize that using the biomaterial-based drug delivery systems (DDS), anti-HIV drugs can selectively accumulate in the infected tissues or cells, while concentrations in non-infected tissues or cells should be much lower (*16-18*). Therefore, side effects should be reduced, lower doses needed and drug administration becomes simplified (*17*). A biomaterial-based DDS should include three or more components: (a) drug; (b) targeting moieties; and (c) a pharmaceutical carrier to link the drugs and targeting moieties. Pharmaceutical carriers include soluble natural or synthetic polymers (collagen, cellulose, chitosan, PEG, PLGA etc.), microcapsules, microspheres, liposomes, micelles and dendrimers. PEGylation, the process of attaching polyethylene glycol (PEG) to drug molecules, has been a highly successful strategy for improving the

pharmacokinetics and pharmacodynamics of pharmaceuticals, especially for protein and peptide therapeutics (*19-25*). Moreover, the shielding effect of PEG decreases nonspecific interactions with negatively charged cellular membranes, resulting in a reduction of nonspecific cellular uptake. Currently used PEGylation approaches that have been enormously successful for treating cancers are not likely to be appropriate for treating HIV infection in viral reservoirs or sanctuary sites such as macrophages, the central nervous system and testis. Therefore, the main goal of this research is to design, synthesize, characterize and evaluate novel polymeric drug conjugates and carriers for enhancing anti-HIV drug bioefficacy by improving their delivery, pharmacokinetics and pharmacodynamics.

In the first part of this research, conjugates were prepared from saquinavir, R.I.CK-Tat9 and poly(ethylene glycol). Anti-HIV activities were assessed by measuring MTT activity in MT-2 cells, an HTLV-I-transformed human lymphoid cell line, infected with HIV-1, while parallel studies were performed in uninfected cells to determine cellular toxicity. The saquinavir and R.I.CK-Tat PEG conjugates retained antiviral activity *in vitro* and showed favorable therapeutic indices. Furthermore, the addition of a releasable saquinavir to the R.I.CK-Tat9-PEG conjugate resulted in a conjugate with the highest *in vitro* potency among the conjugates tested (EC_{50} 15 nM). Mechanistic studies suggest that cell surface targeting of CXCR4 combined with the known biopharmaceutical properties of PEGylation, may act in synergy with known intracellular antiviral mechanisms to increase the overall antiviral effect.

In the second part of this thesis research, fMLF was used to target the formyl peptide receptors (FPRs) on macrophages for the enhanced delivery of PEG-based

nanocarriers. A series of fMLF macrophage-targeted PEG nanocarriers were prepared and tested to delineate the relationship between the molecular features of PEG-fMLF nanocarriers (i.e. number of targeting peptide and PEG sizes) and cell uptake in order to optimize the design of the DDS. The binding and activation of the PEG-fMLF nanocarriers were evaluated *in vitro* using differentiated human monocytic U937 cells. The results suggest that two fMLF residues are adequate for achieving optimal macrophage targeting and 20K may be the optimal PEG size of those studied for macrophage uptake *in vitro*. Based on the results, novel peptide-backbone PEG-fMLF nanocarriers were prepared by coupling the peptide backbone to NHS-PEG-VS and followed by the attachment of the fMLFKC peptide. The peptide-backbone PEG-$(fMLF)_2$ and PEG-$(fMLF)_4$ increased macrophage uptake similarly to nanocarriers derived from commercially available PEGs, suggesting that the peptide-backbone PEG-fMLF nanocarriers retained the ability of targeting and being uptaken by macrophages besides their other advantages over other PEGylated systems. Finally peritoneal macrophage uptake, pharmacokinetics and biodistribution of the PEG-fMLF nanocarriers were studied *in vivo* using rats and mice in order to further delineate the relationship between the *in vivo* tissue dispositional properties and/or cellular uptake and structural characteristics of PEG-fMLF nanocarriers.

CHAPTER 2

BACKGROUND AND SIGNIFICANCE

2.1 HIV and AIDS

Acquired immunodeficiency syndrome (AIDS) is a disease of the human immune system that is caused by the human immunodeficiency virus (HIV). An HIV-infected person is diagnosed with AIDS when his or her immune system is seriously compromised and complications of HIV infection are severe. A diagnosis of AIDS is given to HIV-infected individuals when their $CD4^+$ T-cell count falls below 200 cells/cubic millimeter (mm^3) of blood. Healthy adults usually have $CD4^+$ T-cell counts of 600-1,500/mm^3 of blood. AIDS was first recognized in 1981 and has since become a major worldwide pandemic. An estimated 38.6 million [33.4 million–46.0 million] people worldwide were living with HIV in 2005. An estimated 4.1 million [3.4 million–6.2 million] became newly infected with HIV and an estimated 2.8 million [2.4 million–3.3 million] lost their lives to AIDS (*26*). (Figure 2.1). In the United States, more people than ever were living with HIV in 2005: 1.2 million [720,000–2.0 million] people (*26*). AIDS is the fifth leading cause of death among all adults aged 25 to 44 in the United States (*27*).

The infectious nature of AIDS was established in 1983 when Dr. Francoise Barre-Sinoussi from Luc Montagnier's group at the Pasteur Institute isolated a retrovirus from the lymph node of a 33-year-old Caucasian patient with signs and symptoms that often precede AIDS. Gallo's group also discovered the new virus independently in 1984 (*28,*

29), although there has been some controversy regarding priority. The new virus was initially named lymphadenopathy-associated virus (LAV) and later received the designation of human immunodeficiency virus (HIV). HIV is a retrovirus that infects cells that express the CD4 receptor including T-helper lymphocytes, macrophages, and dendritic cells (DCs) (*30*). By killing or damaging $CD4^+$ T cells of the body's immune system, HIV progressively destroys the body's ability to fight infections and certain cancers. The virus is carried in infected $CD4^+$ T cells, macrophages and DCs, and also exists as a free virus in blood, semen, vaginal fluid, or milk. There are two major variants of HIV have been identified, HIV-1 is most prevalent in central Africa, North America, Europe, Asia and Australia. HIV-2 is endemic in West Africa and is now spreading in India. HIV-2 is less virulent than HIV-1, rarely causes full-blown AIDS syndrome, and is not as widely and rapidly spread as HIV-1. HIV has a diameter of 1/10,000 of a millimeter and is spherical in shape (Figure 2.2). The outer coat of the virus, known as the viral envelope, is composed of two layers of lipids, taken from the membrane of a human cell when a newly formed virus particle buds from the cell. Embedded in the viral envelope are proteins from the host cell, as well as 72 copies of a complex HIV protein that protrudes through the surface of the virus particle (virion). This protein, known as Env, consists of a cap made of three molecules called glycoprotein (gp) 120, and a stem consisting of three gp41 molecules that anchor the structure in the viral envelope. Within the envelope of a mature HIV particle is a bullet-shaped core or capsid, made of 2,000 copies of another viral protein, p24. The capsid surrounds two single strands of HIV RNA, each of which has a copy of the virus's nine genes. Three of these genes, *gag, pol,* and *env*, contain information needed to make structural proteins for new virus particles.

Six regulatory genes, *tat, rev, nef, vif, vpr,* and *vpu*, contain information necessary to produce proteins that control the ability of HIV to infect a cell, produce new copies of virus, or cause disease.

The ability of HIV to enter particular cell type, known as the cellular tropism of the virus, is determined by the expression of specific receptors for the virus on the surface of those cells. HIV enters cells by means of a complex of two noncovalently associated viral glycoproteins, gp120 and gp41, in the viral envelope. The gp120 portion of the glycoprotein complex binds with high affinity to the cell-surface molecule called cluster designation 4 (CD4). This glycoprotein draws the virus to $CD4^+$ T cells, DCs and macrophages, which also express CD4. Infection typically begins when an HIV particle, which contains two copies of the HIV RNA, encounters a $CD4^+$ cell (Figure 2.3). The binding of gp120 to CD4 results in a conformational change in the gp120 molecule allowing it to bind to a second molecule on the cell surface known as a co-receptor. Two chemokine receptors, known as CCR5 (chemokine C-C motif receptor 5), which is predominantly expressed on DCs, macrophages, and $CD4^+$ T cells, and CXCR4 (chemokine C-X-C motif receptor 4), expressed on activated T cells, are the major co-receptors for HIV (*31*). The envelope of the virus and the cell membrane then fuse and lead to entry of the virus into the cell. In the cytoplasm of the cell, HIV reverse transcriptase copies viral RNA into DNA in the infected cell and this DNA "provirus" is then integrated into the host cell chromosome. The RNA transcripts produced from the integrated viral DNA serve both as mRNA to direct the synthesis of the viral proteins and later as the RNA genomes of the new viral particles, which escape from the cell by budding from the plasma membrane, each in a membrane envelope.

It appears that macrophage-tropic isolates of HIV are preferentially transmitted by sexual contact as they are the dominant viral phenotype found in newly infected individuals. Virus is disseminated from an initial reservoir of infected DCs and macrophages. Infection of $CD4^+$ T cells via CCR5 occurs early in the course of infection and continues to occur, with activated $CD4^+$ T cells accounting for the major production of HIV throughout infection. Late in infection, in approximately 50% of cases, the viral phenotype switches to a T-lymphocyte-tropic type that utilizes CXCR4 co-receptors, and this is followed by a rapid decline in $CD4^+$ T-cell count and progression to AIDS.

Cells of macrophage lineage play an important role in the initial stage of HIV-1 infection and continue to do so throughout the course of infection (*32*). Productively infected macrophages have been found in both untreated patients and those receiving HAART (*33*). HIV-1 infection of macrophages can be productive but noncytopathic, permitting macrophages to serve as long-lived sources of HIV production. More importantly they represent major viral reservoirs and are responsible for the relapse of the infection and the development of resistance on discontinuation of treatment. The tissue distribution of macrophages defines the anatomical reservoirs of HIV. In the body, macrophages colonize the primary lymphoid organs such as fetal bone marrow, liver, thymus and secondary lymph organs such as spleen, adult bone marrow, lymph nodes, gut- and mucosal-associated lymphoid tissue (GALT and MALT), in addition to other major organs such as the brain, lungs, kidney (*34*) (Figure 2.4). Throughout the course of HIV infection, macrophages have been implicated in carrying virus across the blood-brain barrier and in establishing and maintaining HIV infection within the central nervous system (CNS), probably the most important anatomical HIV reservoir. *In situ*

hybridization and immunohistochemical analyses revealed that tissue macrophages in the lymph nodes, spleen, gastrointestinal tract, liver, and kidney sustain high plasma virus loads in rhesus macaques after the depletion of $CD4^+$ T cells by a highly pathogenic simian immunodeficiency virus/HIV type 1 chimera (SHIV) (*35*). Viral particles have also been identified in kidney (*36*), brain (*37*) and the cerebrospinal fluid (*38*). There are many more HIV-1 infected cells in lymph nodes than in the blood, which in any case contains fewer than 2 percent of total body lymphocytes (*39*). Taken together, it is clear that macrophages are not only the primary target of HIV infection in patients but are an important source of HIV persistence during HAART (*40, 41*). Therefore, tissue macrophages represent a key challenge for eradicating HIV by current antiviral treatment. Better drug delivery is needed to suppress viral replication inside macrophages in order to improve anti-HIV therapy.

2.2 Problems in Current HIV Infection Treatment

Until the 1990s, there was no effective treatment for AIDS. The introduction of HAART for HIV-infected individuals in 1992, a treatment regimen consisting of a combination of at least three antiretroviral drugs, has greatly reduced the number of viral copies in blood to an undetectable level and has slowed the progression of the disease in patients with HIV infection. HAART has dramatically changed the clinical course of infection in many infected individuals and has led to a substantial decline in the incidence of AIDS and AIDS-related mortality in the United States (*42-46*) and other developed countries (*47, 48*). This has turned HIV disease from a death sentence to a manageable chronic disease.

All of the compounds used in HAART belong to one of the following classes: (i) nucleoside reverse transcriptase inhibitors (NRTIs): i.e., zidovudine, didanosine, zalcitabine, stavudine, lamivudine, abacavir, emtricitabine and nucleotide reverse transcriptase inhibitors (NtRTIs) (i.e., tenofovir disoproxil fumarate); (ii) non-nucleoside reverse transcriptase inhibitors (NNRTIs): i.e., nevirapine, delavirdine, efavirenz, emivirine; (iii) protease inhibitors (PIs): i.e., saquinavir, indinavir, ritonavir, nelfinavir, amprenavir, lopinavir, kaletra (lopinavir and ritonavir), and atazanavir, and (iv) a viral fusion inhibitor: i.e., Fuzeon (T2, Enfuvirtide).

2.2.1 HIV Protease Inhibitor Saquinavir

HIV protease is classified as an aspartic protease and is essential for the production of infectious virions. During the late stages of the HIV replication cycle, multiple copies of the viral *gag* and *gag-pol* polypeptides combine with two molecules of viral RNA and envelope proteins to form immature virus particles. Viral protease then cleaves the *gag* and *gag-pol* polypeptides to form mature virus particles that can recognize and infect other target cells. Inhibiting viral protease leads to the release of immature, noninfectious, virions that halt the spread of virus to uninfected cells. Inhibitors of HIV protease do not effect mammalian proteases due to the dissimilarity of HIV protease and the human aspartic proteases (e.g. renin)(*49*). There are 8 protease inhibitors (PIs) that have been approved by FDA for the treatment of HIV infections. They all share the same structural scaffold, i.e., a hydroxyethylene (instead of the normal peptidic) bond, which makes these compounds peptidomimetic but nonscissile substrate analogues for the HIV protease.

Saquinavir (SQV) was the first HIV-protease inhibitor approved by the U.S. Food and Drug Administration (Figure 2.5). Its structure mimics the phenylalanine-proline cleavage sequence at positions 167 and 168 of the gag-pol polyprotein (*50*). Thus, SQV prevents cleavage of gag and gag-pol protein precursors in acutely and chronically infected cells, arresting maturation and blocking nascent virions from becoming infectious (*51*). However, therapeutic use of SQV suffers from problems of low absorptive and high secretory permeability, bioconversion to inactive metabolites, and poor solubility (*52, 53*). The oral bioavailability of SQV in clinical formulations is low and/or variable with limited penetration into the lymphatic and central nervous systems (CNS) (*9, 54*). Its low and variable bioavailability is primarily attributed to metabolism by cytochrome P-450 3A. Recent results published by our group (*55*) and others (*56*) suggest that multiple membrane transporters may also contribute significantly to the delivery problems of SQV. Clearly, better drug delivery methods are required to enhance the bioavailability of SQV and to reduce the associated variability observed in the clinic.

2.2.2 HIV Tat Inhibitor R.I.Tat9

Some new anti-HIV drug candidates under investigation have alternate mechanisms of action. For example, ALX40-4C (*57, 58*) blocks viral coreceptor CXCR4 and TAK-779 (*59*) blocks coreceptor CCR5. T-20 (*60, 61*) and T-1249 (*4, 62, 63*) inhibit virus-cell fusion by binding to the viral envelope glycoprotein gp-41. Tat antagonists (*64, 65*) interrupt viral transcription. NCp7 (nucleocapsid p7) inhibitors (*66*) hamper viral assembly and budding.

HIV-1 encodes a small non-structural protein, Tat (trans-activator of transcription), which is essential for transcriptional activation of virally encoded genes. Viruses with deletion of the Tat-function are non-viable (*67*). Efficient replication and gene expression of HIV-1 involves a specific interaction of the Tat viral protein, with the trans-activation responsive element (TAR), a highly stable stem-loop RNA structure (*68*). The transactivation responsive (TAR) RNA is the 5'-leader sequence of the HIV-1 mRNA genome and interacts with the Tat protein during transcription. Tat and the positive transcription elongation factor (PTEFb) complex bind to TAR to promote efficient transcription of the full-length HIV genome (*69*). In the absence of the TAR-Tat interaction, viral transcription is inefficient, which makes this RNA-protein complex an important target for therapeutic intervention of HIV replication. The interaction with TAR is mediated by a nine-amino acid region (RKKRRQRRR, residues 49-57) of the Tat protein (Figure 2.6). The Tat-derived basic arginine-rich peptide alone binds TAR RNA with high affinity *in vitro* (*64*). The basic arginine-rich domain (amino acid residues 48-59) in Tat forms the Tat nuclear/nucleolar localization signal (*70, 71*), and this domain is also essential for TAR RNA binding *in vivo* and is sufficient for TAR recognition *in vitro* (*72*). The peptidic compound, N-acetyl- RKKRRQRRR-(biotin)-NH2, containing the 9-amino acid sequence of Tat protein basic domain, was shown to inhibit both Tat-TAR interaction *in vitro* and HIV-1 replication in cell culture (*64*).

Small Tat peptides have also been shown to inhibit HIV replication in cultured T-cells by interaction with the CXCR4 HIV co-receptor present on the surface of T cells, thereby blocking infection by T-tropic HIV-1 strains (*73-75*). A schematic picture of Tat peptide inhibition of CXCR4-dependent HIV-1 infection is shown in Figure 2.7. Tat

inhibitors may also have translational effects (*76*). However, Tat peptides have certain disadvantages, such as high systemic clearance due to *in vivo* degradation, non-specific binding to other biological components, and rapid renal clearance due to their low molecular weight and positive charges (*77*). In our studies, we have utilized R.I.CK (retro-inverso-D-cysteine-lysine)-Tat9, N-acetyl-ckrrrqrrkkr-NH_2, which consists of D-amino acids assembled in the reverse order of the natural L-amino acid Tat9 peptide, N-acetyl-RKKRRQRRR-NH2. Thus, R.I.CK-Tat9 has a similar shape and charge distribution to the natural L-amino acid peptide but is more stable to proteases and retains pharmacological activity (*78*). Furthermore, by attachment of R.I.CK-Tat9 to a large PEG carrier molecule, it should be possible to reduce the renal clearance of and the non-specific binding by the peptide moiety.

2.2.3 Macrophages and HIV-1 Infection

Macrophages are the major differentiated cell of the mononuclear phagocyte system, which comprises bone marrow monoblasts and promonoblasts, peripheral monocytes and tissue macrophages (*79*). The precursors of macrophages are monocytes, promonocytes, and monoblasts. All of these cells come from a common progenitor called the colony-forming unit, granulocyte-macrophages. Monoblasts, the least mature cell of the mononuclear phagocyte system, firstly differentiate into monocytes, remain in the bone marrow for 24 h and then enter the peripheral blood. From the peripheral blood, monocytes migrate to extravascular tissue where they differentiate into macrophages. Macrophages colonize the liver (kupffer cells), lungs (alveolar-interstitial macrophages), spleen, lymph nodes, thymus, gut, marrow, brain, connective tissue and serous cavities

(*79*). They play a critically prominent role in host defense against many infectious agents, including bacteria, viruses, protozoa and parasites.

2.2.3.1 Macrophages as Primary Target of HIV-1

Since M-tropic strains of HIV are preferentially transmitted from person to person (*80*), cells of macrophage lineage are among the first cells infected with the virus (*81*). Both blood monocytes and tissue macrophages can be infected with HIV-1, although monocytes are significantly less susceptible than macrophages (*82-85*). Monocytes in cultures must undergo differentiation to macrophages to become maximally susceptible to productive infection by M-tropic viruses that use CCR5 as a coreceptor (*84, 85*). Resident tissue macrophages are major targets for HIV-1, being susceptible to HIV-1 infection *in vitro* on the day of isolation (*84, 86-88*). The percentage of HIV-infected macrophages within tissues may be high, with reports ranging from 1 to 50% depending on the specific tissue site (*89-94*). Similar to tissue macrophages, monocyte-derived macrophages (MDM) cultured from peripheral blood monocytes are susceptible to HIV-1 infection *in vitro*. They can produce HIV-1 for weeks to months without significant cytopathic effects (*85, 91, 95*).

The ability of macrophages to support HIV-1 replication *in vitro* with minimal or no cytopathicity has been well characterized for a number of years, although the underlying mechanism has been proposed only recently. Studies from two independent groups have characterized the assembly of HIV-1 in subcellular vesicles within macrophages, in contrast to $CD4^+$ T cells, where the virus assembles and buds from the plasma membrane (*96, 97*). In macrophages, HIV-1 virions assemble within late

endosomes of the endocytic vesicle system, which also contain MHC class II glycoproteins and endocytosis-associated molecules such as LAMP-1 and CD63. Under normal circumstances, late endosomes are destined for lysosomal fusion and subsequent peptide degradation, MHC loading and antigen presentation (Figure 2.8). However, HIV-1 infection of macrophages inhibits endosome-lysosome fusion, preserving the HIV-1 virions inside the cells. Hijacking the MHC class II presentation pathway enables transmission of HIV-1 from macrophages to T cells via cell-cell contact during antigen presentation. In addition, it has been proposed that HIV-1 hijacks the exosome or intracellular vesicle trafficking pathway (*98*). Exosomes are produced by exocytosis of endosomes that contain MHC/peptide complexes, to enable antigen-presentation by a wider range of antigen-presenting cells. Transfer of HIV-1 via exosomes represents a noncytopathic mechanism for infection of new cells, which is made possible by the localization of HIV-1 to the endocytic pathway (Figure 2.8). It is also likely that this localization contributes to the preservation of macrophage viability, since endosome synthesis is a normal, ongoing process as opposed to budding from the T cells plasma membrane and related cytopathicity. While the kinetics of virus release from macrophages are slower than from T cells, the lack of HIV-induced cytopathicity enables macrophages to continue secreting HIV-1 for a longer period of time.

2.2.3.2 Macrophages as the Main Reservoir of HIV-1

$CD4^+$ lymphocytes latently infected by HIV-1 are thought to be a major viral reservoir (*99-101*). These cells carry HIV provirus integrated within the cellular genome in a state that is non-replicating or producing incomplete strands of HIV–RNA. This

suggests that HIV–DNA in resting T-lymphocytes is fully quiescent; resumption of virus replication may occur only after activation of resting lymphocytes by exogenous stimuli. Recent observations show that virus quasispecies reappearing in plasma of patients undergoing interruption of successful antiviral therapy are often genetically different from those present, at the same time, in $CD4^+$ lymphocytes latently infected by HIV-1 (*102, 103*). These data strongly suggest that other reservoirs may also be implicated in the rebound of HIV-1 replication during treatment interruptions.

HIV-1-infected monocytes and macrophages are commonly found in blood and tissues of seropositive patients receiving HAART (*104, 105*). Their distribution is widespread in all tissues, including the brain, gut, liver, lungs, lymphoid tissues, spleen and they represent important viral reservoirs throughout the course of HIV-1 disease (*12, 106*) (Figure 2.4). Furthermore, circulating monocytes harbor infectious provirus both in untreated patients and in those undergoing successful HAART (*41*). In addition, the virus life cycle in HIV-1-infected macrophages is quite different from that in $CD4^+$ lymphocytes. Once infected, the large majority of activated $CD4^+$ lymphocytes are rapidly killed by HIV-1 (*107*), while macrophages are relatively resistant to the viral cytopathic effects (*108, 109*). Indeed, macrophages can survive at least 3-4 months after a virus challenge *in vitro*. As a consequence, it is conceivable that the long life span of infected M/M may in part compensate for their relatively low number. However, their contribution to overall daily virus production and release during the slow-phase of virus decay in HAART experienced patients is substantiated. This supports the role of macrophages as not only a primary target of HIV-1 infection, but also as an important

cellular reservoir of HIV-1 able to challenge the attempts to eradicate the virus from patients (*5, 93, 110*).

The role of macrophages as agents for virus dissemination and disease pathogenesis is also well known. Productively-infected M/M can fuse with $CD4^+$ lymphocytes and transfer the virus to these cells (*111*). In addition, infected macrophages are able to trigger apoptosis of lymphocytes (either $CD4^+$ or $CD8^+$) (*112*), astrocytes, and neurons even without directly infecting these cells (this is known as the bystander effect) (*113*).

Taken together, cells of macrophage lineage play an important role not only in the initial stage of HIV-1 infection but also subsequently throughout the course of infection (*32*). Recent reports provide clear evidence that monocytes and macrophages are not only the primary target of HIV infection but are an important source of HIV persistence during HAART in addition to $CD4^+$ T-lymphocytes (*40, 41*). Therefore macrophages represent a key challenge for eradicating HIV by current antiviral treatment, indicating the need for better drug delivery to suppress viral replication inside macrophages in order to improve anti-HIV therapy.

2.2.4 Statement of the Problem

While the remarkable efficacy of protease and reverse transcriptase inhibitor combinations for the treatment of HIV-1 infection has been clearly established *in vitro* and in the clinic, a cure for AIDS remains an elusive goal. HIV particles exist in sites outside of the blood compartment such as the CNS, gastric and male genital tracts, and in cellular reservoirs such T-cells and macrophages. Three cellular reservoirs thus far have

been identified as possible sanctuaries for HIV-1 in the presence of potent antiretroviral therapy: latent $CD4^+$ T cells, macrophages, and follicular dendritic cells (FDCs) (Table 2.1). Viral replication rebounds once the drug therapy is terminated, regardless of the duration of the therapy, primarily due to persistence of replication-competent virus in viral reservoirs and sanctuary sites in body (*5*). Therefore, viral reservoirs and sanctuary sites remain the main obstacles for the eradication of HIV from the body. The major factors that contribute to the formation of viral reservoirs and sanctuary sites are the low and fluctuating drug concentrations due to poor drug absorption and penetration (*4, 114, 115*). The oral bioavailabilities of the HIV protease inhibitors are low and/or variable, with limited penetration into the central nervous system (CNS) (*15*). Saquinavir mesylate was the first drug approved in this class. The two marketed saquinavir capsule formulations have mean oral bioavailabilities that range from 4 to 16% and are highly variable, as indicated by area under the concentration-time curve (AUC) coefficients of variation that are ≥30% (*9*). Saquinavir's low and variable bioavailability is primarily attributed to metabolism by cytochrome P-450 3A4 (*116*). Tat peptide was shown to inhibit both Tat-TAR interaction *in vitro* and HIV-1 replication in cell culture (*64*), as well as inhibit HIV replication in cultured T-cells by interaction with the HIV co-receptor CXCR4 present on the surface of T cells (*73-75*). However, Tat peptides have certain disadvantages, such as high systemic clearance due to *in vivo* degradation, non-specific binding to other biological components, and rapid renal clearance due to their low molecular weight and positive charges (*77*). Therefore, it is becoming more obvious that better drug delivery technologies are required to increase total body persistence and retention of these potent therapeutic agents.

In addition to $CD4^+$ lymphocytes, cells of macrophage lineage represent a key target of HIV infection. The absolute number of infected macrophages in the body is relatively low compared to $CD4^+$ lymphocytes. Nevertheless, the peculiar dynamics of HIV replication in macrophages, their long-term survival after HIV infection, and their ability to spread virus particles to bystander $CD4^+$ lymphocytes, results in their substantial contribution to the pathogenesis of HIV infection. Macrophages are infected during an early stage of HIV infection and are thought to play the role of a Trojan horse by spreading the infection in tissues. Most recent studies point out to a more complex role for macrophages in HIV infection: macrophages contribute to host defense, viral persistence and pathogenesis. Infected macrophages are a reservoir for HIV and modulate apoptosis of T cells present in their vicinity. In addition, macrophages are the most important target of HIV in the central nervous system (*117*). Taken together, persistently-infected macrophages represent a key challenge for therapeutic approaches aimed at decreasing residual virus replication. The protease inhibitors (PIs), acting at post-integrational stages of virus replication, are the only drugs able to interfere with virus production and release from macrophages with established and persistent HIV infection (chronically-infected cells) (*118*). However, because the penetration of PIs into the macrophages is restricted, this effect is achieved at concentrations and doses higher than those effective in de-novo infected $CD4^+$ lymphocytes and thus cause severe drug toxicity during chronic therapy. The insufficient concentrations of PIs due to poor absorption and penetration and/or lack of adherence may cause a resumption of virus replication from chronically-infected macrophages, ultimately resulting in therapeutic failure. For all these reasons, therapeutic strategies aimed at delivering PIs specifically to macrophages to

achieve sufficient concentrations and control of HIV replication in macrophages should be explored.

2.3 Nanotechnology-based Drug Delivery System

2.3.1 Nanotechnology

Nanotechnology, the term derived from the Greek word nano meaning dwarf, is a broad, interdisciplinary topic involving physics, chemistry, biology and engineering at the molecular or nanometer level. Precise drug release into highly specified targets involves miniaturizing the delivery systems to become much smaller than their targets such as cells and intracellular compartments of micron or submicron size. The development of novel drug delivery systems has been impacted to an enormous degree over the past decade by the explosive growth of nanotechnology, and has led to the development of nanoparticles for medical and biotechnological applications.

Nanoparticles can be defined as colloidal systems with a diameter smaller than 1,000 nm (*119*), which have novel optical, electronic, and structural properties that are not available either in individual molecules or bulk solids. Recently, many therapeutic agents including small molecules, proteins, DNA, and peptides have been developed into potent and complex agents. The drug can either be integrated in the matrix or attached to the particle surface. Submicron particles possess a very high surface to volume ratio. As a consequence the dissolution rate is increased according to Noyes Whitney and Kevin equations (*119*). Depending on the particle charge, surface properties and attached targeting groups, nanoparticles can be designed to accumulate preferentially in organs or

tissues. Nanoparticle drug delivery systems, due to their diminutive size, can penetrate into individual cells to allow efficient drug accumulation at targeted locations in the body. By doing so, the toxicity is reduced, drug side effects decreased and treatment efficacy enhanced. Also, therapeutic agents can be loaded into nanoparticles in a manner that prevents their recognition by the immune system. This "stealth" property makes them candidates for carrying antiviral drugs to selectively target HIV-infected cells (*120*). These nanoparticle systems maybe used to carry the drug in a controlled manner from the site of administration to the therapeutic target. Thus, the concept of the "magic bullet" proposed by the Nobel laureate immunologist Paul Ehrlich at the beginning of 20th century may become a reality with the development of nanoparticle drug delivery systems.

2.3.2 Polymeric Nanoparticles for Targeted Delivery

Over the past decade, there has been considerable interest in developing polymeric nanoparticles as effective drug delivery devices (*121-123*). Most systems consist of biocompatible polymers such as polyethylene glycol (PEG), poly lactic acid (PLA), poly lactic/glycolic acid (PLGA) and/or natural polymers like chitosan and gelatine. The drug of interest is either dissolved, entrapped, adsorbed, attached or encapsulated into the nanoparticle matrix. Depending on the method of preparation, nanoparticles, nanospheres or nanocapsules can be obtained with different properties and release characteristics for the encapsulated therapeutic agent. The advantages of using nanoparticles for drug delivery result from their three main basic properties. First,

nanoparticles, because of their small size, can penetrate through smaller capillaries and be taken up by cells, which allows efficient drug accumulation at the target sites. Second, the use of biodegradable materials for nanoparticle preparation allows sustained drug release within the target site over a period of days or even weeks. Third, an insoluble drug can be made water-soluble by introducing solubilizing moieties into the polymer, thereby improving its bioavailability and biodegradability. In general, nanocarriers may (i) protect a drug from degradation, (ii) enhance drug absorption by facilitating diffusion through epithelium, (iii) modify pharmacokinetic and drug tissue distribution profile, and/or (iv) improve intracellular penetration and distribution. However these advantages have to be weighed against their main disadvantages such as costly production, and difficult storage and administration because of physical instability phenomena like aggregation.

Application of nanotechnology in drug delivery is linked to the potential of drug targeting. Treatment of severe disease such as cancer and AIDS generally involves drugs that are highly toxic to healthy tissues. Consequently, their use is considerably limited by the occurence of dramatic side effects. Nanoparticles represent a significant improvement over traditional oral and intravenous methods of administration in terms of efficiency and effectiveness. The delivery of the drug to the target tissue can be achieved primarily in two ways—passive and active. Passive targeting takes advantage of the permeability of tumor tissues and most polymer nanoparticles show higher accumulation into tumors by means of the enhanced permeability and retention (EPR) effect. Active targeting is usually achieved by conjugating the nanoparticle to a targeting moiety, thereby allowing preferential accumulation of the drug in the tumor tissue, within individual cancer cells,

intracellular organelles, or specific molecules in cancer cells. This approach is used to direct nanoparticles to cell surface carbohydrates, receptors, and antigens.

2.3.3 Polymeric Nanoparticles for AIDS Therapy

Providing the optimum treatment of AIDS is a major healthcare challenge in the 21st Century. HIV is localized and harbored in certain inaccessible compartments of the body, such as the CNS, the cerebrospinal fluid, the lymphatic system and in macrophages throughout the body, where it can not be reached by the majority of therapeutic agents in adequate concentrations or where therapeutic agents cannot reside for an adequate duration of time. Currently available therapy can lower the systemic viral load below the detection limit. However, upon discontinuation of treatment, an infection rebound phenomenon from the reservoir sites is observed and the potential for the development of resistance exists. Recent data indicate that low and residual levels of virus found in tissues of the lymphoid and CNS are likely due to insufficient drug levels at those sites. Thus, improvement in the delivery of anti-HIV drugs to these tissues with limited drug penetration or persistence is now a more important next step in advancing anti-HIV therapy than suppressing viral load alone. Nanoparticle-based drug delivery systems may provide an opportunity to facilitate complete eradication of viral load from reservoir sites by delivering anti-HIV drugs to therapeutic targets such as HIV infected cells and viral reservoirs. Liposomal and polymeric nanoparticles have been suggested to achieve better control of targeting toxic antiviral drugs to enhance their bioavailability in infected cells. For instance, liposomes targeted to HIV-infected cells with the ligand for CD4 grafted on their surface increased the efficiency of a liposome-encapsulated protease inhibitor by

almost 10-fold, whereas, at the same time, toxic side effects significantly decreased (*124*). In AIDS therapy, macrophages are a good target since they represent a cell population in the reticulo-endothelial system (RES) that plays an important role in the immunopathogenesis of the disease. The effectiveness of human serum albumin (HSA) and polyhexylcyanoacrylate (PHCA) nanoparticles loaded with PIs and nucleoside analogs (SQV, AZT and ddC) was demonstrated based on their ability to prevent HIV infection in monocytes/macrophages cultures from blood donors (*125, 126*). In acutely infected cells, an aqueous solution of saquinavir showed little antiviral activity at concentrations below 10 nM, whereas a nanoparticulate formulation exhibited a good antiviral effect at a concentration of 1 nM (*126*). In a rat model, intravenously injected colloidal ^{14}C-labeled AZT nanoparticles were detected in the organs of the RES in concentrations as high as 18-fold those of unbound AZT (*125*). Thus, increasing drug concentrations at specific sites where macrophages are abundant may allow a reduction in the dosage and, as a result, a decrease in systemic toxicity (*127*). The IgG-derived immunomodulating peptide tuftsin (Thr-Lys-Pro-Arg) was conjugated to HIV reverse transcriptase inhibitor 3'-azido-3'-deoxythymidine (AZT) (*128*). The AZT-tuftsin chimera possessed the characteristics of both components, including inhibition of reverse transcriptase and HIV-antigen expression, stimulation of IL-1 release from mouse macrophages, and augmentation of the immunogenic function of the cell. Similarly, acetylated low density lipoproteins (AcLDL), ligands for macrophage scavenger receptors, were conjugated to AZT (*129*). A murine macrophage cell line J774.A and a human macrophage cell line U937 took up 10-fold more of the AcLDL-AZT than AZT.

Although nanotechnology is a fast-expanding area of science, application of nanotechnology to antiviral therapy is still in its infancy. Initial studies in cultured cells predict that new antiviral strategies applied in combination with nanotechnology should provide promising and efficient treatment. Further evaluation both *in vitro* and *in vivo* are still required to confirm these studies. However, the lack of convenient animal models of HIV infection currently limits the rate of progress in this field. This area of research is anticipated to lead to the development of novel, sophisticated, multifunctional drug delivery systems which can recognize infected tissues and cells, deliver anti-HIV drugs to target tissues and cells in a controlled manner, and most importantly, eradicate the HIV virus from the body and ultimately cure the AIDS patient.

2.4 *PEGylation for Improved Drug Delivery and Therapy*

Polymers have already been shown to form effective delivery systems for many anticancer agents. However there are few studies using polymers in HIV drug delivery. The potential advantages of improved drug delivery include (*16*): (1) continuous maintenance of drug levels in a therapeutically desirable range; (2) reduction of harmful side effects due to targeted delivery to a particular cell type or tissue; (3) decreased amount of drug needed; (4) decreased number of doses and possibly less invasive drug regimen; and (5) facilitation of drug administration for pharmaceuticals with short in vivo half-lives (e.g. peptides and proteins). These advantages are significant since up to 15% of all hospital admissions, some 100,000 deaths and $136 billion in health costs in the US each year can be attributed to adverse drug events (*130, 131*). Another 10% of hospital admissions are due to a lack of patient compliance (*131, 132*). The advantages must be weighed against the following concerns in the development of each particular drug

delivery system: (1) toxicity of the materials (or their degradation products) from which the drug is released, or other safety issues such as unwanted rapid release of the drug (dose dumping); (2) discomfort caused by the system itself or the means of insertion; and (3) expense of the system due to the drug encapsulation materials or the manufacturing process.

PEGylation, the process of attaching polyethylene glycol (PEG) to drug molecules, has been a highly successful strategy for improving the pharmacokinetics and pharmcodynamics of pharmaceuticals, especially for protein and peptide therapeutics (*19-25*). PEG has the general formula of HO-(CH_2CH_2)n-CH_2CH_2OH with typical molecular weights of 500 to 50,000 Da. PEGs are amphiphilic and dissolve in organic solvents as well as in water; they are also non-toxic and eliminated by a combination of renal and hepatic pathways thus making them ideal to employ in pharmaceutical applications. PEG also has the lowest level of protein or cellular absorption of any known polymer. The FDA has approved PEG for use as lubricants, binders, and vehicle in injectable, topical, rectal and nasal formulations for cosmetics or pharmaceuticals.

2.4.1 PEGylation of Proteins

In the late 1970s, Frank Davis and his colleagues at Rutgers University pioneered the first chemical steps of PEGylation that enabled the protection of proteins from destruction during drug delivery (*133*). Their studies generated the unexpected finding that pegylation also improves the **pharmacokinetic** and **pharmacodynamic** properties of polypeptide drugs by increasing water solubility, reducing renal clearance and limiting toxicity (*133*). Studies of PEG in solution reveal that each ethylene glycol subunit is

tightly associated with two or three water molecules. This binding of water molecules makes pegylated compounds function as though they are five to ten times larger than a corresponding soluble protein of similar molecular mass, as confirmed by size-exclusion chromatography and gel electrophoresis (*19*). The PEG polymer, along with the associated water molecules, acts like a shield to protect the attached drug from enzyme degradation, rapid renal clearance and interactions with cell surface proteins, thereby limiting adverse immunological effects. Pegylation reduces kidney clearance simply by making the molecules larger, and, as the kidneys filter substances basically according to size, larger molecules clear more slowly. Pegylated drugs are also more stable over a range of pH and temperature changes (*134*) compared with their unpegylated counterparts. Consequently, pegylation confers on drugs a number of properties that are likely to result in a number of clinical benefits, such as sustained blood levels that enhance effectiveness, fewer adverse reactions, longer shelf life and improved patient convenience (*21*). However, pegylation can produce a decrease in the *in vitro* activity of proteins, but generally this negative effect is offset in biological systems by an increased half-life. Pegylation can influence the binding affinity of therapeutic proteins to cellular receptors, which results in changes in the bioactivity of polypeptides (*20*).

With first-generation pegylation, the PEG polymer was generally attached to the ε-amino groups of lysines. This resulted in the modification of multiple lysines, and gave mixtures of PEG isomers with different molecular masses. The existence of these isomers makes it difficult to reproduce drug batches, and can contribute to the antigenicity of the drug and poor clinical outcomes. In addition, first-generation approaches mainly used linear PEG polymers with molecular masses of 12 kDa or less. Unstable bonds between

the drug and PEG were sometimes used, which led to degradation of the PEG–drug conjugate during manufacturing and injection. An additional problem was that early pegylation was performed with methoxy–PEG (m–PEG), which was contaminated with PEG diol resulting in the crosslinking of proteins to form inactive aggregates. Diol contamination can reach up to 10–15% (*135*). Despite these limitations, several first-generation pegylated drugs received regulatory approval, including pegademase (Adagen), a pegylated form of the enzyme adenosine deaminase for the treatment of severe combined immunodeficiency disease (SCID), and pegaspargase (Oncaspar), a pegylated form of the enzyme asparaginase for the treatment of leukaemia. In 2001, peginterferon α2b (PegIntron) became available as a once-a-week treatment for hepatitis C. Chronic hepatitis C virus (HCV) infection is the leading cause of liver cirrhosis and liver cancer (*136*), and the principal reason for liver transplants in the United States. PEG-Intron contains a single strand of PEG (MW 12,000 Da) per IFN (MW 19,000 Da). The plasma circulating $t_{1/2}$ of PEG-Intron is about eight times that of native IFN α-2b, allowing for weekly subcutaneous dosing.

Second-generation pegylation chemistry strives to avoid the pitfalls associated with mixtures of isomers, diol contamination, unstable bonds and low-molecular mass m–PEG. Researchers have created an array of chemistries to improve PEG derivatives and their linkages to drugs. For example, using PEG–propionaldehyde instead of PEG–acetaldehyde prevents the formation of impurities in the PEG (by aldol condensation in this case). Generating carboxylic acid intermediates of PEG permit up to 97% of diol impurities to be removed by ion-exchange chromatography before PEG attachment to polypeptide drugs (*134*). An overall goal of second-generation pegylation methods is to

create larger PEG polymers to improve the pharmacokinetic and pharmacodynamic effects seen with lower molecular mass PEGs. In some cases, the changes are dramatic, such as the pegylation of interleukin-6 (IL-6), which increases the half-life of IL-6 100-fold, which in turn results in a 500-fold rise in its thrombopoietic potency (*20*). Another improvement in second-generation PEG polymers is the use of branched structures, in contrast to the solely linear structures found in first-generation PEGs (*134*). Branched PEGs of greatly increased molecular masses — up to 60 kDa or more, compared with the 12 kDa or less found in first-generation PEGs — have been prepared. A branched PEG 'acts' as if it were much larger than a corresponding linear PEG of the same molecular mass. A linear PEG is distributed throughout the body with larger distribution volume while a branched PEG is distributed with a smaller distribution volume and early on delivered to the liver and spleen (*137*). The increase in the hydrodynamic size of $F(ab')_2$ form of a humanized anti-interleukin-8 (anti-IL-8) antibody was about 7-fold by adding one 20 kDa PEG and about 11-fold by adding one branched 40 kDa (*138*). The $F(ab')_2$ conjugate obtained by linking a single branched 40 kDa PEG was found to possess an apparent size of 1600 kDa (protein equivalent), greatly over the kidney ultrafiltration limit, and displayed an AUC after intravenous administration 15.7 higher than the unmodified protein (*138*). Branched PEGs are also better at cloaking the attached polypeptide drug from the immune system and proteolytic enzymes, thereby reducing its antigenicity and likelihood of destruction (*139*). The binding of branched 10 kDa PEG to asparaginase reduced the antigenic character of the protein about 10-fold as compared to the counterpart obtained by modification with 5 kDa PEG (*134*). These results are attributable to the higher molecular weight and “umbrella like” structure of the branched

polymer, which efficiently prevents the approach of anti-protein antibodies and immunocompetent cells. Using the new chemistries described above, second-generation clinical PEG conjugates started to appear in the early 1990s. A second-generation, branched PEG of 40 kDa was then coupled to IFN-α2a (*140*). This version (Pegasys) was approved by FDA in 2002 for the treatment of adults with chronic hepatitis C. Once-weekly injections of Pegasys produce nearly constant blood concentrations of IFN-α2a (Figure 2.9), and renal clearance is reduced 100-fold relative to unpegylated IFN-α2a. Pegylation increases the half-life of IFN-α2a from 9 to 77 hours (*141*).

2.4.2 PEGylation of Peptides

The area of peptide PEGylation is still in its infancy but has generated much interest in the drug delivery community. Hirudin is a naturally occurring anticoagulant polypeptide found in the leech, *Hirudo medicinais*, and consists of 65 amino acids with an approximate *Mw* of 7000 Da. Recombinant hirudin (r-hirudin) has proved to be an effective antithrombotic agent and is currently in clinical trials. It has been determined that r-hirudin is rapidly eliminated from circulation with a terminal $t_{1/2}$ of 50–100 min, thus requiring continuous infusion or multiple daily injections to maintain therapeutic levels. Modification of r-hirudin with two strands of PEG-5000 via urethane bonds affords PEG-hirudin that exhibits a significantly prolonged $t_{1/2}$ resulting in enhanced antithrombotic activity and no observable immunogenicity (*142*). Salmon calcitonin (sCT) is a therapeutic poly-peptide hormone consisting of 32 amino acids (*Mw* 3432 Da). It possesses a disulfide bridge between the 1 and 7 positions and a C-terminal proline

amide residue. PEG modified sCT was prepared using succinimidyl carbonate-PEG as the linking agent to produce mono and di-PEGylated species. Both derivatives showed slightly enhanced pharmacokinetics and lower renal excretion compared to the unmodified peptide. The authors concluded that PEGylated sCTs may have therapeutic potential (*143*).

2.4.3 PEGylation of Small Cancer and HIV Drugs

In contrast to the successful application of permanently bonded PEG to proteins (macromolecules) for drug delivery, only a few small organic drug molecules have been conjugated to PEG. For example, stable amide derivatives of doxorubicin (Dox) and amphetamine were prepared, but only in vitro data was reported (*22, 144*). Permanent PEGylation of paclitaxel was also reported as a means of solubilizing and delivering this very potent anticancer drug (*145*). Water soluble mPEG 5000 paclitaxel-7-carbamates were synthesized but were10-fold less active than the native drug in vitro and non-toxic in mice (*24*). This may be attributed to two reasons: the large PEG substituent blocks activity at the target cells or the PEGylated paclitaxel does not reach the cells in sufficient concentration to produce meaningful results. It was also shown that PEG-CPT prodrug showed greater tumor accumulation (30 fold) in mice bearing subcutaneous HT-29 tumors compared to unmodified CPT (*22*), primarily due to enhanced permeation and retention (EPR) effects. PEG conjugates of indinavir, saquinavir, and nelfinavir were synthesized and the permeation was tested across a Caco-2 cell monolayer (*146*). The PEG-HIV protease inhibitor conjugates were designed for reducing the interactions of the protease inhibitors with plasma proteins, and improving their *in vivo* blood circulation

time. The connection of highly hydrophilic polyethylene glycol moieties to a drug is further expected to decrease its solubility into the cell membrane and consequently its passive diffusion across a cell monolayer and across the intestinal barrier. As expected from a hydrophilicity increase, the conjugation of PEG2000 to Saq and Ind reduced drastically both their absorptive and secretory diffusion and Papp coefficients across the Caco-2 monolayer (*146*). Such PEG-modified prodrugs are therefore limited to intravenous administration. It was concluded from this study that a PEG *prodrug* approach to drug delivery would offer a more effective route for enhancement of therapeutic index.

2.5 Macrophage Targeted Drug Delivery

As discussed above, macrophages play a critically important role in host defense against many infectious agents, including virus, bacteria and parasites. On the other hand, macrophages are not only the primary target of HIV infection but are an important source of HIV persistence during HAART in addition to $CD4^+$ T-lymphocytes (*40, 41*). Therefore, targeting of drugs to macrophages could be an effective strategy for the treatment of HIV infection and AIDS. In addition, macrophages play important roles in the pathogenesis of other diseases such as tuberculosis, influenza, herpes simplex, rheumatoid arthritis, and multiple sclerosis (*147*). Targeting to macrophages could be potentially useful in the treatment of these diseases too. Macrophages possess various receptors such as formyl peptide receptors, mannose receptors, Fc receptors, complement and many other receptors (*148-150*). These macrophage surface receptors determine the control of activities such as activation, recognition, endocytosis, secretion, etc. A useful

approach for promoting the uptake of drugs or drug delivery systems by macrophages is to incorporate into drug conjugates ligands capable of interacting with macrophage surface receptors. Various research groups showed that uptake of ligand-incorporated liposomes targeted to macrophage receptors was significantly higher than liposomes without ligands (*151-155*).

2.5.1 N-formyl Peptide Receptors (FPRs)

N-formyl methionyl peptides are cleavage products of bacterial and mitochondrial proteins, and serve as potent chemoattractants for mammalian phagocytic leukocytes (*156, 157*). The synthetic peptide N-formyl-methionyl-leucyl-phenylalanine (fMLF) binds and activates at least two G protein-coupled receptors (GPCRs), the high-affinity formyl-peptide receptor (FPR) (Figure 2.10) and its low-affinity variant formyl-peptide receptor like-1 (FPRL1), in human phagocytic cells. FPR and PRL1 are expressed at high levels in both peripheral blood monocytes and neutrophils. FPR binds fMLF with high affinity with K_d values in the picomolar to low nanomolar range and is activated by fMLF at correspondingly low concentrations to mediate robust chemotactic and Ca^{2+} mobilizing responses in human phagocytic leukocytes (*158*), while only high concentrations ($\geq$1 μM) of fMLF are capable of inducing Ca^{2+} mobilization in cells transfected to express FPRL1 and fMLF is a poor chemotactic agonist for FPRL1 even in the micromolar concentration range (*159*). After binding to the receptors, fMLF activates phagocytic cells through a typical pertussis toxin (PTX) sensitive, G protein-mediated signaling cascade, which leads to increases in cell migration, phagocytosis, and release of proinflammatory mediators (*148, 160*). Unlike other leukocyte chemoattractants, N-

formyl peptides could originate from either an endogenous source, such as the mitochondrial proteins of ruptured host cells, or an exogenous source, such as the proteins of invading bacterial pathogens. This suggests that the formyl-peptide receptor (FPR) and its variant FPRL1 (FPR-like 1) are involved in host defense against bacterial infection and in the clearance of damaged cells. Recently, additional, more complex roles in HIV infection for these receptors have been proposed. The activation of FPR and/or FPRL1 in monocytes by fMLF resulted in increased cell migration, calcium mobilization and the heterologous down-regulation of the expression and function of chemokine receptors, notably CCR5 and CXCR4, two crucial fusion co-receptors for HIV-1 (*161-164*).

2.5.2 Macrophage Targeted Delivery via N-formyl Peptide Receptors

Therapeutic drugs are generally administered without regard to their tissue distribution, even though only one organ, tissue or cell type might be diseased or infected. By targeting a drug to the site of the disease, it may be possible to achieve a higher and more effective dose where needed and a lower and less toxic dose in unaffected tissues. Macrophage targeting could be especially useful for treatment of AIDS. This objective could potentially be achieved by covalent attachment of the therapeutic agent of choice to a polymeric drug carrier with an attached targeting molecule. Some attempts toward macrophage targeted delivery have been made by targeting to N-formyl peptide receptors using the chemotactic peptide N-formyl-methionyl-leucyl-phenylalanine (fMLF). For example, liposomes containing fMLF were

prepared and their interaction with mouse peritoneal macrophages were studied by the Fidler group(*155*). They found that liposomes containing of fMLF are phagocytosed more efficiently and their phagocytosis is mediated via the fMLF receptors on the macrophage (*155*). Further studies with radioactive fMLF revealed that higher levels of fMLF can be delivered to macrophages by liposomes than in the free, nonencapsulated form (*153*). Treatment of mouse macrophages with liposome-encapsulated fMLF, but not with free fMLF, generated tumoricidal properties in the macrophages (*153*).

2.5.3 Macrophage Targeted Delivery via Other Receptors

Macrophage mannose receptor is a type-I transmembrane glycoprotein consisting of a single subunit (165-170 kDa), with its carboxyl terminus on the cytoplasmic side of the membrane and contains as many as 8 carbohydrate-recognition domains (CRD) (*165, 166*), of which only the segment consisting of CRD's 4-8 possesses receptor activity (*167, 168*). The mannose receptor is expressed by all tissue macrophages (*169, 170*) and displays much higher affinity for multivalent oligosaccharides such as those found on the surfaces of bacteria than for single oligosaccharide. Muller and Schuber (*154*) studied the interaction of neo-mannosylated liposomes with murine kupffer cells and resident peritoneal macrophages using synthetic functionalized mannosyl ligands. Their study showed that mannose residue-conjugated liposomes were associated to peritoneal macrophages and Kupffer cells in about 2–4 times greater amount than were plain unconjugated liposomes. Both in vitro and in vivo uptake of liposomes increased extraordinarily by targeting these carriers through Fc surface receptors of macrophages (*151, 152*). Derksen et al. (*151, 152*) studied rabbit immunoglobulin and modified mouse

monoclonal antibody-incorporated liposomes. Coupling of rabbit immunoglobulin with liposomes increases the uptake by rat liver macrophages more than five times compared with control liposomes (*151*). In vivo study demonstrated that 80–85% of the coupled liposomes were accumulated in the liver within 1 h of the injection (*152*). Another example of such ligands is IgG-derived immunomodulating peptide tuftsin (Thr-Lys-Pro-Arg), which was conjugated to the HIV reverse transcriptase inhibitor 3'-azido-3'-deoxythymidine (AZT) (*128*). The AZT-tuftsin chimera possessed characteristics of both components, including inhibition of reverse transcriptase and HIV-antigen expression, stimulation of IL-1 release from mouse macrophages, and augmentation of the immunogenic function of the cell. Similarly, acetylated low density lipoprotein (AcLDL), a ligand for macrophage scavenger receptors, was conjugated to AZT (*129*). Ten-fold more of the AcLDL-AZT than AZT were taken up by a murine macrophage cell line J774.A and a human macrophage cell line U937.

2.6 Ideal Nanotechnology-based Drug Delivery System for AIDS Therapy

The “ideal” polymeric nanoparticle drug delivery system for AIDS therapy should include a coordinated behavior of the following components:

- Polymeric nanocarrier capable of improving the PK properties of therapeutic agents
- Therapeutic agent (such as anti-HIV agents saquinavir, R.I.Tat etc.)
- Targeting moiety (such as macrophage-targeting groups fMLF, mannose, etc.)
- Other components (such as endosomal escape agent, efflux pump inhibitor, etc.)

The concept is to use novel drug delivery technology to optimize the bioefficacy of the anti-HIV agents and therefore improve AIDS therapy. Typically, drug concentrations from conventional dosage forms are optimized based on drug concentrations in the blood. The assumption is that drug concentrations at the active site(s) are proportional to drug concentrations in the blood. However, this is not true for the HIV anatomical reservoirs such as CNS and testis or the cellular reservoirs such as latent $CD4^+$ T cells and macrophages, that may develop biopharmaceutical "resistance" due to the induction or inhibition of transport proteins or metabolizing enzymes by co-administered drugs. Attaching PEG to drugs has been shown to prolong blood circulation time by preventing glomerular filtration in the kidneys and by preventing interactions with cells (i.e., stealth-like properties). Drugs that are slowly released from PEG as it circulates in the blood eventually make their way to the active site(s) as well as to non-diseased tissues and cells, i.e., the conjugate has improved blood levels but is not targeted to the sites of HIV persistance. Therefore, currently used PEGylation approaches that have been enormously successful for treating other diseases are not likely to be appropriate for treating HIV infection. Dose levels and the frequency of administration are higher when the efficiency of drug delivery is low as it is for many drugs used in HAART. This leads to increased side effects, poor patient adherence to therapeutic regimens and therapeutic failure. Selectively delivering a drug or drugs to the therapeutic active site(s) will allow for a reduction in dosage and frequency of administration and lead to enhanced therapeutic outcomes. The efficacy, toxicity and specificity of the drug delivery system are important issues. The present research will focus on a full evaluation of the "ideal" targeting system, which includes all of the features described previously.

Table 2.1 Cellular and Anatomical Reservoirs and Other Sources of HIV -1.

(Schrager, L.K. and M.P. D'Souza, JAMA, 1998. 280(1): p. 67-71.)

Cellular and Anatomical Reservoirs and Other Sources of Human Immunodeficiency Virus 1 (HIV-1)

Source of HIV*	Time*	Potential Means of Eradication
Sources contributing to rapid-phase decay		
Free virions	<6 h	Potent antiretroviral therapy
Productively infected $CD4^+$ T cells	~1 d	Potent antiretroviral therapy
Resting $CD4^+$ T cells with unintegrated HIV-1 DNA	~16 d	Potent antiretroviral therapy
Cellular reservoirs		
Resting $CD4^+$ T cells with integrated provirus	Months to years	Potent antiretroviral therapy and adjunctive therapies?
Infected macrophages	>14 d	Potent antiretroviral therapy and P-glycoprotein inhibitors?
Virions on follicular dendritic cells	15 d	Potent antiretroviral therapy and adjunctive therapies to hasten virion depletion?
Anatomical reservoirs		
Virions in the central nervous system	Unknown	Potent antiretroviral therapy regimens with improved bioavailability and with P-glycoprotein inhibitors?
Other anatomical reservoirs? (eg, testes?)	Unknown	Potent antiretroviral therapy regimens with improved bioavailability

*Measured as half-life.

Figure 2.1 A global view of HIV/AIDS 38.6 million people [range: 33.4-46 million] living with HIV as of end 2005. (WHO/UNAIDS: http://www.who.int/hiv/facts/hiv2005/en/index.html)

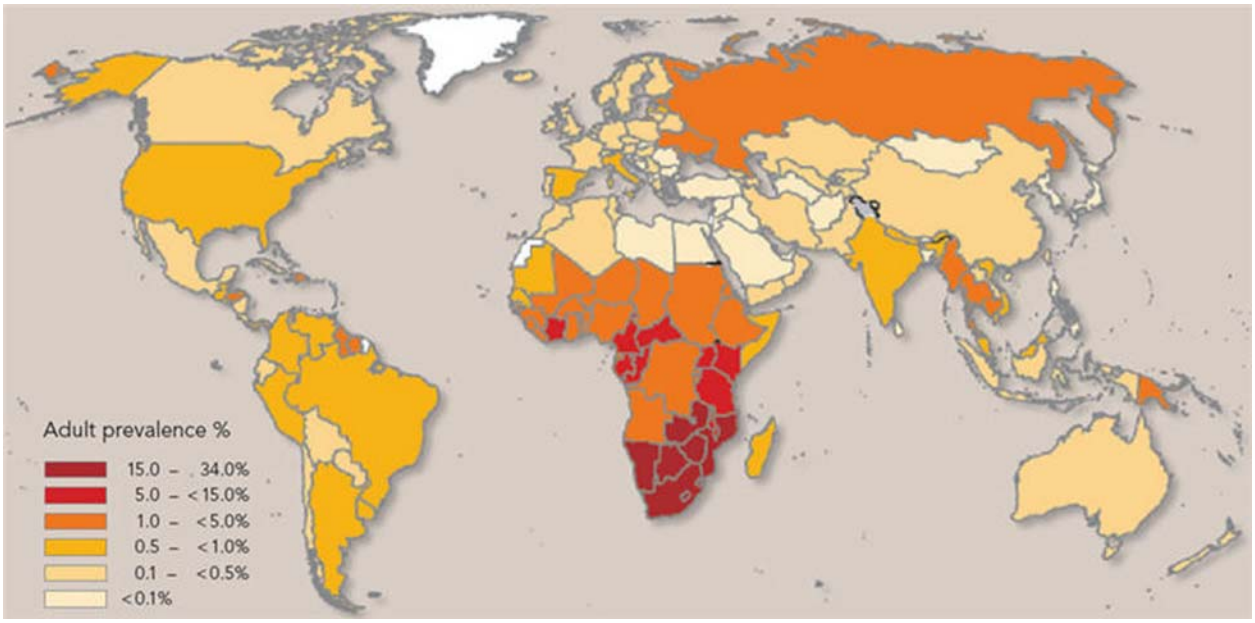

Figure 2.2 Structure of HIV. (National Institute of Allergy and Infectious Diseases: http://www.niaid.nih.gov/factsheets/howhiv.htm)

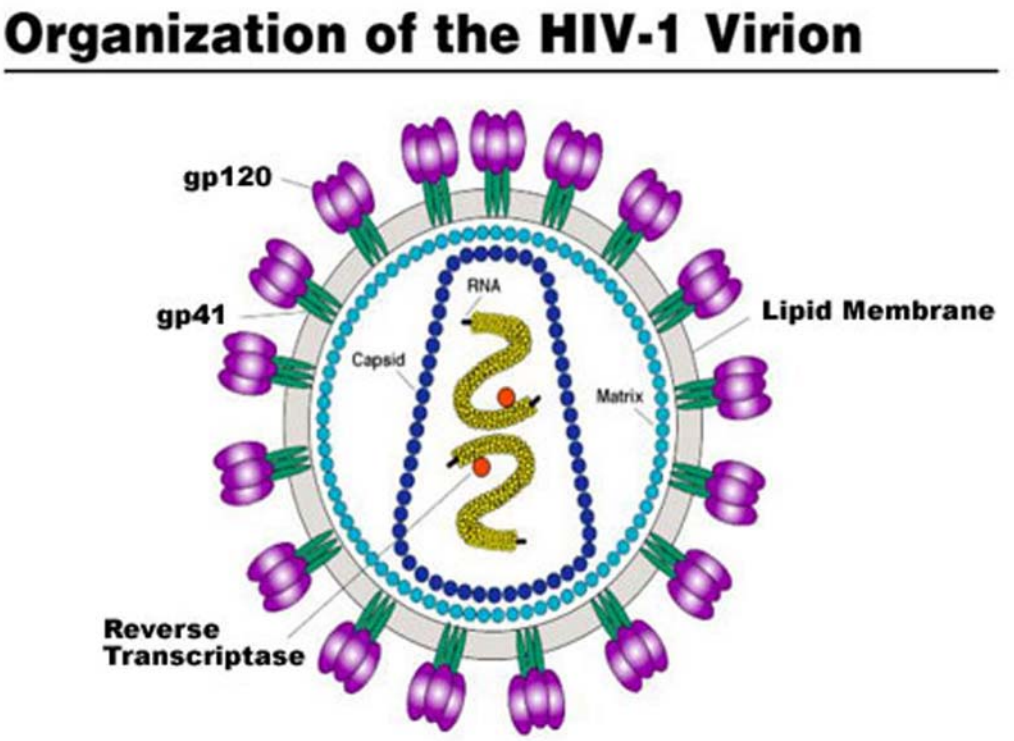

Figure 2.3 Replication cycle of HIV. (Weiss, RA Nature 410, 963-967, 19 April 2001)

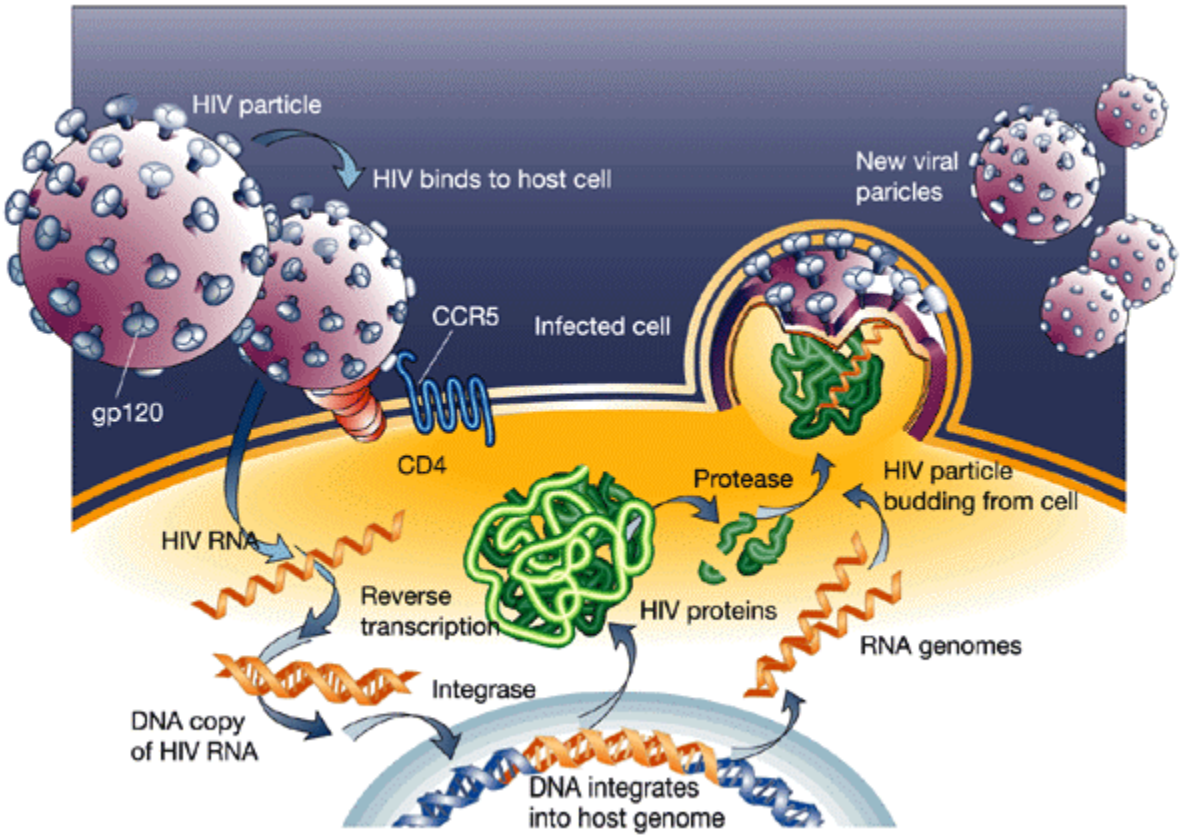

Figure 2.4 Macrophages and HIV-1 infection. Macrophages are not only the primary target but also the main reservoir of HIV infection during HAART.

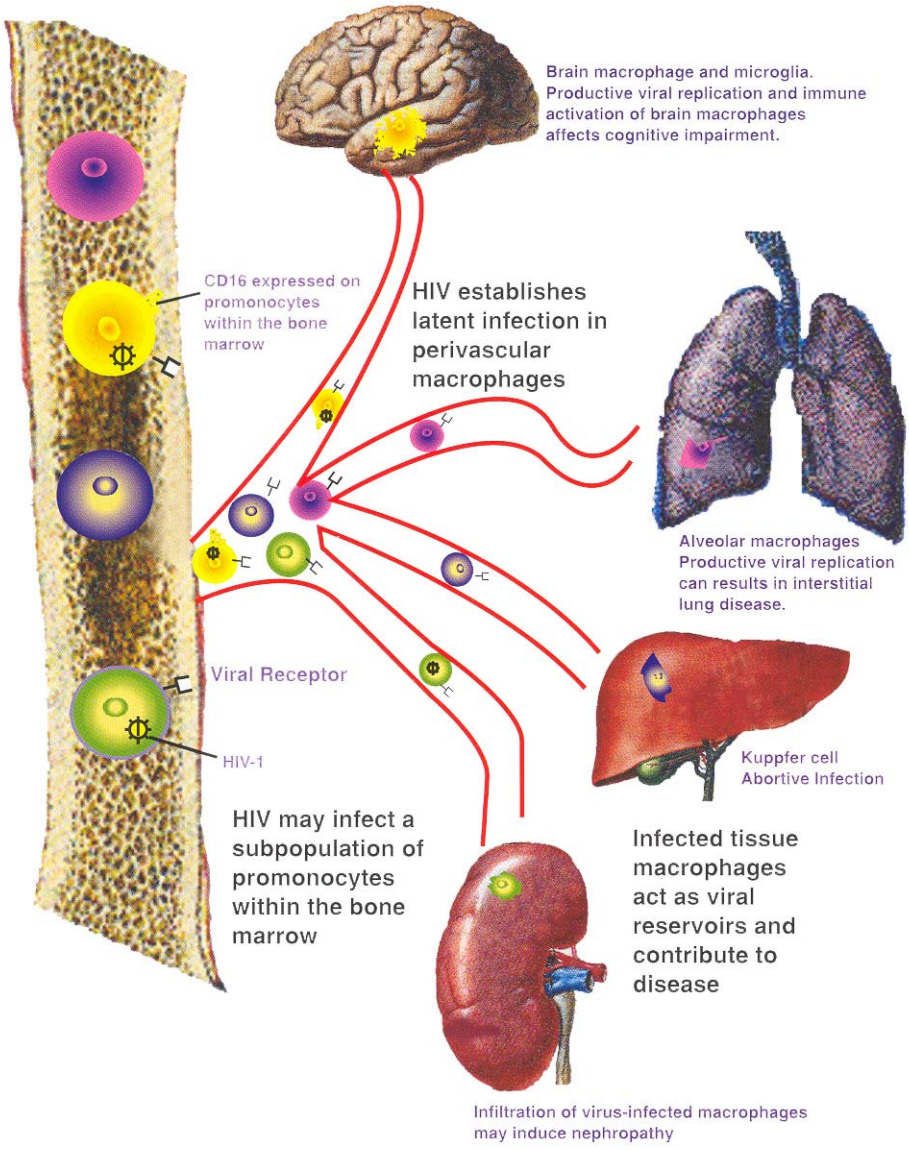

Figure 2.5 Structure of the first FDA approved HIV protease inhibitor saquinavir (Fortovase, Invirase).

(http://www.wiley.com/legacy/college/boyer/0470003790/cutting_edge/aids_therapies/aids_therapies.htm)

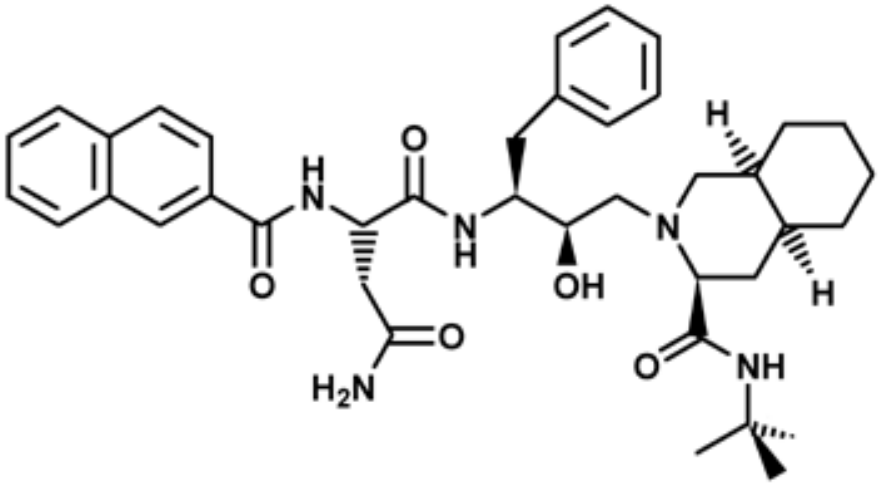

Saquinavir

Figure 2.6 Model of the HIV-1 Tat (49-57)-TAR complex. (http://btcpxx.che.uni-bayreuth.de/INSTITUTE_members/Heinrich_Sticht/structures.html)

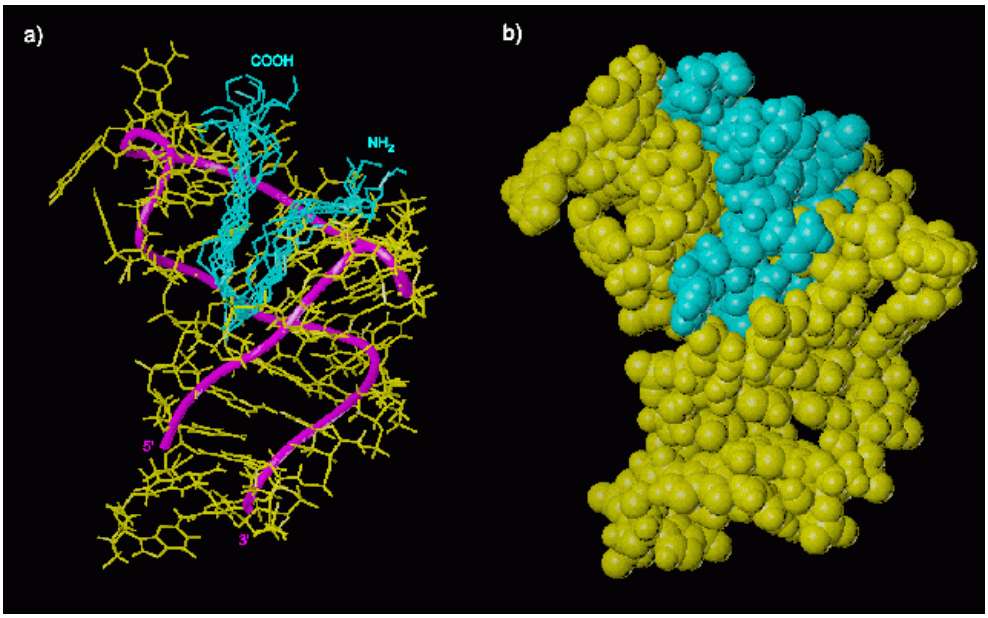

Figure 2.7 A schematic picture of Tat peptide inhibition of CXCR4-dependent HIV-1 infection.

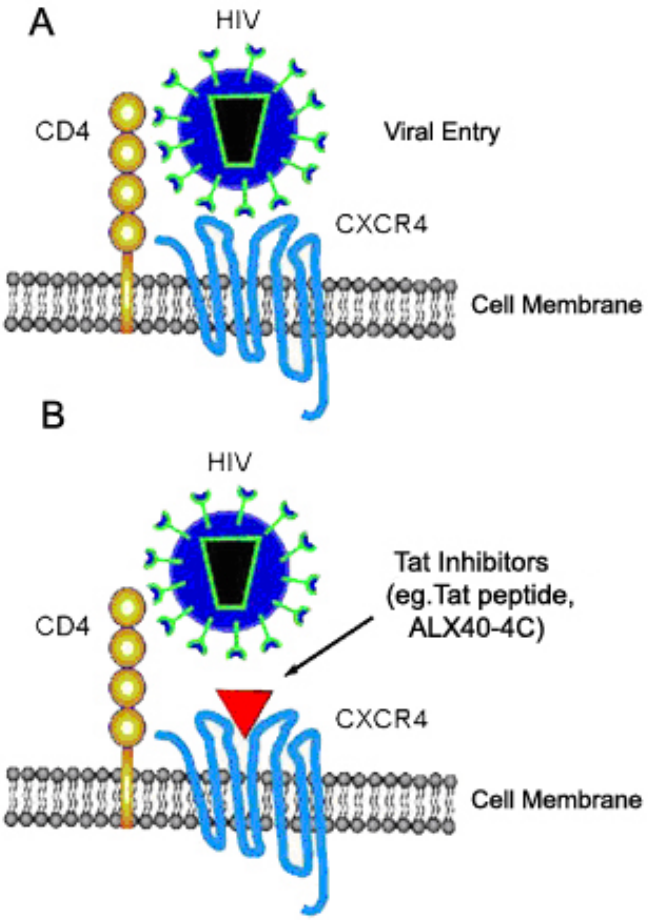

Figure 2.8 HIV-1 virions assemble within late endosomes in HIV infected macrophages**.** (Kedzierska, K, Maslin, CL, Crowe, SM, Medicinal Chemistry Reviews, 2004, 1, 351-360)

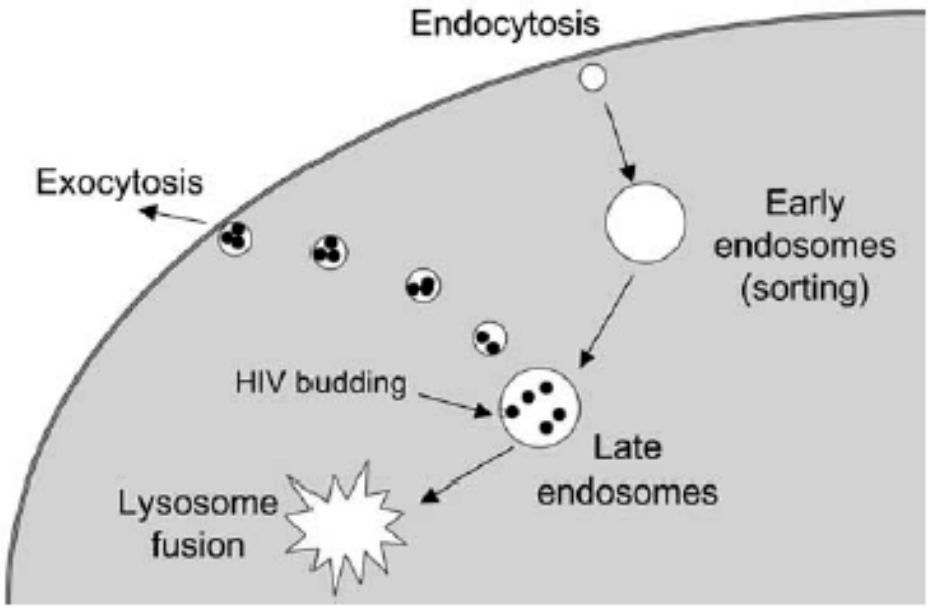

Figure 2.9 Pharmacokinetic profiles for interferon (IFN)-α 2a and 40 kDa polyethylene glycol (PEG)–IFN-α 2a. (Harris, JM, Nature Reviews Drug Discovery **2**, 214-221, 2003)

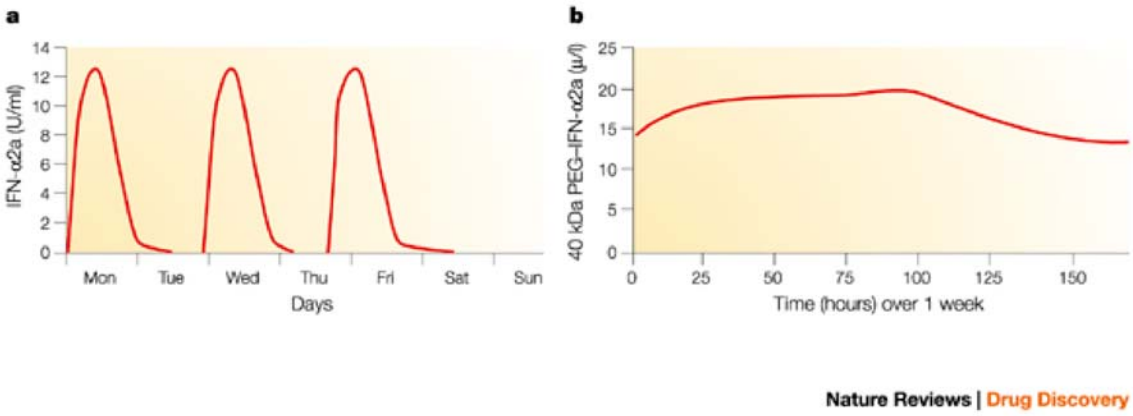

Figure 2.10 Structure of N-formyl peptide receptor. (Prossnitz ER, Ye RD, Pharmacol Ther. 74 (1): 73-102, 1977)

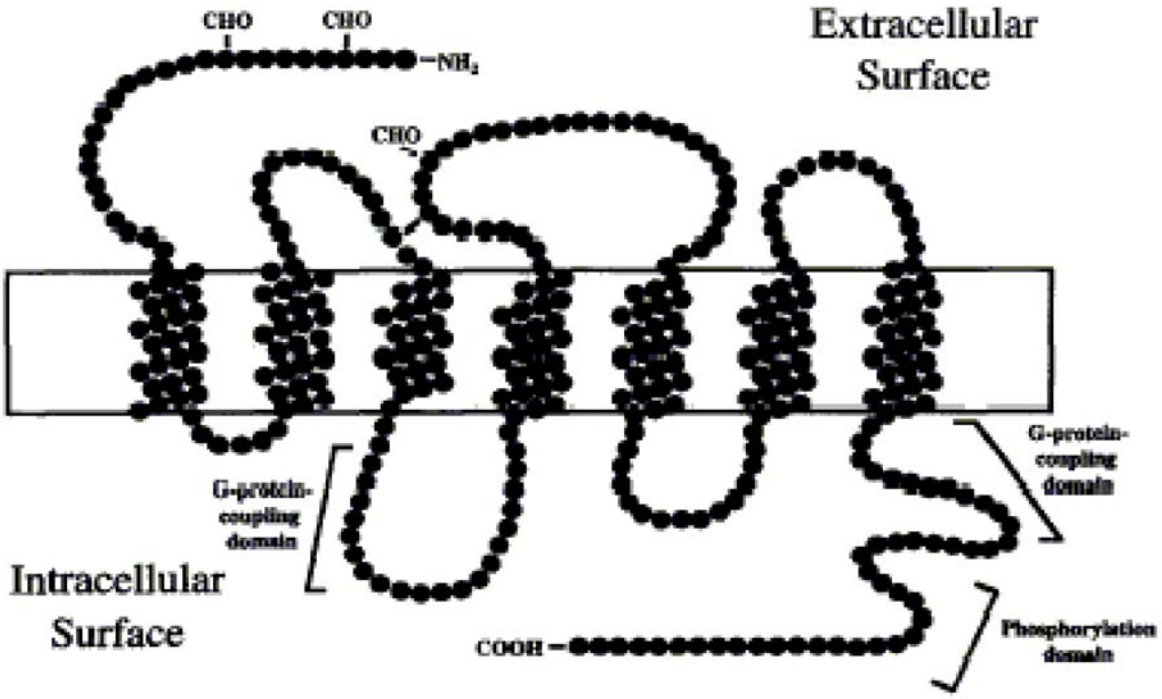

CHAPTER 3

DESIGN, SYNTHESIS, STABILITY AND ANTI-HIV ACTIVITY OF MULTI-COMPONENT NANOPHARMACEUTICALS DERIVED FROM POLY (ETHYLENE GLYCOL), RETRO-INVERSO-TAT NONAPEPTIDE AND SAQUINAVIR

3.1 Introduction:

Most current anti-Acquired Immunodeficiency Syndrome (AIDS) drugs target two key enzymes in the human immunodeficiency virus-1 (HIV-1) replication cycle, reverse transcriptase and protease. While the remarkable efficacy of protease and reverse transcriptase inhibitor combinations for the treatment of HIV-1 infection has been clearly established *in vitro* and in the clinic, not even a single AIDS patient has ever been cured. Accordingly, new anti-HIV drug candidates having alternate mechanisms of action are under investigation. For example, ALX40-4C (*57, 58*) blocks viral coreceptor CXCR4 and TAK-779 (*59*) blocks coreceptor CCR5. T-20 (*60, 61*) and T-1249 (*4, 62, 63*) inhibit virus-cell fusion by binding to the viral envelope glycoprotein gp-41. Tat antagonists (*64, 65*) interrupt viral transcription. NCp7 inhibitors (*66*) hamper viral assembly and budding. To date, combination pharmacotherapy remains the most effective strategy for reducing viral loads in HIV-infected patients. However, given the variety of new

chemical entities under development, combination therapies hold even greater future promise.

A major impediment to successful anti-HIV-1 therapy is the emergence of drug resistant strains harboring mutations in genes encoding these viral enzymes (*171*). Factors that are known or expected to contribute to the failure of highly active antiretroviral therapy (HAART) include pre-existing resistance (*172*), low and fluctuating drug concentrations due to poor drug absorption or patient non-compliance(*4, 114, 115*), and the presence of viral reservoirs and sanctuary sites (*5*). Other mechanisms of resistance are becoming increasingly recognized in AIDS therapy. For example, drug-induced biopharmaceutical "resistance" (i.e., multidrug resistance), an established concept in cancer pharmacotherapy (*173, 174*), occurs when the upregulation of cell efflux transporter activity results in lower cellular exposure and decreased drug efficacy. Therefore, the ability to control blood and cellular drug concentrations is critical for managing the emergence of classical viral and multidrug resistance.

Recent successes with HIV peptide fusion inhibitors such as T20 (e.g., enfuvirtide and fuzeon) (*63*) suggest that small anti-HIV peptides can provide clinical utility complementing the antiviral activity of reverse transcriptase or protease inhibitors. However, many of these peptide drugs are poorly absorbed or are rapidly cleared from the body. HIV-1 encodes a small non-structural protein, Tat (trans-activator of transcription), which is essential for transcriptional activation of virally encoded genes. Viruses with deletion of the Tat-function are non-viable (*175*). Efficient replication and gene expression of HIV-1 requires a specific interaction of the Tat viral protein with the trans-activation responsive element (TAR), a highly stable stem-loop RNA structure (*68*).

The interaction with TAR is mediated by a nine-amino acid basic domain (RKKRRQRRR, residues 49-57) of the Tat protein (Figure 3.1). This domain is essential for TAR RNA binding *in vivo* and is sufficient for TAR recognition *in vitro* (*72*). A Tat-derived basic arginine-rich peptide alone binds TAR RNA with high affinity *in vitro* (*64*). A peptidyl compound, N-acetyl- RKKRRQRRR-(biotin)-NH2, containing the 9-amino acid sequence of Tat protein basic domain, was shown to inhibit both Tat-TAR interaction *in vitro* and HIV-1 replication in cell culture (*64*). In addition to the TAR RNA interaction, the basic domain in Tat has at least three other functional properties. It constitutes a nuclear/nucleolar localization signal (*70, 71*). The basic Tat peptide is also a prototypic cell penetrating peptide that can bring a cargo molecule across the plasma membrane. This was originally discovered when it was observed that Tat protein could freely enter cells (*176*). Small Tat peptides derived from the basic domain have also been shown to inhibit HIV replication in cultured T-cells by interacting with the HIV CXCR4 co-receptor present on the surface of T cells, thereby blocking infection by T-tropic HIV-1 strains (*73-75*). These peptides may also have translational effects (*76*).

Therefore, we have been investigating Tat peptides as therapeutic agents (*64, 76*). Considering the pleiotrophic effects of Tat domain peptides, it is not clear whether the delivery of these peptides to extracellular or intracellular targets or both is important for their antiviral effect. Furthermore, since these Tat peptides have cell penetrating activity (*177*), they can also potentially be used to enhance the cellular uptake of an appended drug(*178*). However, Tat peptides have certain disadvantages, such as high systemic clearance due to *in vivo* degradation, non-specific binding to other biological components, and rapid renal clearance due to their low molecular weight and positive

charges (*77*). A variety of different strategies have improved biopharmaceutical properties of peptide drugs. In our studies, we have utilized retro-inverso (RI) peptides and macromolecular PEG conjugates to overcome the many biopharmaceutical challenges faced by Tat peptides. R.I.CK (retro-inverso-D-cysteine-lysine)-Tat9, N-acetyl-ckrrrqrrkkr-NH_2, consists of D-amino acids assembled in the reverse order of the natural L-amino acid Tat9 peptide, N-acetyl-RKKRRQRRR-NH2. Thus, R.I.CK-Tat9 has a similar shape and charge distribution to the natural L-amino acid peptide but is more stable to proteases and retains pharmacological activity (*78*). PEGylation has been shown to be one of the most successful techniques for improving the pharmacokinetic and pharmacodynamic properties of peptide drugs by increasing stability and reducing renal clearance and protein binding (*179*).

The second agent used in this study, saquinavir (SQV) was the first HIV-protease inhibitor approved by the U.S. Food and Drug Administration. Its structure mimics the phenylalanine-proline cleavage sequence at positions 167 and 168 of the HIV gag-pol polyprotein (*50*). Thus, SQV prevents cleavage of gag and gag-pol protein precursors by HIV protease in acutely and chronically infected cells, arresting maturation and blocking nascent virions from becoming infectious (*51*). However, therapeutic use of SQV suffers from problems of low absorptive and high secretory permeability, bioconversion to inactive metabolites, and poor solubility (*52, 53*). The oral bioavailability of SQV in clinical formulations is low and/or variable with limited penetration into the lymphatic and central nervous systems (CNS) (*9, 54*). While its low and variable bioavailability is primarily attributed to metabolism by cytochrome P-450 3A, recent results published by

our group (*55*) and others (*180*) suggest that multiple membrane transporters may also contribute significantly to the delivery problems of SQV.

In the current study, the preclinical *in vitro* effectiveness of a small peptidic Tat antagonist, R.I.CK-Tat9, alone or in combination with saquinavir on multifunctional poly(ethylene glycol) (PEG)-based bioconjugates is demonstrated. We showed that the PEG conjugates of R.I.CK-Tat9 and R.I.CK(biotin)-Tat9 both displayed similar antiviral activity with EC_{50} of 1.47 μM and 1.5 μM, respectively, which was weaker than that of the non-PEGylated forms (Figure 3.6 and Table 3.1). The activity of SQV in drug conjugates compared to the maximal achievable antiviral efficacy of free SQV (EC_{50} = 15 nM) was reduced with addition of $PEG_{3.4k}$ alone (EC_{50} = 900 nM), but restored with the addition of R.I.CK-Tat9 to the SQV-$PEG_{3.4k}$ conjugate (EC_{50} = 15 nM), the same *in vitro* potency as free SQV. However, the mechanism of enhancement for the SQV-$PEG_{3.4K}$-R.I.CK-Tat9 conjugates was not clearly established and needs further investigation.

3.2 Material and Methods:

3.2.1 Material

Fluorenylmethoxycarbonyl (Fmoc)-amino acid derivatives, MBHA Rink amide resin, BOP (benzotriazol-1-yl-oxytris(dimethylamino)phosphonium hexafluorophosphate) and HOBt (*N*-hydroxybenzotriazole) were purchased from Calbiochem-Novabiochem Corp. (La Jolla, CA). mPEG-NHS (MW ~3.4 kDa) and 8-arm PEG-$(NH_2)_8$ (MW ~10 kDa) were obtained from Nektar Therapeutics (Huntsville, AL).

N-maleimidobutyryloxysuccinimide ester (GMBS) was obtained from Pierce Biotechnology (Rockford, IL). NHS-carboxyfluorescein, glutathione (GSH), DIEA (diisopropylethylamine), aldrithiol, piperidine, hydrazine, acetic anhydride, diethyl ether, Dde (1-(4,4-dimethyl-2,6-dioxocyclohex-1-ylidene)ethyl), EDT (ethanedithiol), TIS (triisopropyl silane), DMAP (4-(dimethylamino)pyridine), DIPC (1,3-diisopropylcarbodiimide), anhydrous dimethylformamide (DMF), and anhydrous dimethyl sulfoxide (DMSO) were obtained from Sigma-Aldrich (St.Louis, MO). Dichloromethane (DCM) obtained from Sigma was dried over calcium hydride and freshly distilled prior to use. Trifluoroacetic acid (TFA) obtained from Aldrich was distilled with H_2SO_4 before use. SQV from commercially purchased capsules (Inverase, Roche) was extracted with methanol. Chemical reactions were carried out under a nitrogen atmosphere. The purity of all new compounds was checked by mass spectrometry, TLC, and/or NMR.

3.2.2 Synthesis of R.I.CK-Tat9 and SQV Conjugates

R.I.CK-Tat9 and its derivatives, compounds **1-3** (Figure 3.2) were synthesized manually on a MBHA Rink amide resin (Novabiochem, La Jolla, CA) via Fmoc chemistry in the presence of 3 folds coupling activating reagents, BOP and HOBt (Sigma-Aldrich, St. Louis, MO). The ε-Dde (1-(4,4-dimethyl-2,6-dioxocyclohex-1-ylidene)ethyl) protecting group (in the N-terminal lysine residue) was selectively removed using 2 % hydrazine in DMF and reacted to attach the appended groups biotin-NHS or carboxyfluorescein-NHS (Sigma-Aldrich, St. Louis, MO) on solid support. The peptides were then acetylated, cleaved and purified on a Vydac C_{18} column (10 μm, 2.2 x

25 cm, Vydac, Hesperia, CA) with detection at 220 nm and fluorescence of labeled peptides was detected at 535 nm (emission) and 485 nm (excitation). The purified products were lyophilized and confirmed by electrospray ionization mass spectra **(**ESI-MS**)**.

In the synthesis of R.I.CK-Tat9-PEG bioconjugates (Figure 3.3), the eight amino groups of PEG_{10K}-$(NH_2)_8$ (MW 10 kDa, 8-arm branched, Nektar Therapeutics, Huntsville, AL) (4) were first activated with three-fold molar excess of the heterobifunctional cross-linker, N-maleimidobutyryloxysuccinimide ester (GMBS) (Pierce Biotechnology, Rockford, IL), in DMF to form a maleimide activated PEG (5). The reaction was stirred overnight at room temperature. The product was precipitated with cold ether and dried under vacuum to yield the solid PEGylated product. The GMBS linker essentially converts a primary amino group to a maleimide group that can react with a thiol group to form a stable thioether bond. This activated intermediate 5 was reacted with a three-fold molar excess of 1, 2 and 3, respectively, with coupling reagents HOBt (4-fold molar excess) and BOP (3-fold molar excess) in DMF. DIEA (diisopropylethylamine, 1 % v/v) was added to adjust to neutral pH. The products were recrystallized from cold ether and dried under vacuum overnight. These bioconjugates 6-8 were purified using size-exclusion chromatography using a Sephacryl S-100 column (Amersham, Piscataway, NJ) in 0.1 M PBS, pH 7.4, with detection at 220 nm (for 6 and 7). For 8, fluorescence was detected at 535 nm (emission) and 485 nm (excitation). The formation of the bioconjugates (6-8) was confirmed by MALDI-TOF mass spectrometry and the concentrations of bioconjugates were determined by amino acid analysis.

In the synthesis of the SQV conjugates (Figure 3.4), the active hydroxyl function of SQV (9, extracted from Inverase, Roche) was esterified with Fmoc-Cys(S-Trt)-COOH using DIPC (1,3-diisopropylcarbodiimide) / DMAP [4-(dimethylamino)pyridine] as coupling reagent. SQV-Cys ester (10) was obtained with 82% yield after Fmoc removal with piperidine, followed by TFA (trifluoroacetic acid) -deprotection of the Trt (trityl) group. The esterification of the hydroxyl of SQV after silica gel purification was confirmed by ESI-MS and ^{1}H and ^{13}C NMR. ESI-MS (m/z): 774.5 $(M+H)^{+}$; 796.5 $(M+Na)^{+}$. PEGylation of 10 was carried out using $PEG_{3.4k}$-NHS in the presence of DIEA/DCM to give 11. This product was purified using gel permeation chromatography (Sephadex LH-20 column in DMF, 239 nm) resulting in 70 % yield. The formation of 11 was confirmed by MALDI-TOF (m/z (%) 3837.6) and ^{1}H and ^{13}C NMR. The thiol group of the cysteine in PEGylated form of SQV-Cys-ester (11) was then activated with 2,2'-dithiodipyridine. Addition of 1 to the activated PEGylated form of SQV-Cys-ester (11) gave 12 with 65% yield after gel permeation purification. Mass spectrometry of these products demonstrated peaks at the expected molecular weights using MALDI-TOF (m/z (%) 5447.6.

3.2.3 Release kinetics of R.I.CK-Tat9 by cleavage of thioether bond

The stability of fluorescein-labeled PEG_{10k}-$(R.I.CK\text{-}Tat9)_8$ bioconjugates was investigated in PBS (pH 7.4) and rabbit plasma, at 37°C. The stability of the bioconjugates was also investigated in PBS (pH 7.4) at 37°C by treating them with 5 μM glutathione (GSH) (Sigma-Aldrich, St. Louis, MO), a physiologically relevant reducing reagent that is responsible for intracellular reductive environment inside cells. Initially,

different concentrations (0.01 – 10.0 μM) of R.I.CK(fluorescein)-Tat9 were dissolved separately in PBS (pH 7.4) and in plasma and their fluorescence measured by Tecan fluorescence microplate reader (excitation at 485 nm, emission at 535 nm) to obtain calibration curves in PBS (pH 7.4) and in plasma. Thereafter, the bioconjugate solutions were incubated separately in PBS (pH 7.4) and in spiked rabbit plasma at 37°C, along with GSH treated bioconjugates in PBS (pH 7.4) at 37°C. Aliquots were withdrawn at different time points and centrifuged at 14,000 x g for 90 min with a Microcon™ filter (molecular weight cut-off = 10,000 Da) (Amicon Inc., Beverly, MA). The drug moiety cleaved from the bioconjugate during the incubation passes through the filter whereas the drug moiety that remains linked to the PEG carrier is retained. [Note that a PEG polymer of 3,400 Da behaves as a >10,000 Da peptide on ultrafiltration.] The retentates resulting from the different incubation time points were withdrawn and subjected to fluorescence detection. Each measurement was done in duplicate. The concentrations of the bioconjugates were determined from a fluorescence calibration curve that was established in the same media. The rate constant (k) was obtained from the linear plot of $\ln(\text{bioconjugate})_t$ versus incubation time, t (h), where $[\text{bioconjugate}]_t$ = concentration of bioconjugate at different incubation time, t, (Figure 3.5). The half-life ($t_{1/2}$) of the cleavage of thioether bond from the bioconjugates was calculated from the relation $t_{1/2} = 0.693 / k$ where k is the slope of the linear plot.

3.2.4 Release kinetics of SQV by cleavage of ester bond

A fluorogenic protease inhibition assay was used to measure the hydrolysis kinetics of SQV-Cys ester which was the common intermediate for all the synthesized R.I.CK-

Tat9-SQV bioconjugates. The chemical stability of this ester was determined in PBS at pH 7.4 and in spiked plasma both measured at 37ºC as reported earlier (*181*).

3.2.5 Antiviral Assays

The in vitro anti-HIV activity of PEG conjugates was determined by a MTT-based HIV-1 susceptibility assay reported previously (*181*) using MT-2 cells, an HTLV-1-transformed human T-cell leukemia cell line, infected with the HIV-1 strain LAV-Vbu3. The cytotoxicity of the conjugates was evaluated in parallel. The MT-2 cells were grown in RPMI 1640 DM (Dutch modification) medium supplemented with 20% FBS (fetal bovine serum), 1% w/v pen-strep, and 1% w/v L-glutamine and maintained at 37°C in 5% CO_2 in an incubator. The cultured MT-2 cells were diluted to 2×10^5 cells/mL and infected at a multiplicity of infection (MOI) of 0.01 (1 viral particle per 100 cells), causing the death of 90% of the cells 5 days later. The tested conjugates were diluted with RPMI 1640 medium and were added to the cultured MT-2 cells after viral infection. Each conjugate was tested in triplicate for its antiviral activity. Cell viability was measured by the colorimetric MTT test at 540 nm, which is directly proportional to the number of living cells. The conjugate EC_{50} and LC_{50} values were determined from the curves of the percentage of viral cell killing and cytotoxicity against compound concentration (Table 3.1, Figure 3.6).

3.3 Results:

3.3.1 Synthesis of R.I.CK-Tat9 and SQV Conjugates

A series of R.I.CK-Tat9 and SQV bioconjugates was synthesized and characterized. The peptides, L-Tat9, R.I.CK-Tat9, R.I.CK(biotin)-Tat9, and R.I.CK(ε-carboxyfluorescein)-Tat9 (Figure 3.2) were synthesized, purified and their structures were confirmed by electrospray ionization mass spectrometry (ESI-MS). For R.I.CK-Tat9 PEG bioconjugates, the thiol group of the cysteine residue at the N-terminus of R.I.CK-Tat9 or its derivatives was linked to the amino groups of branched 8-arm PEG_{10K}-$(NH_2)_8$ through a stable thioether bond using a heterobifunctional cross-linker N-maleimidobutyryloxysuccinimide ester (GMBS) (Figure 3.3). These bioconjugates were purified using size-exclusion chromatography on a Sephacryl S-100 column. The formation of each bioconjugate was confirmed by MALDI-TOF mass spectrometry and the concentration of each bioconjugates was determined by quantitative amino acid analysis. The overall design for all SQV conjugates was to link the various components using covalent bonds that varied in their stability properties (Figure 3.4). A biodegradable ester bond was made between the hydroxyl group of SQV and the carboxyl group of Cys. The esterification of the hydroxyl of SQV was confirmed by ESI-MS and ^{1}H and ^{13}C NMR. The thiol group of Cys was used to attach R.I.CK-Tat9 and its derivatives via a reducible disulfide bond, while the amino group of Cys was used to attach $PEG_{3.4k}$ via a more stable amide bond. The thiol group of the cysteine in PEGylated form of SQV-Cys-ester was activated with 2,2'-dithiodipyridine. Then, disulfide bond formation resulted from addition of R.I.CK-Tat9 to the activated PEGylated form of SQV [SQV-Cys($PEG_{3.4k}$)(TP)], giving SQV-Cys($PEG_{3.4k}$)(R.I.CK-Tat9), in 65% yield after gel permeation purification. Mass spectrometry using MALDI-TOF of these products demonstrated peaks at the expected molecular weights.

3.3.2 Stability studies

The stability of the covalent linkages attaching pharmacophores to the conjugates was determined. R.I.CK-Tat9 was linked to PEG_{10K} using a relatively stable thioether bond. The stability of this bond was assessed by incubating PEG10K-[R.I.CK(fluorescein)-Tat9]$_8$ bioconjugates in PBS (pH 7.4), spiked plasma or PBS (pH 7.4) with 5 μM reduced glutathione (GSH) at 37°C. Aliquots were withdrawn at different time points and centrifuged at 14,000 x g for 90 min with a 10 kDa cut-off Microcon™ filter. The conjugated R.I.CK(fluorescein)-Tat9 was retained in the filter as retentates and separated from the cleaved free R.I.CK(fluorescein)-Tat9 that passed through the filter. Thereafter, the fluorescence of conjugated R.I.CK(fluorescein)-Tat9 was measured using a Tecan fluorescence microplate reader with an excitation wavelength at 485 nm and an emission wavelength at 535 nm. This method was used rather than measuring fluorescence in the flow-through, since the concentration of cleaved R.I.CK(fluorescein)-Tat9 could not be quantified due a high degree of adsorption caused by its positive charges (unpublished data). The calibration curves of fluorescein-labeled R.I.CK-Tat9 in PBS (pH 7.4) and in plasma were linear with correlation coefficients of 0.9993 and 0.9997, respectively. The concentration of the bioconjugates decreased with time (Figure 3.5). Plots of ln[(bioconjugate)$_t$] against incubation time (t) were linear within the concentration range studied indicating that cleavage occurs by a first order process (Figure 3.5). The PEG_{10k}-[(R.I.CK(fluorescein)-Tat9]$_8$ bioconjugate showed a longer half-life ($t_{1/2}$ = 50.6 h) in PBS (pH 7.4) than in plasma ($t_{1/2}$ of 24.4 h). The half-life of

this bioconjugate decreased significantly from 50.6 h to 10.5 h in the presence of 5 μM GSH in PBS (pH 7.4).

SQV was linked to R.I.CK-Tat9 through a SQV-Cys ester bond. The stability of the ester was evaluated in PBS at pH 7.4 and in spiked plasma, measured at 37ºC using a recently developed fluorogenic protease assay for free SQV (*181*). The release of active SQV was observed with half-lives of 14 h and 0.9 h in PBS at pH 7.4 and in spiked plasma, respectively (*181*).

3.3.3 Anti-HIV Activity

The anti-HIV activity of each bioconjugate derived from R.I.CK-Tat9 and SQV was evaluated *in vitro* in HIV-infected MT-2 cells utilizing an established antiviral assay (*181*) (Figure 3.6, Table 3.1). The L-form of Tat9 showed weak anti-HIV activity (EC_{50} = 51.3 μM) while the retro-inverso form of Tat peptide showed much stronger anti-HIV activity (EC_{50} =0.85 μM). Biotin appended to the R.I.CK-Tat9 peptide greatly enhanced the activity of the peptide (EC_{50} = 0.018 μM), possibly due to the increased cellular uptake (~30-fold) conferred by biotin (*182*). The conjugation with a 10 kDa branched PEG might be expected to enhance the stability of the peptide by protecting it from attack by peptidases, even though the unnatural D-amino acids in the R.I. peptides may already confer ample protease-resistance. We found that R.I.CK-Tat9 is released from PEG_{10k}-$(R.I.CK\text{-}Tat9)_8$ conjugates very slowly ($t_{1/2}$=50.6 h) and that most of the fluorescence labeled PEG_{10k}-$(R.I.CK\text{-}Tat9)_8$ conjugate remained bound to the MT-2 cell surface rather than being internalized. Thus, the PEG conjugates of R.I.CK-Tat9 and R.I.CK(biotin)-Tat9 both displayed similar antiviral activity with EC_{50} of 1.47 μM and 1.5 μM,

respectively, which was weaker than that of the non-PEGylated forms (Figure 3.6 and Table 3.1). This result suggests that the intracellular inhibitory effect of Tat peptide may be quantitatively more important than the extracellular blocking of HIV infection previously described for Tat-based peptides, although targeting cell surface receptors might still be an important secondary mechanism of viral inhibition by either biotinylated or non-biotinylated peptides.

The activity of SQV in drug conjugates compared to the maximal achievable antiviral efficacy of free SQV (EC_{50} = 15 nM) was reduced with addition of $PEG_{3.4k}$ alone (EC_{50} = 900 nM), but restored with the addition of R.I.CK-Tat9 to the SQV-$PEG_{3.4k}$ conjugate (EC_{50} = 15 nM), the same *in vitro* potency as free SQV.

The cytotoxicities of the R.I.CK-Tat9 and SQV bioconjugates were measured by incubating non-infected MT-2 cells in the presence of different concentrations of the bioconjugates for 5 days at 37ºC. The cytotoxicity (LC_{50}) of all the tested bioconjugates was in the low micromolar range (12.5 – 46.8 μM). The L-form of Tat9 showed the poorest therapeutic index with essentially equivalent EC_{50} and LC_{50}. In contrast, a number of the multi-component bioconjugate molecules such as R.I.CK(biotin)-Tat9 and SQV-$PEG_{3.4k}$-R.I.CK-Tat9 exhibited very favorable therapeutic indices of 2600 and 833, respectively. The ratios of LC_{50} / EC_{50} (i.e., *in vitro* therapeutic index) are shown in Table 3.1.

3.4 Discussion:

While recent advances in anti-AIDS therapeutics have resulted in the introduction of more potent drugs, a cure for HIV infection remains an elusive goal. Many factors contribute to the inability of current therapeutic regimens to cure HIV infection.

However, central to the problem is the variability of drug concentrations in the blood and target tissues resulting from poor patient adherence to complicated regimens, the inability of these potent agents to selectively target infected tissues, and the poor penetration or retention of drugs in reservoir and sanctuary sites. It is becoming more obvious that better drug delivery and targeting technologies are required to increase total body persistence, target cell exposure and retention of these potent therapeutic agents. In the current study, we have produced and tested the first of a series of nanoscale drug delivery vehicles in order to better target HIV infected cells and possibly to provide novel modes of action.

The present report describes the design, synthesis and initial characterization of a series of PEG-based bioconjugates in order to achieve maximum therapeutic payload of Tat peptide, to explore multi-drug delivery on one bioconjugate and to determine the potential role of Tat in the cellular uptake and HIV inhibition by the conjugates. These bioconjugates were designed (i) to carry multiple copies of the R.I.CK-Tat9 drug linked by stable thioether bonds to 8-arm polyethylene glycol (PEG), (ii) to carry multiple drugs such as SQV for combination therapy, (iii) to have an extended biological and chemical half-life, (iv) to selectively release appended drug molecules inside the cell because of the differential in reducing capacity between blood and the internal cell environment and finally, (v) to enhance cellular uptake of the drug and bioconjugate through the use of uptake enhancing moieties like biotin attached to the R.I.CK-Tat9. These modifications were designed to increase the therapeutic peptide's bioavailability, biodistribution and delivery into HIV sanctuary sites of both the therapeutic Tat peptide and appended drugs, exemplified here by SQV.

The current study is aimed at improving the therapeutic potential of a Tat-antagonistic compound R.I.CK-Tat9. It is an analog of the nine amino acid sequence of the TAR-binding basic domain of Tat protein in which the direction (polarity) of the amino acid sequence is reversed and the chirality of each amino acid residue is inverted from L to D. Retro-inverso analog peptides are expected to have shapes and charge distributions of their side chains similar to the natural L-amino acid peptides, but are highly resistant to proteolysis (*183, 184*). Furthermore, Wender et. al. found that the L-, D- and R.I. forms of Tat9 showed similar cellular uptake in serum-free medium, while in the presence of serum the D-form was modestly more active and the R.I. form much more active than the L-form, indicating the likely role of proteolysis in limiting the activity of natural peptides (*185*). The current results show that R.I.CK-Tat9 had a 60-fold higher anti-HIV activity than L-Tat9, consistent with the enhanced stability and/or increased intracellular availability of R.I.CK-Tat9.

Choudhury et al. showed that Tat9-C(biotin) with S-biotinylation of the cysteine residue was taken up 30-fold more efficiently by Jurkat cells than was unbiotinylated Tat9-C (3% versus 0.1%, respectively) (*64*). This was attributed to increased hydrophobic interactions with the plasma membrane (*182*) and it was hypothesized that biotinylation would result in enhanced inhibiton of transactivating activity by the biotinylated compound. The current results confirm this hypothesis since the biotinylated RI-Tat9 was 47 times more potent than the RI-Tat9 and was approximately as potent as SQV in inhibiting HIV-1.

The central hypothesis of the current study is that improved delivery would result in an enhancement in the pharmacological properties of Tat inhibitors, in particular

R.I.CK-Tat9. Thus, it was anticipated that PEGylation of R.I.CK-Tat9 would enhance the pharmacological properties *in vivo* for more effective delivery. The PEG residues were chosen to avoid *in vivo* binding of R.I.CK-Tat9 to plasma proteins and rapid elimination from the blood (*186*). Thus, PEGylation provides a way to increase the stability and body persistence of the R.I.CK-Tat9, which could result higher *in vivo* activity. However, the PEG conjugates reduced the antiviral activity of R.I.CK-Tat9 or R.I.CK(biotin)-Tat9 in cell culture experiments (Table 3.1). The thioether bonds, used in the linkage between R.I.CK-Tat9 or R.I.CK(biotin)-Tat9 and PEG were very stable, insuring that Tat was not released from the conjugate. These results suggest the quantitatively more important antiviral effect of R.I.CK-Tat9 depends upon its release from PEG, presumably reflecting a requirement for entry into infected cells.

3.5 Conclusions:

In the current study, the preclinical *in vitro* effectiveness of a small peptidic Tat antagonist, R.I.CK-Tat9, alone or with saquinavir using PEG-based bioconjugates was demonstrated. While PEG-linkage alone did not potentiate the activity of R.I.CK-Tat9, the addition of SQV to R.I.CK-Tat9-PEG bioconjugates significantly enhanced the anti-retroviral activity to the level comparable to free SQV. These bifunctional conjugates were more potent than the PEG conjugates with R.I.CK-Tat9 or SQV alone. These results demonstrate that the macromolecular bioconjugates could deliver drugs to multiple targets, bringing drug delivery systems down to the molecular level. Since *in vitro* studies of anti-HIV activity do not account for factors that would enhance *in vivo* potency (e.g., increased body persistence and decreased binding), it is quite possible that the advantages

of SQV-$PEG_{3.4K}$R.I.CK-Tat9 conjugates over the parent drugs could become evident by *in vivo* testing. In addition, all of the bioconjugates demonstrated low cytotoxicity.

The modular approach for producing a targeted nanopharmaceutical delivery system that we have taken allows for appending different drug combinations or combinations of drugs and cellular uptake enhancing agents in order to maximize the therapeutic effect. Therefore PEG bioconjugates could constitute a powerful delivery system for either single drug administration or combination therapy. However, further mechanistic studies are needed to optimize the structure (e.g. size, shape and other features) of the PEG bioconjugates. Additional studies are needed to assess the potential *in vivo* benefits (long half-life, lower clearance rate) of these conjugates.

Table 3.1 Anti-HIV activity (EC_{50}) and cytotoxicity (LC_{50}) data of R.I.CK-Tat9 based bioconjugates in MT-2 cell culture infected with HIV-1 strain LAV-Vbu3 (MOI of 0.01)[a].

Compound	Number	EC_{50} (μM)	R[b]	LC_{50} (μM)	Therapeutic Index (LC_{50} / EC_{50})
L-Tat9	-	51.3	-	53.8	1
R.I.CK-Tat9	1	0.85	-	29.8	35
R.I.CK(biotin)-Tat9	2	0.018	0.02	46.8	2600
PEG_{10K}-(R.I.CK-Tat9)$_8$	8	1.47	1.7	29.1	20
PEG_{10K}-(R.I.CK(biotin)-Tat9)$_8$	9	1.50	1.8	29.7	20
SQV($MeSO_3H$) (control)	12	0.015	-	25	1667
SQV-Cys-$PEG_{3.4K}$	14	0.90	60	4.5	50
SQV-Cys(R.I.CK-Tat9)-$PEG_{3.4K}$	15	0.015	1	12.5	833

[a] R is the ratio of the EC_{50} of the bioconjugate to that of its parent drugs R.I.CK-Tat9 or SQV.
[b] Several assays of each compound were done with variations in the virus stock, dosage and days of incubation.

Figure 3.1. Schematic representation of Tat peptide, the basic domain in the viral Tat protein containing residue 49-57.

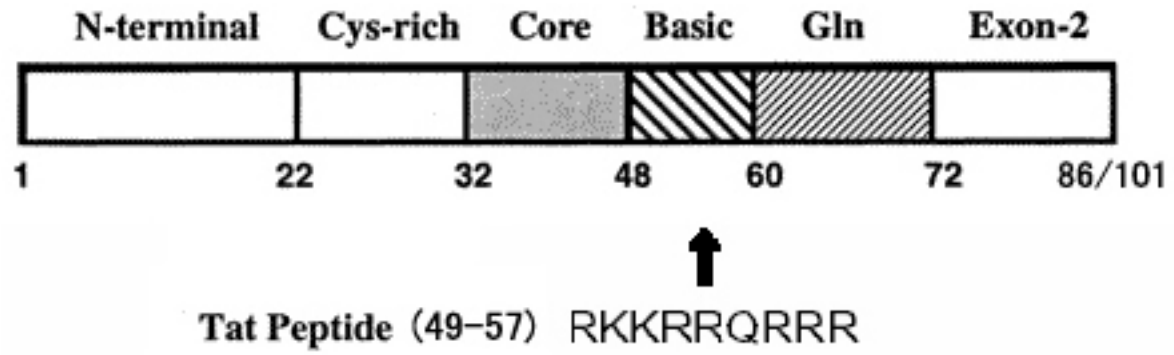

Figure 3.2 Schematic representation of R.I.CK-Tat9 and its derivatives.

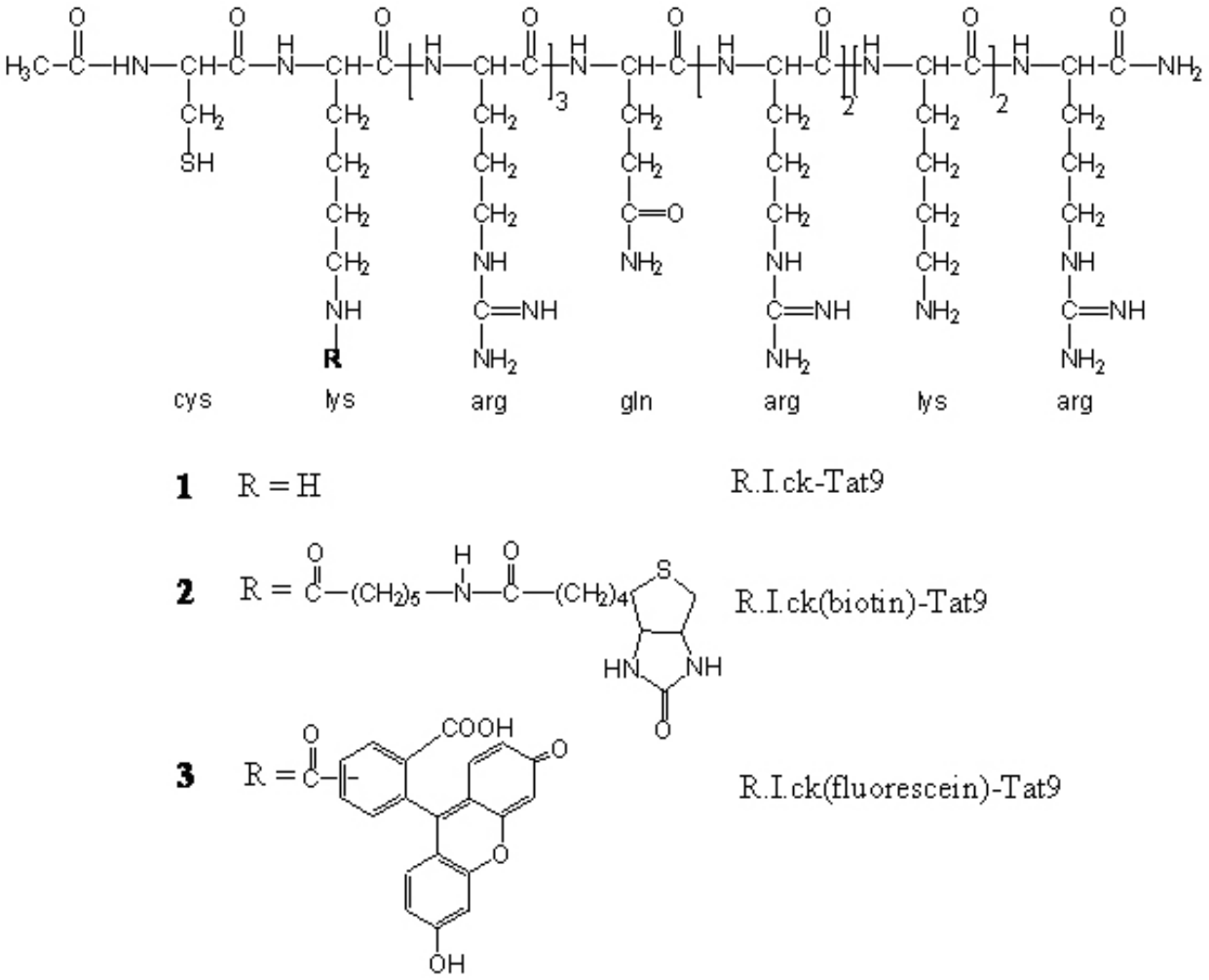

Figure 3.3 Synthetic scheme of Tat-PEG bioconjugates with 8 copies of R.I.CK-Tat9.

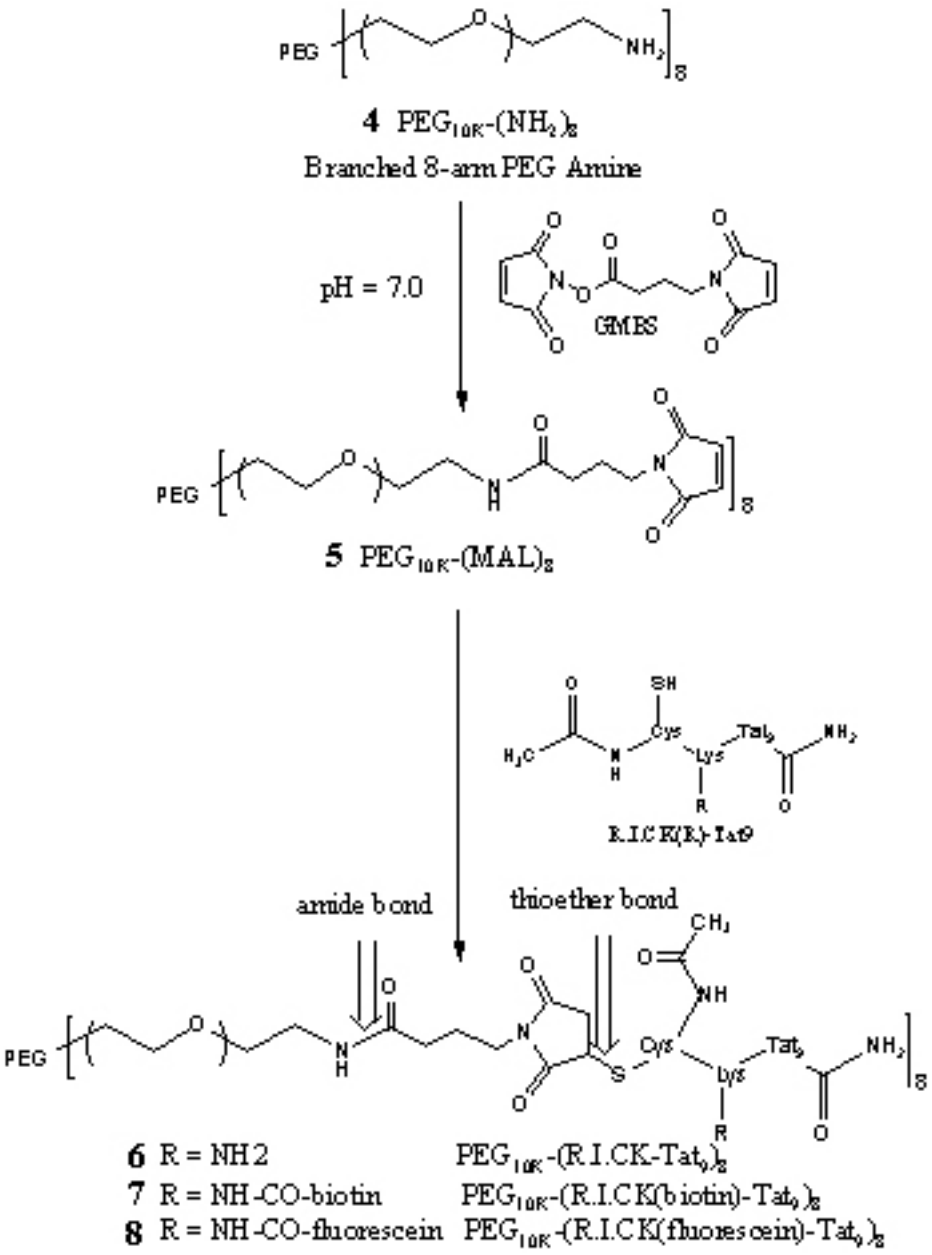

Figure 3.4 Synthetic scheme of Tat-SQV bioconjugates (i) 3 equivalents Fmoc-Cys(S-Trt)-COOH in CH_2Cl_2 with DIPC/DMAP; (ii) 20% piperidine in CH_2Cl_2 ; (iii) TFA/CH_2Cl_2 (1:1); (iv) 2 equivalents Fmoc-$PEG_{3.4K}$-NHS in CH_2Cl_2 with DIEA; (v) 2 equivalents 2,2/-Dithiodipyridine in DMSO; (vi) 2 equivalents. R.I.CK-Tat9 in DMSO.

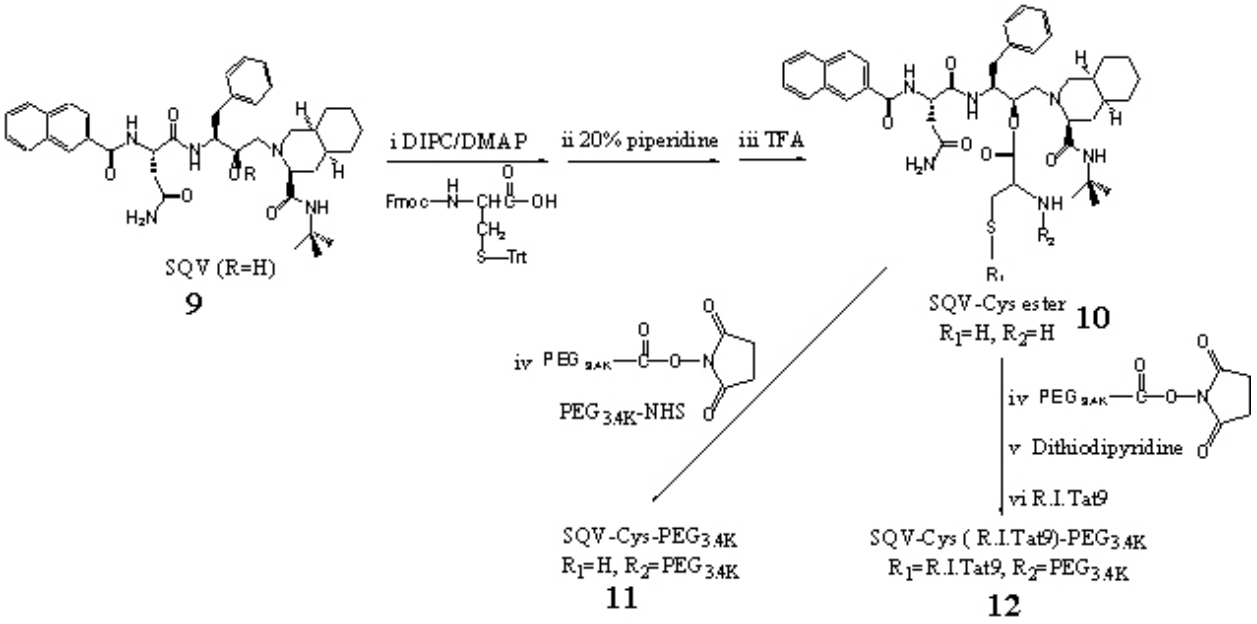

Figure 3.5 Panel A: Release of R.I.CK(fluorescein)-Tat9 from PEG_{10K}-$[(R.I.CK(fluorescein)\text{-}Tat9]_8$ in PBS (pH 7.4) (■), in plasma (▲) or PBS (pH 7.4) with 5μM GSH (▼) at 37°C respectively, using fluorescence detection at excitation wavelength 485nm and emission wavelength 535nm. The concentrations of the bioconjugates were determined from fluorescence calibration curves that were established in the same media. All measurements were done in duplicates. **Panel B:** Plot of $\ln(\text{bioconjugate})_t$ versus incubation time (t) of the PEG-$[R.I.CK(fluorescein)\text{-}Tat9]_8$ in PBS (pH 7.4) (■), in plasma (▲) or PBS (pH 7.4) with 5μM GSH (▼) at 37°C respectively. The rate constant (k) is the slope of this linear plot. The half-lives ($t_{1/2}$) for the thioether bond cleavage were calculated using the relation $t_{1/2} = 0.693/k$.

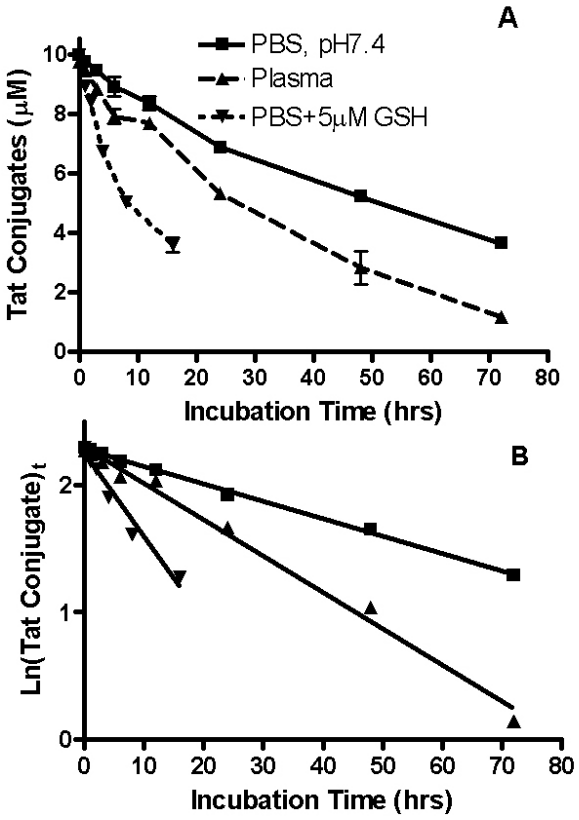

Figure 3.6 Representative data from MTT assays showing the anti-HIV activity (EC_{50}) of Tat and SQV compounds using MT-2 cells infected with HIV-1 strain Vbu 3 at 0.01 MOI. Cytotoxiciy (LC_{50}) was determined usjng uninfected cells. [TB: R.I.CK(biotin)-Tat9, TP: PEG_{10K}-(R.I.CK-Tat9)$_8$, TBP: PEG_{10K}-(R.I.CK(biotin)-Tat9)$_8$, SQV: saquinavir, SP: SQV-Cys- $PEG_{3.4K}$, SPT: SQV- $PEG_{3.4K}$-R.I.CK-Tat9]

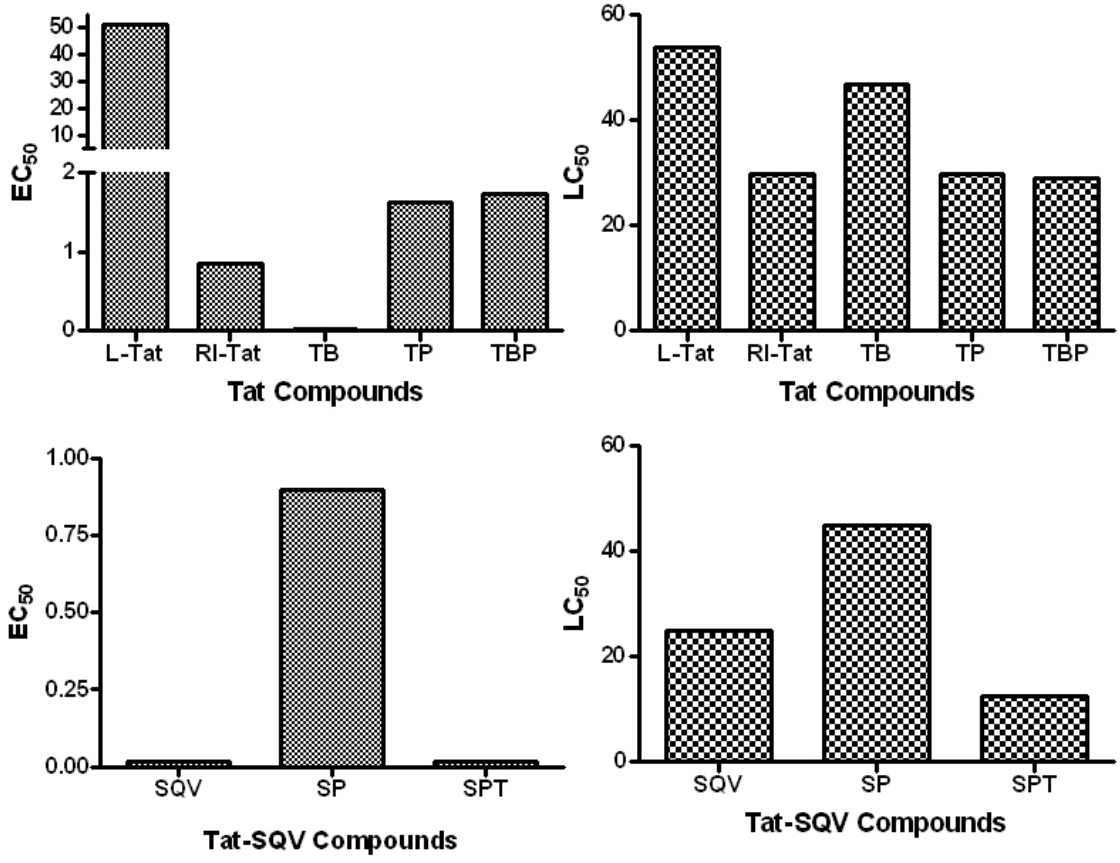

CHAPTER 4

UPTAKE MECHANISM OF MULTI-COMPONENT NANOPHARMACEUTICALS DERIVED FROM POLY (ETHYLENE GLYCOL) AND RETRO-INVERSO-TAT NONAPEPTIDE

4.1 Introduction:

The remarkable efficacy of protease and reverse transcriptase inhibitor combinations for the treatment of HIV-1 infection has been clearly established *in vitro* and in the clinic (*187*). However, due to the rapid development of viral resistance against these drugs, it has been necessary to develop new chemotherapeutic agents directed against other viral targets in order to improve current anti-HIV combination therapies. This is of special importance in view of the failure of current highly active antiretroviral therapy (HAART) regimens due to emerging of resistant HIV-1 strains. Development of inhibitors against the HIV encoded non-structural protein, Tat (trans-activator of transcription), is highly important and might even be critical in the fight against AIDS. Tat is a small (14 kDa) multifunctional viral protein essential for viral replication and the progression of AIDS. The primary role of Tat protein in the HIV life –cycle is trans-activation of the transcription from HIV long terminal repeat (LTR). Viruses with deletion of the Tat-function are non-viable (*175*). Efficient replication and gene expression of HIV-1 requires a specific interaction of the Tat viral protein with the trans-activation responsive element (TAR), a highly stable stem-loop RNA structure (*68*). The

interaction with TAR is mediated by a nine-amino acid basic domain (RKKRRQRRR, residues 49-57) of the Tat protein (Figure 3.1). This domain is essential for TAR RNA binding *in vivo* and is sufficient for TAR recognition *in vitro* (*72*). A Tat-derived basic arginine-rich peptide alone binds TAR RNA with high affinity *in vitro* (*64*). A peptidyl compound, N-acetyl- RKKRRQRRR-(biotin)-NH2, containing the 9-amino acid sequence of Tat protein basic domain, was shown to inhibit both Tat-TAR interaction *in vitro* and HIV-1 replication in cell culture (*64*). In addition to the TAR RNA interaction, the basic domain in Tat has at least three other functional properties. It constitutes a nuclear/nucleolar localization signal (*70, 71*). The basic Tat peptide is also a prototypic cell penetrating peptide that can bring a cargo molecule across the plasma membrane. This was originally discovered when it was observed that Tat protein could freely enter cells (*176*). Small Tat peptides derived from the basic domain have also been shown to inhibit HIV replication in cultured T-cells by interacting with the HIV CXCR4 co-receptor present on the surface of T cells, thereby blocking infection by T-tropic HIV-1 strains (*73-75*). These diverse functions of Tat are mainly provided by the basic domain of the protein and could be imitated by short peptides representing them. Thus, development of Tat protein inhibitor/antagonist comprises an important direction in anti-AIDS drug discovery.

Therefore, we have been investigating Tat peptides as therapeutic agents (*64, 76*). We have previously reported (*188*) a Tat-antagonistic compound, *N*-acetyl-Arg-Lys-Lys-Arg-Arg-Gln-Arg-Arg-Arg-Cys(S-biotin)-NH2 (Tat10-biotin or Tat9-C-biotin), which contains the nine amino acid sequence of the TAR-binding basic domain of Tat protein. Tat9-C-biotin avidly competes with Tat for binding to TAR and inhibits Tat-dependent

gene expression of a stably transfected chloramphenicol acetyltransferase (CAT) gene expressed from the HIV-1 long terminal repeat (LTR) in cultured Jurkat cells (*188*). This Tat antagonist also inhibits acute infection of MT2 cells by HIV-1, as assayed by syncytium induction, cytotoxicity and production of reverse transcriptase (*188*). Subsequently, Tat9-K(biotin), which resembles Tat9-C(biotin) except that the cysteine-S-biotin moiety is replaced by lysine-ε-N-biotin, was synthesized (*76*). Tat9-K(biotin) and Tat9-C(biotin) showed similar ability to compete with Tat protein binding to the TAR domain of viral RNA preventing Tat-dependent gene expression in cultured cells. In our recent report (*189*), we utilized retro-inverso (RI) peptides and macromolecular PEG conjugates to overcome many of the biopharmaceutical challenges faced by Tat peptides. R.I.CK (retro-inverso-D-cysteine-lysine)-Tat9, N-acetyl-ckrrrqrrkkr-NH_2, consists of D-amino acids assembled in the reverse order of the natural L-amino acid Tat9 peptide, N-acetyl-RKKRRQRRR-NH2. Thus, R.I.CK-Tat9 has a similar shape and charge distribution to the natural L-amino acid peptide but is more stable to proteases and retains pharmacological activity (*78*). PEGylation has been shown to be one of the most successful techniques for improving the pharmacokinetic and pharmacodynamic properties of peptide drugs by increasing stability and reducing renal clearance and protein binding (*179*). In addition, a second anti-HIV agent, saquinavir (SQV) was conjugated with R.I.CK-Tat9-PEG in order to achieve the synergistic effect of SQV on HIV protease and Tat peptides on both HIV Tat-TAR binding and/or on the cell surface receptor CXCR4.

In Chapter 3, we showed that the PEG conjugates of R.I.CK-Tat9 and R.I.CK(biotin)-Tat9 displayed similar antiviral activity with EC_{50} of 1.47 μM and 1.5

μM, respectively, which was weaker than that of the non-PEGylated forms (Figure 3.6 and Table 1). The activity of SQV in drug conjugates compared to the maximal achievable antiviral efficacy of free SQV (EC_{50} = 15 nM) was reduced with addition of $PEG_{3.4k}$ alone (EC_{50} = 900 nM), but restored with the addition of R.I.CK-Tat9 to the SQV-$PEG_{3.4k}$ conjugate (EC_{50} = 15 nM), the same *in vitro* potency as free SQV. However, the mechanism of enhancement for the SQV-$PEG_{3.4K}$-R.I.CK-Tat9 conjugates was not clearly established since, in addition to targeting intracellular TAR, Tat possesses cell penetrating properties (*190, 191*) that may promote conjugate uptake into the cell and/or may exert anti-HIV-1 activity by means of cell surface binding to CXCR-4 receptors (*73-75*). In the current study, the mechanism of enhanced activity of the SQV-$PEG_{3.4K}$-R.I.CK-Tat9 conjugates was addressed by flow cytometry and confocal microscopy using fluorescein-labeled nanopharmaceuticals. The current results suggest that the increased anti-HIV activity of SQV-$PEG_{3.4K}$-R.I.CK-Tat9 is due to both enhanced intracellular uptake and synergistic inhibitory effects of SQV on HIV protease and Tat peptides on both CXCR4 co-receptor interactions and/or HIV-1 transcriptional activation.

4.2 Material and Methods:

4.2.1 Materials

Fluorenylmethoxycarbonyl (Fmoc)-amino acid derivatives, MBHA Rink amide resin, BOP (benzotriazol-1-yl-oxytris(dimethylamino)phosphonium hexafluorophosphate) and HOBt (*N*-hydroxybenzotriazole) were purchased from

Calbiochem-Novabiochem Corp. (La Jolla, CA). mPEG-MAL (MW ~3.4 kDa), and 8-arm PEG-$(NH_2)_8$ (MW ~10 kDa) were obtained from Nektar Therapeutics (Huntsville, AL). N-maleimidobutyryloxysuccinimide ester (GMBS) was obtained from Pierce Biotechnology (Rockford, IL). NHS-carboxyfluorescein, DIEA (diisopropylethylamine), aldrithiol, piperidine, hydrazine, acetic anhydride, diethyl ether, Dde (1-(4,4-dimethyl-2,6-dioxocyclohex-1-ylidene)ethyl), EDT (ethanedithiol), TIS (triisopropyl silane), DMAP (4-(dimethylamino)pyridine), DIPC (1,3-diisopropylcarbodiimide), anhydrous dimethylformamide (DMF), and anhydrous dimethyl sulfoxide (DMSO) were obtained from Sigma-Aldrich (St.Louis, MO). Dichloromethane (DCM) obtained from Sigma was dried over calcium hydride and freshly distilled prior to use. Trifluoroacetic acid (TFA) obtained from Aldrich was distilled with H_2SO_4 before use. R.I.CK(fluorescein)-Tat9 was synthesized manually on a MBHA Rink amide resin (Novabiochem, La Jolla, CA) via Fmoc chemistry. The purity of all new compounds was checked by mass spectrometry, TLC, and/or NMR.

4.2.2 Synthesis of fluorescence labeled Tat-PEG conjugates

In the synthesis of R.I.CK-Tat9-PEG bioconjugates (**14**) (Figure 4.1), R.I.CK(fluorescein)-Tat9 was conjugated to mPEG-MAL by the reaction of the thiol group of R.I.CK(fluorescein)-Tat9 with the maleimide group on mPEG-MAL (**13**), which formed a stable thioether bond between PEG and R.I.CK(fluorescein)-Tat9. The eight amino groups of PEG_{10K}-$(NH_2)_8$ (MW 10 kDa, 8-arm branched, Nektar Therapeutics, Huntsville, AL) (**4**) were first activated with three-fold molar excess of the

heterobifunctional cross-linker, N-maleimidobutyryloxysuccinimide ester (GMBS) (Pierce Biotechnology, Rockford, IL), in DMF to form a maleimide activated PEG (**5**). The reaction was stirred overnight at room temperature. The product was precipitated with cold ether and dried under vacuum to yield the solid PEGylated product. The GMBS linker essentially converts a primary amino group to a maleimide group that can react with a thiol group to form a stable thioether bond. This activated intermediate **5** was reacted with a three-fold molar excess of R.I.CK(fluorescein)-Tat9. with coupling reagents HOBt (4-fold molar excess) and BOP (3-fold molar excess) in DMF. DIEA (diisopropylethylamine, 1 % v/v) was added to adjust to neutral pH. For control, the eight amino groups of 8-arm PEG amine were reacted with carboxyfluorescein-NHS in the presence of 1%DIEA in DMF to yield PEG_{10K}-$(fluorescein)_8$ (**15**) lacking Tat peptides. The products were recrystallized from cold ether and dried under vacuum overnight. The bioconjugates were purified using size-exclusion chromatography using a Sephacryl S-100 column (Amersham, Piscataway, NJ) in 0.1 M PBS, pH 7.4, with fluorescence detection at 535 nm (emission) and 485 nm (excitation). The formation of the bioconjugates was confirmed by MALDI-TOF mass spectrometry and the concentrations of bioconjugates were determined by amino acid analysis.

4.2.3 Confocal Microscopy

MT2 cells were treated with fluorescein-labeled R.I.CK-Tat9 or its conjugates for 24 hours. Where indicated, a fluid phase endocytosis marker, tetramethylrhodamine-Dextran/10 kDa (Invitrogen/Molecular Probe), was used at 0.25 mg/mL in co-incubation

with a fluorescein-labeled compound. All images were taken of live cells on a Leica TCS SP2 Spectral Confocal Microscope using the XYZ mode and 0.25 micrometer per section. The fluorescence wavelength windows for different dyes were well separated to ensure no breach-through from one dye to another.

4.2.4 Flow Cytometry

MT-2 cells were grown to 2 days post-confluency and aliquots of 2 x 10^6 cells were washed briefly and incubated in 96-well microplates with 1 μM PEG_{10K}, R.I.CK(fluorescein)-Tat9, $PEG_{3.4K}$-R.I.CK(fluorescein)-Tat9 and PEG_{10K}-$[R.I.CK(fluorescein)\text{-}Tat9]_8$ bioconjugate for 24 hours. Trypan blue staining was used for quenching of cell surface bound fluorochrome emission. After the 24 hours incubation with tested conjugates, the medium was immediately removed from the wells. Part of the cells were washed and resuspended in 0.02 M sodium acetate buffer (pH 5.8). The remaining cells were suspended in sodium acetate buffer containing 0.2 mg/mL trypan blue. After 20 s, the cells were washed twice and resuspended in the sodium acetate buffer. The total cell associated fluorescence was then analyzed by flow cytometry using a Coulter EPICS PROFILE equipped with a 25 mW argon laser. For each analysis, 10,000 to 20, 000 events were accumulated. The total cell associated fluorescence was the cell associated fluorescence of cells without quenching by trypan blue. The intracellular fluorescence was the cell associated fluorescence of cells quenched by trypan blue. The cell surface bound fluorescence is the difference between the total cell associated fluorescence and the intracellular fluorescence.

4.3 Results:

4.3.1 Synthesis of R.I.CK(fluorescein)-Tat9 Conjugates

A series of R.I.CK-Tat9 bioconjugates was synthesized and characterized. The peptides R.I.CK(ε-carboxyfluorescein)-Tat9 were synthesized manually on a MBHA Rink amide resin (Novabiochem, La Jolla, CA) via Fmoc chemistry, then purified and confirmed by electrospray ionization mass spectrometry (ESI-MS). In the synthesis of R.I.CK-Tat9-PEG bioconjugate (14) (Figure 4.1.A), R.I.CK(fluorescein)-Tat9 was conjugated to mPEG-MAL by the reaction of the thiol group of R.I.CK(fluorescein)-Tat9 with the maleimide group on mPEG-MAL (13), which formed a stable thioether bond between PEG and R.I.CK(fluorescein)-Tat9. For eight copies R.I.CK-Tat9 PEG bioconjugates, the thiol group of the cysteine residue at the N-terminus of R.I.CK(fluorescein)-Tat9 was linked to the amino groups of branched 8-arm PEG_{10K}-$(NH_2)_8$ through a stable thioether bond using a heterobifunctional cross-linker N-maleimidobutyryloxysuccinimide ester (GMBS) (Figure 4.1.B). For control, the eight amino groups of 8-arm PEG amine were reacted with carboxyfluorescein-NHS in the presence of 1%DIEA in DMF to yield PEG_{10K}-$(fluorescein)_8$ (15)lacking Tat peptides (Figure 4.1.B). The products were recrystallized from cold ether and dried under vacuum overnight. These bioconjugates were purified using size-exclusion chromatography on a Sephacryl S-100 column. The formation of each bioconjugate was confirmed by MALDI-TOF mass spectrometry and the concentration of each bioconjugates was determined by quantitative amino acid analysis.

4.3.2 Flow Cytometry

Flow cytometry (Figure 4.2) showed that MT2 cells incubated with fluorescein-labeled control PEG lacking Tat peptides had a low fluorescence and no cell-associated fluorescence by fluorescence microscopy (data not shown), indicating PEG did not bind or enter the cells. In contrast, cells incubated with 1 μM (concentrations of conjugates containing Tat9 are indicated in Tat9 equivalents) R.I.CK(fluorescein)-Tat9, $PEG_{3.4k}$-R.I.CK(fluorescein)-Tat9, or PEG_{10k}-$[R.I.CK(fluorescein)\text{-}Tat9]_8$ had significant amounts of total cell-associated fluorescence, with cells incubated with $PEG_{3.4k}$-R.I.CK(fluorescein)-Tat9 and PEG_{10k}-$[R.I.CK(fluorescein)\text{-}Tat9]_8$ having twice as much fluorescence as cells incubated with R.I.CK(fluorescein)-Tat9. When the cell surface-bound fluorescence was quenched with trypan blue, 93.8 % of the total cell-associated fluorescence was intracellular in cells incubated with R.I.CK(fluorescein)-Tat9, 53.6 % of total in cells incubated with $PEG_{3.4k}$-R.I.CK(fluorescein)-Tat9, and only 19 % in cells incubated with PEG_{10k}-$[(R.I.CK(fluorescein)\text{-}Tat9]_8$. Since it is known that arginine-rich peptides bind to CXCR4, this suggests that multivalent Tat9 binding to CXCR4 on the cell surface impedes conjugate internalization.

4.3.3 Confocal Microscopy

Confocal microscopy studies (Figure 4.3) showed that in cells incubated with 1 μM R.I.CK(fluorescein)-Tat9 or $PEG_{3.4k}$-R.I.CK(fluorescein)-Tat9, there was significantly higher fluorescence intracellularly than on the cell surface. On the other hand, cells

incubated with PEG_{10k}-[R.I.CK(fluorescein)-Tat9]$_8$ showed primarily cell surface bound fluorescence. Note that in Figure 4.3, only a middle section of the cells is presented for each compound. This result is consistent with the results from flow cytometry.

Since the targets of both SQV (HIV-1 protease) and one of the Tat targets (HIV-1 mRNA TAR region) are in the cytosol compartment and since flow cytometry shown in Figure 4.2 and the confocal pictures shown in Figure 4.3 can not distinguish the intracellular fluorescence from the cytosol and endosome compartments, we incubated the cells with either R.I.CK(fluorescein)-Tat9 or $PEG_{3.4k}$-R.I.CK(fluorescein)-Tat9 and a fluid phase endocytosis marker, tetramethylrhodamine-labeled dextran (10 kDa). The results (Figure 4.4) showed that at relatively high concentrations (7 μM) of R.I.CK(fluorescein)-Tat9 or $PEG_{3.4k}$-R.I.CK(fluorescein)-Tat9 (green) were mainly co-localized with the fluid phase endocytosis marker rhodamine-dextran (red) in punctate dots (orange/yellow in the merged panels, Figure 4.4D & 4.4H), suggesting a predominantly endosomal location. Only in cells incubated with R.I.CK(fluorescein)-Tat9, was there some faint green fluorescence that was not co-localized with the fluid phase endocytosis marker (arrows in Figure 4.4D), suggesting some cytosolic localization.

Overall, the confocal data are consistent with the observation from the flow cytometry results that the majority of R.I.CK-Tat9 is within cells, the majority of PEG_{10k}-(R.I.CK-Tat9)$_8$ is on the cell surface, and $PEG_{3.4k}$-R.I.CK-Tat9 is roughly equally distributed between cell surface and intracellular locales. The confocal data further suggest that after exposure to 1 μM conjugate, intracellular R.I.CK-Tat9 and $PEG_{3.4k}$-R.I.CK-Tat9 are all predominantly within endosomes. Since the cytosol accounts for the

vast majority of cellular volume, any R.I.CK-Tat9 and $PEG_{3.4k}$-R.I.CK-Tat9 molecules that escaped from endosomes, or entered the cytosol directly from outside the cell, would be diluted. As a result, the detection of cytosolic fluorescence is not suffiently sensitive and we cannot rule out the presence of a small fraction R.I.CK-Tat9 and $PEG_{3.4k}$-R.I.CK-Tat9 in the cytosol. Therefore, the potent anti-HIV-1 activity of SQV-$PEG_{3.4k}$-R.I.CK-Tat9 due to addition of the R.I.CK-Tat9 moiety could be attributable to a variety of factors including the inhibitory effect of Tat9 peptide on viral interaction with co-receptor CXCR4 and/or on HIV-1 transcriptional activation, either of which might be synergistic with SQV inhibition of HIV protease.

4.4 Discussion:

An oligocationic peptide compound (ALX40-4C), designed to mimic the basic domain of the HIV-1 Tat (*58*), was also found to interfere with viral entry through the inhibition of the chemokine receptor CXCR4 on the host cell membrane (*57*). The blocking of viral entry resulted in a more potent response than the inhibition of transactivation by that compound (*58*). To delineate whether the anti-viral mechanism of the R.I.CK-Tat9 conjugates is by inhibition of transactivation or by blocking of cell surface co-receptor, R.I.CK-Tat9 was labeled with the fluorescence tag carboxyfluorescein-NHS and conjugated to $PEG_{3.4K}$ and PEG_{10K}. Flow cytometry showed 93.8%, 53.6%, and 19.0% of total cell-associated R.I.CK(fluorescein)-Tat9, $PEG_{3.4K}$-R.I.CK(fluorescein)-Tat9, and PEG_{10K}-[R.I.CK(fluoroescein)-Tat9]$_8$, respectively, were within the cells. In contrast, the control fluorescein labeled PEG lacking the Tat peptide,

PEG_{10K}-(fluorescein)$_8$, showed little cell association by flow cytometry and no cell surface binding by fluorescence microscopy (data not shown). The confocal microscopy studies showed that cells incubated with 1 μM R.I.CK(fluorescein)-Tat9 or $PEG_{3.4K}$-R.I.CK(fluorescein)-Tat9 showed significantly higher intracellular fluorescence, while cells incubated with PEG_{10K}-[R.I.CK(fluorescein)-Tat9]$_8$ showed primarily cell surface-associated fluorescence. These results suggested that the observed anti-HIV activity of the uncleavable PEG_{10K}-(R.I.CK-Tat9)$_8$ conjugates is a result of the binding of the conjugate to the cell surface CXCR4 receptor, consistent with observations from other groups (*57, 58*). However, the reduced potency of the conjugates relative to free R.I.CK-Tat9 suggests that this peptide may have more anti-HIV-1 activity at intracellular sites than at the cell surface. These results support the model that the most potent mechanism of action of this peptide agent is inhibition of the transcriptional effects of the viral Tat protein.

Certain aspects of the performance of PEG conjugates (e.g., plasma persistence and protein binding) can only be studied *in vivo* and are not addressed in the current study. The known *in vivo* advantages of PEGylation of various pharmacophores indicates the potential that PEG-based bioconjugates could display useful therapeutic properties of increased plasma half-life (*133*), lower cytotoxicity (*192*), and reduced protein binding, which could outweigh the observed reduction in efficacy seen in this study for some PEGylated drugs. This will require further future study in *in vivo* models and is beyond the scope of the current studies.

Multiple-drug cocktail regimens have been associated with recent successes in improving the quality of life of patients with AIDS. However, delivery of drugs to the

bloodstream rather than to many of the known sites of high levels viral replication may not insure that the maximal therapeutic effect will be obtained. A potential first step in achieving this is to better control the exposure of infected cells to multiple therapeutic agents. In this proof-of-principle study, the prototypical protease inhibitor, SQV, was conjugated to $PEG_{3.4K}$ and $PEG_{3.4K}$-R.I.CK-Tat9. The conjugation of PEG to SQV yielded a much less active prodrug conjugate SQV-Cys- $PEG_{3.4K}$ with EC_{50} at 900 nM. The 60-fold lower activity of the conjugate compared to the parent drug could be due to the slow cleavage of the ester bond and/or low cell uptake of the conjugate. However, the addition of Tat to SQV-Cys- $PEG_{3.4K}$ resulted in a conjugate with an EC_{50} of 15 nM, the same *in vitro* potency as the free SQV. The increased activity of SQV-$PEG_{3.4K}$-R.I.CK-Tat9 relative to $PEG_{3.4K}$-R.I.CK-Tat9 may be attributable to a variety of factors including the enhanced intracellular uptake by the bifunctional conjugates containing both Tat peptide and SQV, or the synergistic effects of SQV on HIV protease and Tat peptides on both HIV Tat-TAR binding and/or on cell surface receptor CXCR4. All these results suggest that higher anti-HIV activity was mainly due to the enhanced intracellular uptake of SQV-$PEG_{3.4K}$-R.I.CK-Tat9 resulting in improved delivery of SQV. However, the synergistic effects of SQV on HIV protease and Tat peptides on both HIV TAR and/or CXCR4 may also contribute to the enhancement. In addition, with the known *in vivo* advantages of PEG conjugates, the conjugates may be even much more potent in patients. Thus the *in vivo* activity and biopharmaceutical properties will have to be further studied in an *in vivo* model.

4.5 Conclusions:

In the current study, the preclinical *in vitro* effectiveness of a small peptidic Tat antagonist, R.I.CK-Tat9, alone or with saquinavir in PEG-based bioconjugates was demonstrated. While PEG-linkage alone did not potentiate the activity of R.I.CK-Tat9, the addition of SQV to R.I.CK-Tat9-PEG bioconjugates significantly enhanced the anti-retroviral activity to the level comparable to free SQV. These bifunctional conjugates were more potent than the PEG conjugates with R.I.CK-Tat9 or SQV alone. These results demonstrate that the macromolecular bioconjugates could deliver drugs to multiple cellular targets. Since *in vitro* studies of anti-HIV activity do not account for factors that would enhance *in vivo* potency (e.g., increased body persistence and decreased binding to nontarget tissues), it is likely that the advantages of SQV-$PEG_{3.4K}$R.I.CK-Tat9 conjugates over the parent drugs could become evident by *in vivo* testing. In addition, all of the bioconjugates demonstrated low cytotoxicity.

The modular approach we have taken for producing a targeted nanopharmaceutical delivery system allows for appending different drug combinations or combinations of drugs and cellular uptake enhancing agents in order to maximize the therapeutic effect. Therefore, PEG bioconjugates could constitute a powerful delivery system for either single drug administration or combination therapy. However, further mechanistic studies are needed to optimize the structure (e.g. size, shape and other features) of the PEG nanocarriers. Additional studies are needed to assess the potential *in vivo* benefits (long half-life, lower clearance rate) of these conjugates.

Figure 4.1 Synthetic scheme of Tat-PEG bioconjugates with single (3A) or multiple copies (3B) of R.I.CK-Tat9 and fluorescein-labeled control PEG lacking Tat peptides.

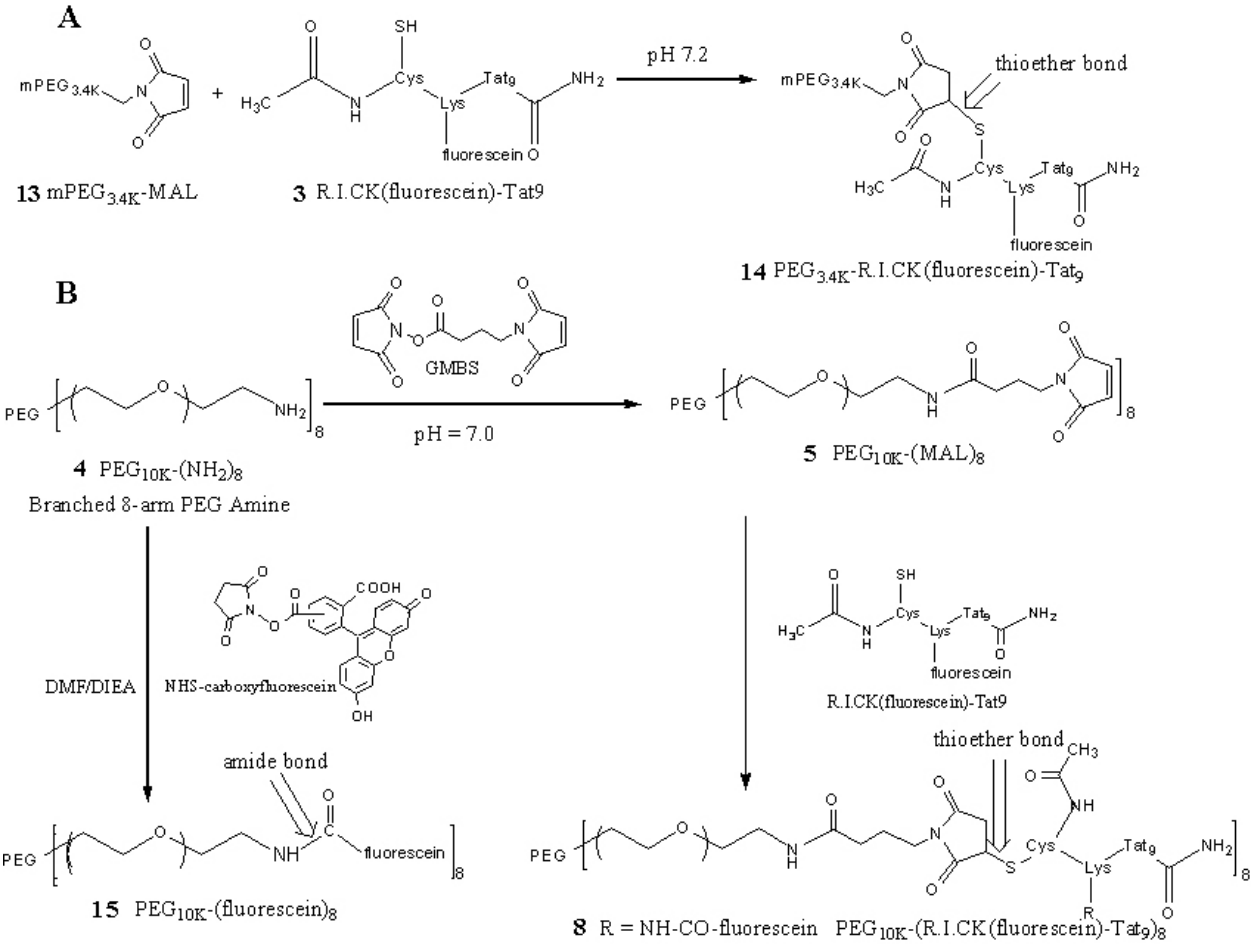

Figure 4.2 Quantitative data from flow cytometry showing the intracellular fluorescence and cell surface bound fluorescence of fluorescein-labeled PEG_{10K} [PEG-$(fluo)_8$], R.I.CK-Tat9 (R.I. Tat9), $PEG_{3.4K}$-R.I.CK-Tat9 (PEG-Tat), and PEG_{10K}-(R.I.CK-Tat9)$_8$ [PEG-(Tat)8] after 24 hrs incubation with MT-2 cells at 37ºC for 24 hrs. The total cell associated fluorescence was quantified by flow cytometry. The intracellular fluorescence was measured after the cell surface-bound fluorescence was quenched by 0.2mg/mL trypan blue at pH 5.8. The cell surface bound fluorescence is the difference between the total cell associated fluorescence and the intracellular fluorescence.

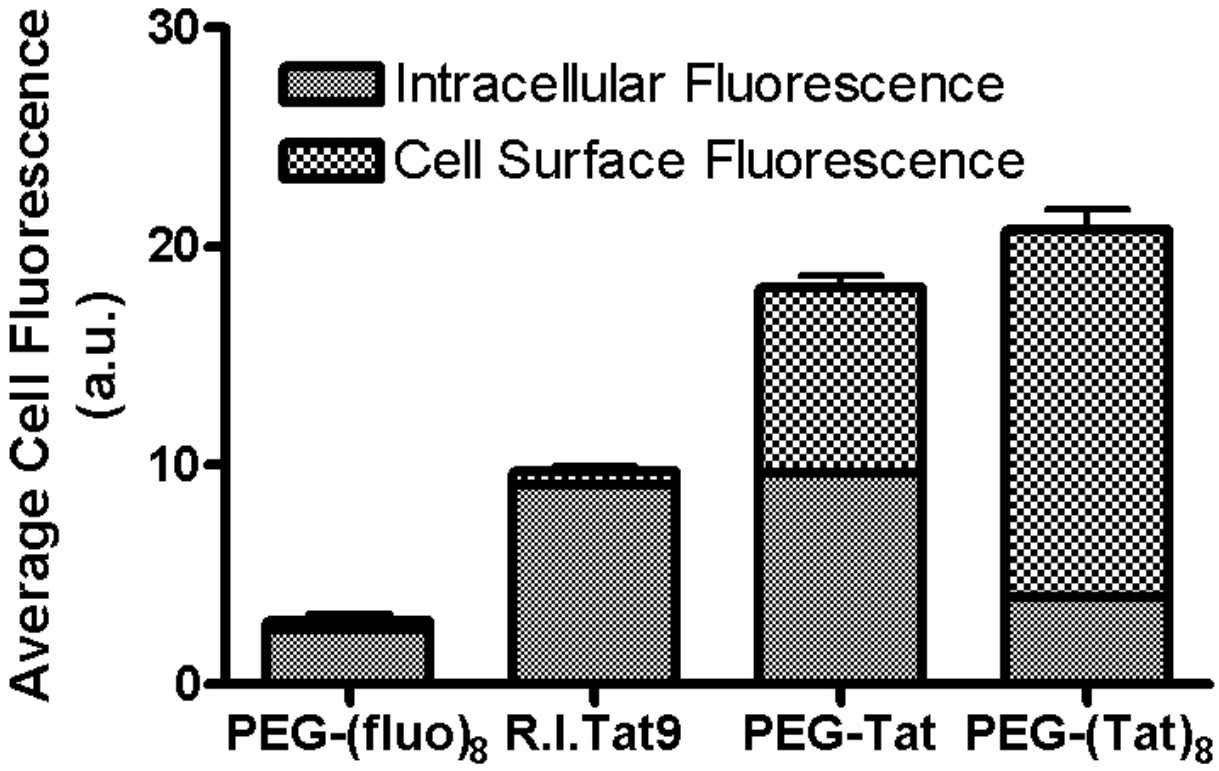

Figure 4.3 Fluorescence microscopic images of suspended MT-2 cells incubated with R.I.CK(fluorescein)-Tat9 (A, B), $PEG_{3.4K}$-R.I.CK(fluorescein)-Tat9 (C, D) and PEG_{10K}-$[R.I.CK(fluorescein)\text{-}Tat9]_8$ (E, F) for 24 hours (all 1μM relative to Tat9). (A, C and E show fluorescence images while B, D and F are light images generated by differential interference contrast (DIC) of the same fields. All focal planes are through the middle of the cells. A and C show bright intracellular fluorescence, while E shows primarily cell surface bound fluorescence.

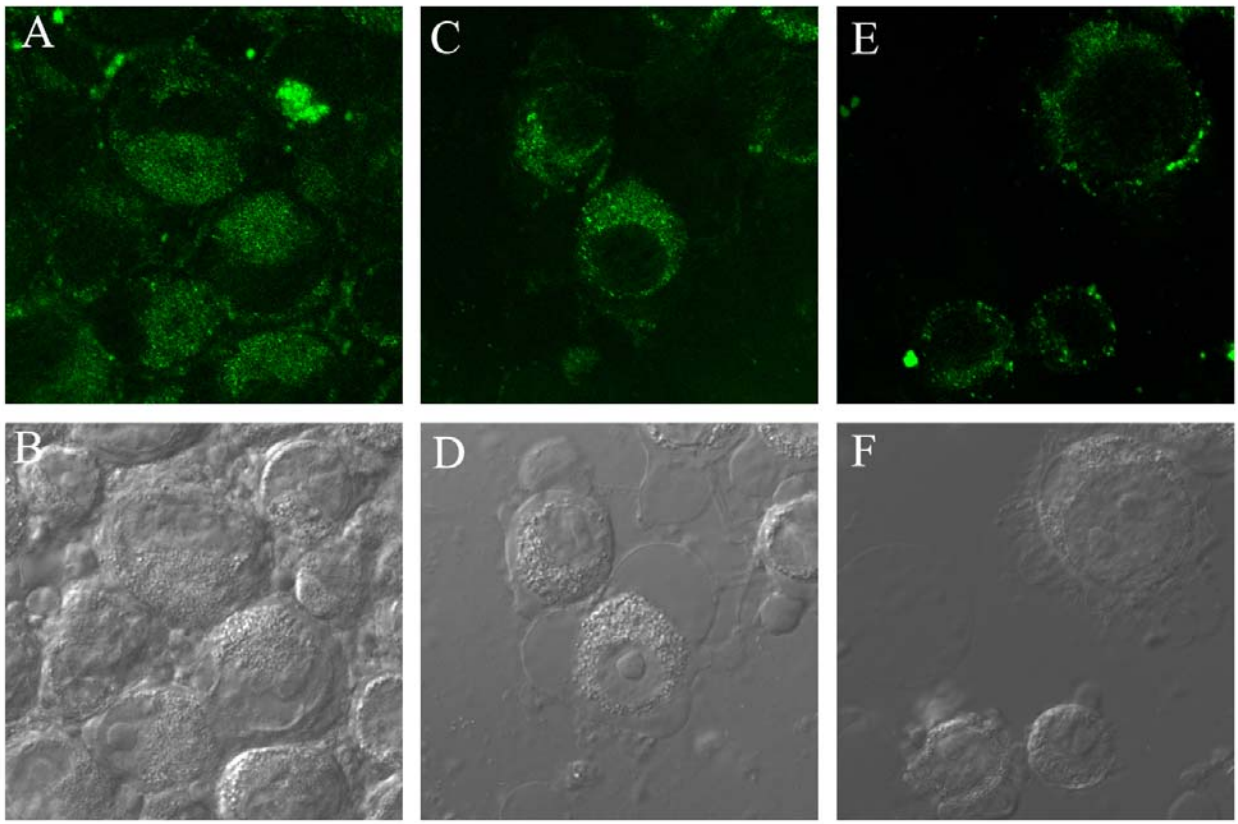

Figure 4.4 Confocal microscopic images of suspended MT2 cells incubated with R.I.CK(fluorescein)-Tat9 (A-D) or $PEG_{3.4K}$-R.I.CK(fluorescein)-Tat9 (E-H) in the presence of endocytosis marker rhodamine-dextran at 37ºC for 24 hours. A and E show fluorescein fluorescence (green), B and F are DIC images, C and G show rhodamine-dextran (red), and D and H show overlaying of the green and red images. Colocalization of two dyes (orange-yellowin the overlay images) implies endosomal uptake of $PEG_{3.4K}$-R.I.CK-Tat9. Cells incubated with R.I.CK(fluorescein)-Tat9 showed some faint green fluorescence that was not co-localized with the fluid phase endocytosis marker (arrows in Figure 4.4D), suggesting some cytosolic localization.

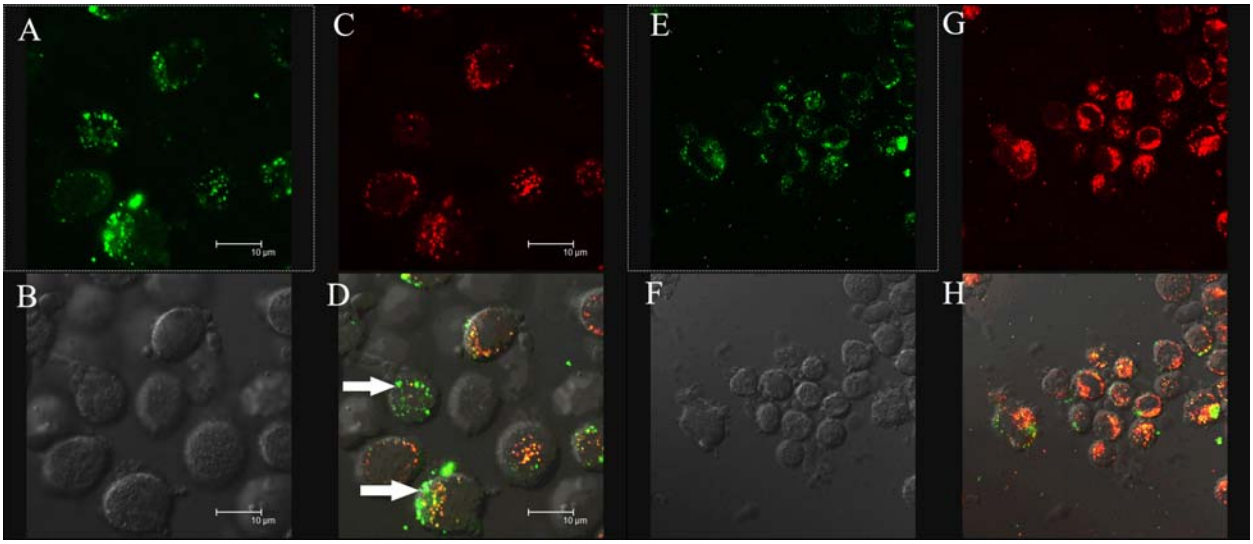

CHAPTER 5

DESIGN, SYNTHESIS AND EVALUATION OF MULTI-VALENT MACROPHAGE-TARGETED PEG-fMLF NANOCARRIERS I: OPTIMIZING SIZE AND COPY NUMBER FOR PEG-fMLF (N-FORMYL-METHIONYL-LEUCYL-PHENYLALANINE) NANOCARRIER UPTAKE BY MACROPHAGES

5.1 Introduction:

Infection by human immunodeficiency virus type 1 (HIV-1) is the cause of acquired immunodeficiency syndrome (AIDS). AIDS is characterized by the severe impairment of the immune system functions resulting in a profound decrease in the number of CD4+ T cells. The advent of highly active antiretroviral therapy (HAART), a multiple drug treatment regimen, has led to a dramatic decrease in both the morbidity and mortality of HIV patients (*3*). Despite this success, curing HIV infection has remained an elusive goal due to many challenges including low and fluctuating drug concentrations due to poor drug absorption or patient non-adherence (*4*), the presence of viral reservoirs and sanctuary sites (*5*), and drug toxicity during chronic therapy (*193*).

Macrophages are infected early during HIV infection and play an important role throughout the course of infection (*32*). Viral strains that establish infection in the new host are macrophage-tropic in over 95% of early asymptomatic individuals (*32, 194*). HIV enters macrophages via the interaction with surface receptor CD4 (cluster

designation 4) and coreceptor CCR5 (chemokine C-C motif receptor 5). Individuals bearing a homozygous deletion of the CCR5 molecule (CCR5Δ32) are highly resistant to HIV-1 infection despite multiple sexual exposures (*195, 196*). HIV-1 infection of macrophages is productive but noncytopathic, permitting macrophages to serve as long-lived sources of HIV production and to play the role of a Trojan horse by spreading infection in tissues. Infected macrophages are found in all tissues including the brain, gut, liver, lungs, lymphoid tissues and spleen. More significantly they represent major viral reservoirs and are responsible for the relapse of infection and development of resistance on discontinuation of treatment. Taken together, macrophages represent a key target and an important HIV cellular reservoir for therapeutic approaches aimed at decreasing replication of residual virus that survives HAART (*33*).

Among the major causes of HIV treatment failure, insufficient drug exposure due to poor penetration into viral reservoirs is one of the areas where little progress has been made and efforts are generally lacking. Macrophage–specific drug delivery could significantly improve current anti-HIV therapy by improving therapeutic efficacy, minimizing systemic toxicity and simplifying administration regimens. Targeting could possibly be achieved by covalently attaching a drug to a macrophage-specific ligand via a polymeric nanocarrier. A number of natural ligands for macrophage targeting have been explored. An example of such a ligand is IgG-derived immunomodulating peptide tuftsin (Thr-Lys-Pro-Arg), which was conjugated to the HIV reverse transcriptase inhibitor 3'-azido-3'-deoxythymidine (AZT) (*128*). The AZT-tuftsin chimera possessed characteristics of both components, including inhibition of reverse transcriptase and HIV-antigen expression, stimulation of IL-1 release from mouse macrophages, and

augmentation of the immunogenic function of the cell. Similarly, acetylated low density lipoprotein (AcLDL), a ligand for macrophage scavenger receptors, was conjugated to AZT (*129*). A 10-fold increase in the uptake of AcLDL-AZT was observed as compared to AZT in murine (J774) and human (U937) macrophage cell lines.

N-formyl peptides are cleavage products of bacterial and mitochondrial proteins, and serve as potent chemoattractants for mammalian phagocytic leukocytes. The synthetic peptide N-formyl-methionyl-leucyl-phenylalanine (fMLF) is the first identified and most potent chemoattractant for human macrophages (*197*). fMLF binds to the formyl peptide receptor (FPR) with high affinity (10-30 nM) and to its variant FPRL1 with low affinity (*197*). When the free fMLF chemotactic peptide binds to a phagocytic cell, rapid receptor-mediated internalization takes place (*198*). After binding to the receptors, fMLF activates phagocytic leukocytes through a G protein-mediated signaling cascade resulting in increased cell migration, calcium mobilization and the heterologous down-regulation of the expression and function of chemokine receptors, notably CCR5 and CXCR4, two crucial fusion co-receptors for HIV-1 (*197*). fMLF has been used for imaging of infection and inflammation (*199*).

Previous work by Pooyan et al. showed that increasing the number of fMLF residues (up to eight) attached to a single PEG polymer results in enhanced avidity (K_d = 0.18 nM) for neutrophil-like differentiated HL-60 cells relative to free fMLF (K_d = 28 nM) (*200*). A PEG polymer bearing four fMLF and four digoxigenin residues showed specific enhancement in binding to differentiated HL-60 cells and mouse peritoneal macrophages *in situ* relative to a polymer lacking fMLF. Furthermore, increasing copy numbers of fMLF increased avidity more potently than it increased cell activation,

suggesting that toxicity due to excessive phagocyte activation might not be a problem. These results suggest that biopolymer based conjugates bearing multiple fMLF residues can be used as an effective drug targeted delivery system for delivery to phagocytic cells. To successfully develop a nanocarrier delivery system, in general, requires understanding (1) the relationship between cell uptake and the copy number, size and shape of the constituent PEG chains, (2) the avidity and specificity of the interactions between the ligands appended to the nanocarriers and the cognate receptors on the target cell and (3) the chemical reactions required for synthesis of such macromolecules, including stability of the conjugates prior to administration and disassembly and release of the active drug after reaching the target site.

In the present study, a series of PEG nanocarriers with different numbers of fMLF and various PEG sizes and shapes were designed, synthesized and evaluated *in vitro* for targeting to human U937 cells induced to differentiate into a macrophage phenotype. The relationship between the molecular features of PEG-fMLF nanocarriers (i.e., number of targeting peptide and PEG sizes) and cell uptake was elucidated. The current studies demonstrated the feasibility of using macrophage-targeted nanocarriers for enhancing drug uptake in macrophages *in vitro*.

5.2 Materials And Methods

5.3.1 Materials

N-formyl-Met-Leu-Phe-Lys-Cys-amide and the backbone peptides acetyl-Cys(thiopyridine)-(β-Ala- β-Ala-Lys)$_n$-amide (n=2, 4) were synthesized via Fmoc

Chemistry by the W.M. Keck Facility (New Haven, CT). N-hydroxysuccinimide (NHS)-PEG-vinyl sulfone (VS) [NHS-PEG-VS] (MW ~5 kDa), mPEG-MAL (MW ~5.5 kDa), mPEG-$(MAL)_2$ (MW ~5.5 kDa, 20 kDa, 40 kDa), mPEG-NH_2 (MW ~5 kDa) and 4-arm PEG-$(NH_2)_4$ (MW ~10 kDa) were obtained from Nektar Therapeutics (Huntsville, AL). N-maleimidobutyryloxysuccinimide ester (GMBS) was obtained from Pierce Biotechnology (Rockford, IL). NHS-carboxyfluorescein was obtained from Sigma-Aldrich (St. Louis, MO). Fluo-4 AM (acetoxymethyl ester) was obtained from Molecular Probes (Eugene, OR). DMF **(**dimethylformamide), DIEA (diisopropylethylamine), acetonitrile (ACN), trifluoroacetic acid (TFA), ether and other chemical reagents were purchased from Sigma-Aldrich (St. Louis, MO).

5.3.2 Synthesis and Characterization of PEG-fMLF Nanocarriers

PEG_{5k}-fMLF (fMLFK(FLUORESCEIN)C-$mPEG_{5K}$): $mPEG_{5K}$-maleimide (11.2 mg, 2 mmol) was dissolved in 1 mL phosphate-buffered saline (PBS, pH=7.4) at room temperature. To this were added 3 equivalents of fMLFKC (4 mg, 6 mmol). The reaction was stirred overnight at room temperature. Excess solvent was removed under reduced pressure. The solid PEGylated product was further reacted with 3 equivalents of NHS-carboxyfluorescein (3 mg, 6 mmol) and 1% DIEA (5 μL) in 500 μL DMF. The reaction was stirred for 3 hrs at room temperature. The final product was recrystallized from cold ether, washed three times to remove impurities and dried under vacuum. Then the dried product was dissolved in ~5 mL ddH_2O and was subjected to dialysis against ddH_2O for two days in the dark. The solution was dried under vacuum to yield the purified product.

$PEG_{5K,\ 20K,\ 40K}$ -$(fMLF)_2$ ($[fMLFK(FLUORESCEIN)C]_2$-$mPEG_{5K,\ 20K,\ 40K}$): $mPEG_{5K}$-$(maleimide)_2$ (11.4 mg, 2 mmol) was dissolved in 1 mL phosphate-buffered saline (PBS, pH=7.4) at room temperature. To this were added 3 equivalents of fMLFKC (8 mg, 12 mmol). The reaction was stirred overnight at room temperature. The excess solvent was removed under reduced pressure. The solid PEGylated product was further reacted with 3 equivalents of NHS-carboxyfluorescein (6 mg, 12 mmol) and 1% DIEA (5 µL) in 500 µL DMF. The reaction was stirred for 3 hrs at room temperature. The final product was recrystallized from cold ether, washed three times to remove impurities and dried under vacuum. Then the dried product was dissolved in ~5 mL ddH_2O and was subject to dialysis against ddH_2O for two days in the dark. The solution was dried under vacuum to give the powder of purified product. $[fMLFK(fluorescein)C]_2$-$mPEG_{20K,\ 40K}$ were synthesized using a similar approach (Scheme 5.1).

PEG_{10k}-$(fMLF)_4$ $[fMLFK(FLUORESCEIN)C]_4$-PEG_{10K}: PEG_{10K}-$(NH_2)_4$ (20 mg, 2 mmol) was first activated with three-fold molar excess of the heterobifunctional cross-linker GMBS in DMF to form a maleimide activated PEG. The reaction was stirred overnight at room temperature. The product was precipitated with cold ether and dried under vacuum to yield the solid PEGylated product. The GMBS linker essentially converts a primary amino group to a maleimide group that can react with a thiol group to form a stable thioether bond. This activated intermediate was reacted with 3 equivalents of fMLFKC (16 mg, 24 mmol) in 1 mL phosphate-buffered saline (PBS, pH=7.4) at room temperature. The reaction was stirred overnight at room temperature. The excess solvent

was removed under reduced pressure. The reaction product was further reacted with 3 equivalents of NHS-carboxyfluorescein (12 mg, 24 mmol) and 1% DIEA (5 μL) in 500 μL DMF. The reaction was stirred for 3 hrs at room temperature. The final product was recrystallized from cold ether, washed three times to remove impurities and dried under vacuum. Then the dried product was dissolved in ~5 mL ddH_2O and was subject to dialysis against ddH_2O for two days in the dark. The solution was dried under vacuum to yield the purified product.

PEG_{5k} ($mPEG_{5K}$-FLUORESCEIN): The amino groups of $mPEG_{5k}$-NH_2 (5 mg, 1 mmol) were reacted with 3 equivalents of NHS-carboxyfluorescein (1.5 mg, 3 mmol) and 1% DIEA (5 μL) in 500 μL DMF to yield $mPEG_{5k}$-fluorescein. The reaction was stirred for 3 hrs at room temperature. The final product was recrystallized from cold ether, washed three times to remove impurities and dried under vacuum. Then the dried product was dissolved in ~5 mL ddH_2O and was subject to dialysis against ddH_2O for two days in the dark. The solution was dried under vacuum to give the purified product.

PEPTIDE-BACKBONE PEG-fMLF NANOCARRIERS: To achieve a branch shape and multiple coupling sites, peptide-backbone PEG nanocarriers were designed and synthesized (Scheme 5.2). In order to synthesize fMLF PEG nanocarriers with two copies of fMLF (Scheme 5.2), the backbone peptide acetyl-Cys(thiopyridine)-β-Ala-β-Ala-Lys-β-Ala-β-Ala-Lys-amide (1.4 mg, 2 mmol) was reacted with 2 equivalents of NHS-PEG_{5k}-VS (40 mg, 8 mmol) and 1% DIEA (5 μL) in 500 μL DMF. The reaction was carried out at room temperature for 3 hours. The PEGylated intermediate acetyl-Cys(thiopyridine)-

[β-Ala-β-Ala-Lys(PEG_{5k}-VS)]$_2$-Amide was purified by size exclusion chromatography on a TSK Gel-3000pw column. The structure of the product in elution fractions was confirmed by MALDI-TOF mass spectrometry, and peak fractions were pooled and dried under vacuum. The PEGylated intermediate was dissolved in 1 mL phosphate-buffered saline (PBS, pH=7.4) at room temperature. To this was added 3 equivalents of fMLFKC (8 mg, 12 mmol). The reaction was stirred overnight at room temperature. The product was then treated with 5 molar excess of dithiothreitol (DTT) for another 2 hours. The product was dialyzed against ddH_2O for two days. Then, the excess solvent was removed under reduced pressure. The solid PEGylated product was further reacted with 3 equivalents of NHS-carboxyfluorescein (6 mg, 12 mmol) and 1% DIEA (5 μL) in 500 μL DMF. The reaction was stirred for 3 hrs at room temperature. The final product was recrystallized from cold ether, washed three times to remove impurities and dried under vacuum. Then the dried product was dissolved in ~5 mL ddH_2O and was subject to dialysis against ddH_2O for two days in the dark. The solution was dried under vacuum to give the purified product. The PEG nanocarrier with four copies of fMLF and fluorescein was synthesized by a similar scheme (Scheme 5.2).

5.3.3 Size Exclusion Chromatography (SEC)

Purified nanocarriers were dissolved in ddH_2O at a final concentration of ~1 mg/mL. The solution was loaded into a Waters HPLC equipped with a SEC TSK-GEL G3000PW HPLC column (Tosoh Corp., Japan). The mobile phase was 100% ddH_2O and the flow rate was 1 mL/min. Eluents were monitored for absorbance at 220 nm with a Waters UV detector.

5.3.4 MALDI-TOF Mass Spectrometry

Mass spectrometry was performed using an Applied Biosystems Voyager DE Pro matrix assisted laser desorption time of flight mass spectrometer (MALDI-TOF). The instrument was operated in the linear positive ion mode at 25.0 kV utilizing delayed extraction (100 nanoseconds). Data were collected over a mass range of 2000-10000 M/z with 100 shots per spectrum. Samples were dissolved in 50:50 H_2O:ACN with 0.1% TFA at ~10 mg/mL. The matrix solution was (10 mg/mL) α-cyano-4-hydrocinnamic acid (10 mg/mL) in 50:50 H_2O:ACN with 0.1% TFA. A sample (4 μL) was combined with 1 μL of matrix solution. This mixture was then spotted onto the sample plate and allowed to dry. The instrument was externally calibrated by analysis of a three-component peptide mixture over a mass range of ~1000-10000 M/z. Data analysis consisted of baseline correction and noise reduction utilizing Data Explorer software version 5.1 (Applied Biosystems). The difference in the molecular weights of final nanocarrier and unreacted PEG corresponds with the molecular weight additions on the PEG skeleton (Figure 5.1).

5.3.5 Amino Acid Analysis

Amino acid analysis of the free fMLF, PEG_{5k}-fMLF, PEG_{5K}-$(fMLF)_2$, PEG_{10k}-$(fMLF)_4$ and peptide based PEG_{10k}-$(fMLF)_2$, PEG_{20k}-$(fMLF)_4$ nanocarriers was performed at the Protein Facility of the Iowa State University Office of Biotechnology (Ames, Iowa) to confirm the presence and concentration of fMLF on PEG nanocarriers. The sample was transferred to a hydrolysis tube and dried under vacuum. The tube is placed in a vial containing 6 N HCl and a small amount of phenol and the samples were

hydrolyzed by the HCl vapors under vacuum for 65 minutes at 150°C. Following hydrolysis, the sample was dissolved in distilled water containing EDTA. An aliquot containing approximately 1 nmole of each amino acid was placed on a sample slide and derivatization was done under basic conditions for 30 minutes with phenylisothocyanate (PITC). The resulting phenylthiocarbamyl (PTC) derivatives were separated by reverse phase chromatography and quantitated by absorbance at 254 nm.

5.3.6 Stability in PBS And Rabbit Plasma

The stability of the fluorescein labeled PEG-fMLF nanocarriers was tested in 10 mM PBS (pH 7.4) and rabbit plasma at 37 °C for 24 hours. The nanocarrier solutions were incubated separately in 10 mM PBS (pH 7.4) or in spiked rabbit plasma at 37°C. Aliquots were withdrawn at different time points and centrifuged at 14,000 x*g* for 90 min with a Microcon™ filter (molecular weight cut-off = 3,000 Da) (Amicon Inc., Beverly, MA). The free fMLF cleaved from the PEG nanocarrier during the incubation passes through the filter whereas the fMLF that remains linked is retained. The eluents and retentates resulting from the different incubation time points were withdrawn and subjected to fluorescence detection. Each measurement was done in triplicate.

5.3.7 Cell Lines

The U937 cell line was used, which was isolated from a patient suffering histiocytic lymphoma and later found capable of terminal differentiation upon induction into a macrophage phenotype. U937 cells were grown in RPMI 1640 DM medium supplemented with 10% FBS (fetal bovine serum). They differentiated into macrophage-

like cells after treatment with 1 mM dibutyryl-cAMP for 48 hrs. The U937 cell line is potentially an excellent model system to study formyl peptide receptors because, in the undifferentiated state, these cells do not express formyl peptide receptors and showed no movement toward any stimuli (*201, 202*). A variety of differentiating agents induce U937 cells toward a more mature phenotype in which they express formyl peptide receptors and display migratory properties similar to peripheral blood monocytes or neutrophils.

5.3.8 Expression of Formyl Peptide Receptors

Total RNA was extracted from U937 and differentiated U937 cells. RNA (2 μg) was used as template for RT-PCR. The sense oligonucleotide primer 5′-CTGCTGGTGCTGCTGGCAAG-3′ and antisense primer 5′-AATATCCCTGACCCCATCCTCA-3′ based on the sequences flanking the human FPRL1 coding region (1.1 kb) were designed to amplify FPRL1. The sense primer 5′-CTCCAGTTGGACTAGCCACA-3′ (nucleotide 1639–1658 in the exon 2) and antisense primer 5′-CCATCACCCAGGGCCCAATG -3′ (nucleotide 5341–5359 in the coding region of exon 3) were designed to amplify human FPR. The sense primer 5'-GCTCG TCGTC GACAA CGGCT C-3' and the antisense primer 5'-CAAAC ATGAT CTGGG TCATC TTCTC-3' for beta-actin were used as controls. RT-PCR was performed using the MJ Research PTC200 PCR system (Watertown, MA).

5.3.9 Time-Dependent Uptake of PEG-fMLF Nanocarriers in Differentiated U937 Cells

U937 cells were differentiated into macrophage-like cells after treatment with 1 mM dibutyryl-cAMP for 48 hrs. The cells were seeded on 24-well polycarbonate plates at the density of 1×10^5 cells/mL. The cells were washed twice with uptake buffer (Hanks Balanced Salt Solutions (HBSS) with 20 mM HEPES to adjust pH to neutral). Subsequently the cells were incubated with fluorescein-labeled PEG-fMLF nanocarriers for 1, 2, 4 or 8 hrs at either 37 °C. At the end of incubation period the cells were washed twice with ice-cold uptake buffer to stop uptake. The cells were subsequently resuspended in uptake buffer. The total cell-associated fluorescence was then analyzed by flow cytometry using a Coulter EPICS PROFILE (Fullerton, CA) equipped with a 25 mW argon laser. For each analysis, 10,000 to 20,000 events were accumulated.

5.3.10 Temperature-Dependent Uptake of PEG-fMLF Nanocarriers by Differentiated U937 Cells

Differentiated U937 cells were incubated with fluorescein-labeled PEG-fMLF nanocarriers for 4 hrs at 37 °C and/or 4°C. At the end of incubation period the cells were washed twice with ice-cold uptake buffer to stop uptake. The cells were subsequently resuspended in uptake buffer. The total cell-associated fluorescence was then analyzed by flow cytometry as described above.

5.3.11 U937 Cell Uptake Studies

To study the specificity of the interaction between the PEG-fMLF nanocarriers and the formyl peptide receptors, uptake inhibition studies were carried out in undifferentiated U937 cells. These cells are known to express only low levels of FRPL1

and no FPR. U937 cells were seeded on 24-well polycarbonate plates at the density of 1×10^5 cells/ml. The uptake experiments were performed according to the procedure described above at 37 °C for 4 hrs.

5.3.12 Uptake Inhibition Studies by Free fMLF Peptide

The involvement of formyl peptide receptors in differentiated U937 cell uptake of PEG-fMLF nanocarriers was also investigated using inhibition studies. Free fMLF peptide (5 μM), a competitive substrate of formyl peptide receptor, was co-incubated with 50 nM fluorescein-labeled PEG, mPEG-fMLF, mPEG-$(fMLF)_2$ or PEG-$(fMLF)_4$ nanocarriers. Uptake assays were performed as described above at 37 °C and 4°C for 4 hrs.

5.3.13 Uptake by Fluorescence Microscopy

Differentiated U937 cells were incubated in 24-well microplates with 50 nM fluorescein-labeled PEG, mPEG-fMLF, mPEG-$(fMLF)_2$ or PEG-$(fMLF)_4$ nanocarriers for 4 hrs. After incubation, the cells were washed twice and resuspended in Hanks Balanced Salt Solutions (HBSS). The stained cell suspension was placed on slides and covered with coverslips. The slides were then observed under a Zeiss Axiostar Plus fluorescence microscope (Thornwood, NY) with an objective magnification of 63× and an Insight digital camera (Sterling, MI) with proper filter sets. Digital images were taken with the Insight digital camera and its companion Spot software.

5.3.14 Calcium Mobilization

Differentiated U937 cells were loaded with 4 μmol/L fluo-4 AM in HBSS for 30 min at 37°C in the dark. The cells were washed and incubated for 30 min at room temperature to allow the Fluo-4 AM dye to completely de-esterify. The cells were washed, resuspended in HBSS, and treated with 1 μM PEG-fMLF nanocarriers at 37 °C. Fluorescence readings were obtained using a Tecan fluorescence plate reader for 400 s at 2 s intervals.

5.3.15 Statistical Analysis

All statistical tests were performed using GraphPad Instat (GraphPad Software, Inc., San Diego, CA). A minimal p-value of 0.05 was used as the significance level for all tests. One-way analysis of variance and Tukey test was performed on the uptake data. All data are reported as means ± S.D. of three observations, unless otherwise noted. The graphs were plotted using GraphPad Prism 4.01 (GraphPad Software, Inc., San Diego, CA).

5.3 Results

5.3.1 Synthesis and Characterization of PEG-fMLF Nanocarriers

The PEG-fMLF nanocarriers $mPEG_{5K}$-fMLF, $mPEG_{5K}$-$(fMLF)_2$, PEG_{10K}-$(fMLF)_4$ were prepared by coupling the fMLFKC to mPEG-MAL, mPEG-(MAL)2 and PEG-$(NH_2)_4$ according to the procedures described above (Scheme 5.1). All nanocarriers were purified by removal of low molecular weight contaminants using 3 kDa dialysis bags in ddH_2O for 2 days. The structures of purified products were confirmed by a combination

of SEC, MALDI-TOF and amino acid analysis. Amino acid analysis of the final nanocarrier showed the presence of methionine, leucine, phenylalanine, lysine and cysteine in the proper ratios (Table 1). Matrix Assisted Laser Desorption/Ionization Time-of-Flight (MALDI-TOF) Mass Spectrometry accurately determined the molar masses, the sequencing of repeat units, and the recognition of polymer additives and impurities. The nanocarriers were characterized using an Applied Biosystems Voyager DE Pro MALDI-TOF spectrometer (Foster City, CA) (Figure 5.1). The MALDI-TOF method was used to confirm the formation of polydisperse polymeric nanocarriers. A comparison of MALDI-TOF spectra of unreacted mPEG-MAL (MW ~5518 Da) with that of the fMLFK(fluorescein)C-mPEG (~6560 Da) and [fMLFK(fluorescein)C]$_2$-mPEG (~7604 Da) revealed average mass peak shifts of ~1040 Da and ~2080 Da, respectively, confirming that the polymeric nanocarriers created were derivatized with either fMLFK(fluorescein)C (1042 Da) or [fMLFK(fluorescein)C]$_2$ (2084 Da). Thus although the polymer is polydisperse due to variations in number of ethylene glycol repeats, the fMLFK(fluorescein) content of each preparation is monodisperse.

Novel peptide-backbone nanocarriers were prepared by coupling the peptide backbone, acetyl-Cys(TP)- (β-Ala-β-Ala-Lys-)$_n$ –amide (n=2, 4) to a heterobifunctional PEG, NHS-PEG-VS (Scheme 5.2). The NHS moiety reacts specifically with the ε-amine group of backbone peptide and the VS group is used for attachment of PEG to the sulfhydryl (SH) moiety of the fMLFKC peptide. The linkages formed amide (for NHS) and thioether (for VS) bonds between PEG and the fMLFKC and the peptide backbone, respectively. Both bonds are highly stable under physiological conditions. The thiol group of the cysteine moiety in the peptide backbone provides a site suitable for

attachment of a drug moiety. This moiety is protected by thiopyridine, which is an excellent leaving group and hence can be readily reacted with sulfhydryl containing drugs or peptides. TP is replaced by fMLFKC during the synthesis via a reversible thiol linkage. Thus the product was further reacted with DTT in order to remove the reversibly linked fMLFKC peptide. The targeting moiety fMLFKC in the nanocarrier is thus only attached via stable and non-reversible thioether linkage. The β-alanine moiety in the scaffold serves as a "spacer" reducing steric hindrance during the PEGylation reaction. Scaffold (peptide-based PEG carrier) size was varied by using peptide backbones of different lengths, which could be conjugated with different (2 or 4) numbers of copies of NHS-PEG-VS, in reactions proceeding to complete peptide derivatization. The Cys thiol group in the backbone peptide is not used in the particular conjugates described herein. Instead, it must be protected, such as in a disulfide form with the -S-tButyll group. If needed, this protecting group can be removed by a reducing agent without disturbing any other bonds in the conjugate.

5.3.2 Stability in PBS and Plasma

The stability of the fluorescein labeled PEG-fMLF nanocarriers were tested in 10 mM PBS (pH 7.4) and rabbit plasma at 37 °C for 24 hours. For non-peptide PEG-fMLF nanocarriers, the linkages formed a thioether bond between fMLFKC and PEG and an amide bond between the fMLFKC and the fluorescein. For peptide backbone PEG nanocarriers, the linkages formed amide (from NHS) bonds between PEG and the peptide backbone or thioether (from VS) bond between PEG and fMLFKC, respectively. All bonds were highly stable under physiological conditions. The nanocarriers were also very

stable in PBS and plasma during 24 hours of incubation at 37^{o}C with less than 3% degradation occurring after 24 hours.

5.3.3 Expression of Formyl Peptide Receptors

The expression of the formyl peptide receptor in the cell lines used was confirmed using gene expression analysis by RT-PCR. Differentiated U937 cells expressed high level of the formyl peptide receptor (FPR, 500 bp RT-PCR product) transcripts and formyl peptide receptor-like 1 (FPRL1, 1100 bp RT-PCR product) transcripts, while undifferentiated U937 cells only expressed low levels of FRPL1 and no detectable FPR (Figure 5.2).

5.3.4 Time-Dependent Uptake of PEG-fMLF Nanocarriers in Differentiated U937 Cells

The time course of PEG-fMLF nanocarrier uptake into macrophage-like differentiated U937 cells at 37°C showed a progressive increase in uptake at 1 hr, 2 hrs, and 4 hrs, with steady state apparently being reached at 4 hrs (Figure 5.3). Flow cytometry results showed that PEG_{5k} lacking fMLF had very low uptake at all time points during the incubation. In general, the attachment of 1, 2 or 4 copies of fMLF to PEG significantly increased nanocarrier uptake at all time points. Specifically, PEG_{5K}-fMLF enhanced macrophage uptake about 15-fold ($p<0.05$) after 4 hours of incubation at 37°C compared to the control PEG_{5k}. PEG_{5k}-$(fMLF)_2$ and PEG_{10k}-$(fMLF)_4$ further increased uptake about 45 and 60-fold ($p<0.01$) compared to the control PEG_{5k}, respectively.

5.3.5 Uptake in U937 Cells

To confirm the uptake specificity of PEG-fMLF nanocarriers, a comparison was made between the uptake in U937 cells expressing low levels of FPRL1/no FPR and differentiated U937 cells expressing high levels of FPR and FPRL1 (Figure 5.4). The uptake of the control PEG_{5k} was low and showed no significant difference between undifferentiated and differentiated U937 cells. In contrast, the uptake of PEG-fMLF nanocarriers with 1, 2 or 4 copies of fMLF was significantly higher in differentiated as compared to undifferentiated U937 cells ($p<0.01$). PEG_{5k}-fMLF uptake in differentiated U937 cells increased 1.52-fold as compared to undifferentiated U937 cells. Similarly, PEG_{5k}-$(fMLF)_2$ and PEG_{10k}-$(fMLF)_4$ increased 3.76-fold and 3.65-fold, respectively. Significantly higher uptake in differentiated U937 cells expressing FPR and FPRL1 is consistent with the uptake specifically mediated by the formyl peptide receptors.

5.3.6 Temperature Dependence of PEG-fMLF Nanocarriers Uptake in Differentiated U937 Cells

The uptake of PEG-fMLF nanocarriers in differentiated U937 cells after 4 hours of incubation at 4°C showed significantly lower cell uptake than at 37ºC (Figure 5.5). Non-derivatized PEG_{5k} showed similar low uptake levels at both temperatures. PEG_{5k}-fMLF uptake at 4°C was only 46.2% of that at 37ºC, while the ratio of 4°C:37ºC for PEG_{5k}-$(fMLF)_2$ and PEG_{10k}-$(fMLF)_4$was 40% and 41.6%, respectively. The main difference between 4°C and 37ºC is the magnitude of active uptake. The temperature-dependence of PEG-fMLF nanocarrier uptake suggested that the mechanism involves receptor-mediated active uptake.

5.3.7 Uptake Inhibition Studies

The specificity of this interaction was further investigated using differentiated U937cells incubated with PEG-fMLF nanocarriers in the presence of 5 μM free fMLF (Figure 5.6). The presence of 100-fold excess fMLF significantly inhibited the average uptake of PEG-fMLF nanocarriers in differentiated U937 cells. The inhibition led to a relative decrease in uptake of PEG-fMLF nanocarriers with 1, 2 and 4 copies of fMLF to 31.5%, 14.8% and 13.5%, respectively. Excess fMLF did not affect the uptake of PEG_{5k} significantly. Taken together, these results suggest that PEG-fMLF nanocarrier uptake was mediated by formyl peptide receptors.

5.3.8 Effect of PEG Sizes on PEG-fMLF Nanocarriers Uptake

To evaluate the effect of PEG size on the macrophage uptake, PEG-$(fMLF)_2$ prepared using 5K, 20K or 40K PEGs were incubated with differentiated U937 cells for 4 hours at 37ºC (Figure 5.7). Increasing PEG size from 5 kDa to 20 kDa slightly enhanced the uptake of PEG-$(fMLF)_2$ by about 14.4% ($p<0.05$). However, when PEG size increased to 40 kDa, the uptake of PEG-$(fMLF)_2$ decreased by 38.6% ($p<0.05$) suggesting that 20 kDa may be an optimal size.

5.3.9 Peptide-Based PEG Nanocarriers

The PEG-fMLF nanocarriers synthesized from commercially-available multifunctional PEGs showed enhanced macrophage uptake. However, the limited ability to produce such PEGs with defined numbers of cargo moieties, especially in high

numbers, limits their use as nanocarriers when multiple targeting or therapeutic moieties are necessary. Thus a novel peptide-backbone PEG nanocarrier was designed and synthesized to overcome this limitation. The peptide-PEG scaffold is comprised of the peptide backbone, acetyl-Cys(TP)-[β-Ala-β-Ala-Lys]$_{2, 4}$-amide. PEG is attached to the scaffold via the ε-amine group of lysine. The heterobifunctional PEG (NHS-PEG-VS) is linked to the scaffold by a stable amide linkage that is the result of the succinimidyl reaction with the e-amino group of lysine. The targeting moieties are appended to the other end of the PEG. The peptide-backbone acetyl-C-[AAK(PEG_{5K}-(fMLFK(fluorescein)C]$_2$-amide and acetyl-C-[AAK(PEG_{5K}-(fMLFK(fluorescein)C]$_4$-amide demonstrated increased macrophage uptake after 4 hrs of incubation at 37°C, about 4.2 and 5.7-fold more than PEG-fMLF (Figure 5.8), respectively. This is similar to but slightly higher than PEG-$(fMLF)_2$ and PEG-$(fMLF)_4$ derived from the PEGs. The results indicate that the number of attached targeting groups has much greater impact on the extent of the macrophage uptake than other factors such as the shape of the nanocarriers or geometric distribution of attached groups.

5.3.10 Fluorescence Microscopy

Cells incubated with the control fluorescein-labeled PEG_{5k} lacking fMLF showed no signal by fluorescence microscopy (Figure 5.9A). PEG_{5k}-fMLF showed faint fluorescence in cells, suggesting weak uptake (Figure 5.9B). The presence of punctate fluorescence suggested that the nanocarriers were internalized via endocytosis, which is typical of macromolecular uptake. PEG_{5k}-$(fMLF)_2$, and PEG_{10k}-$(fMLF)_4$ exhibited strong fluorescence throughout the cell, suggesting significantly higher binding/uptake to cells.

The representative histogram of flow cytometry results for PEG_{5k} (PEG), PEG_{5k}-fMLF, PEG_{5k}-$(fMLF)_2$, and PEG_{10k}-$(fMLF)_4$ (Figure 5.9E) confirmed the microscopic observations.

5.3.11 Calcium Mobilization

All PEG-fMLF nanocarriers showed decreased ability to activate macrophages cells, relative to free fMLF, as measured by transient stimulation of release of calcium ions from intracellular stores into the cytoplasm. The change of cytoplasmic calcium concentration was monitored by the fluorescent calcium indicator Fluo-4 AM preloaded in the cell cytoplasm. The linkage to PEG decreased calcium release by about 40% in all PEG-fMLF nanocarriers compared to free fMLF peptide (Figure 5.10). Interestingly, the linkage to PEG not only decreased macrophage activation of fMLF but also delayed the starting time of activation. This time delay and reduced activation by fMLF linked to PEG versus free fMLF was observed in our previous study in differentiated HL-60 cells (*200*) and may reflect a difference in the molecular pathways for macrophage activation and ligand internalization mediated by the same formyl peptide receptors.

5.4 Discussion:

The clinical potential of anti-HIV agents has been limited by a variety of factors such as drug toxicity for uninfected cells and development of drug resistance, which leads to sub-therapeutic drug levels and the formation of viral reservoirs. Better drug delivery and targeting technologies are required to specifically increase target cell exposure to these potent therapeutic agents. Therefore, drug delivery systems specifically targeted to

macrophage cell surface receptors could potentially improve therapeutic efficacy and minimize systemic toxicity of anti-HIV drugs.

fMLF was chosen as the targeting moiety for the formyl peptide receptor on macrophages. fMLF resembles the amino terminus of unprocessed eubacterial proteins and binds avidly to the formyl peptide receptors on the surface of macrophages, where it serves as a chemoattractant, triggers cellular activation, and enters the cells to which it binds (*148*). The potential of using fMLF as a targeting peptide to deliver PEG nanocarriers to macrophages was investigated in this study. The peptide fMLF was chosen as the targeting agent for several reasons. First, formyl peptide receptors are specifically expressed on phagocytic cells such as macrophages, dendritic cells and neutrophils. Secondly, fMLF specifically binds to formyl peptide receptors on macrophages with high affinity. Thirdly, fMLF activates macrophages and down-regulates the co-receptors of HIV entry, CCR5 and CXCR4. The down-regulation of CCR5 co-receptor by fMLF could potentially inhibit viral entry in macrophages, which might potentiate the therapeutic effects of such targeted nanoparticles.

In the current study, multiple copies of fMLF were conjugated to various PEG nanocarriers and evaluated for targeting to human macrophage-like differentiated U937 cells. The number of copies (1, 2 and 4) of fMLFKC conjugated to a single PEG nanocarrier was evaluated in order to determine the effects on avidity and macrophage uptake. Previous work by us has shown that increasing the number of fMLF residues (up to eight) attached to a single PEG polymer results in enhanced avidity (K_d = 0.18 nM) for neutrophil-like differentiated HL-60 cells relative to free fMLF (K_d = 28 nM), with less enhancement of activation than of binding by increasing fMLF number (*200*). In the

current study we show that increasing the number of fMLF residues attached to a single PEG polymer from one to two resulted in significantly enhanced uptake (~ 4-fold, $p<0.05$) in macrophage-like differentiated U937 cells, while further increasing this number from two to four only resulted in a modest increase in uptake. While the molecular basis of enhanced avidity by multivalency (i.e., multiple ligands attached to a single polymeric carrier molecule) is not proven, it is likely due to multimeric ligands interacting with multiple cellular receptors.

PEG was chosen as the pharmaceutical nanocarrier for macrophage-targeted drug delivery system because of our long experience with this polymer class. PEGylation, the process of attaching polyethylene glycol (PEG) to drug molecules, has been a highly successful strategy for improving the pharmacokinetics and pharmacodynamics of pharmaceuticals, especially for protein and peptide therapeutics (*19-25*). In previous reports from our laboratory, we have shown that multi-component macromolecular conjugates consist of PEG, saquinavir and R.I.CK-Tat retained antiviral activity *in vitro* and showed favorable therapeutic indices (*181, 203*). Studies of PEG in solution showed that each ethylene glycol sub-unit is tightly associated with two or three water molecules. The binding of water to PEG makes PEGylated compounds behave physically as though they are 3 to 9 times larger than a corresponding soluble protein of similar molecular weight (*204, 205*). In drug conjugates, PEG polymers with associated water molecules act like a shield to protect the attached drug from enzymatic degradation, inhibit interactions with cell surface proteins and provide increased size to prevent rapid renal filtration and clearance. These “stealth” properties of PEG have proven to be very valuable in prolonging drug persistence in the systemic circulation. However, the

inability of PEG to interact with cell-surfaces theoretically limits its use as a biomaterial for cell-surface or intracellular drug delivery and targeting. Therefore, the very property of PEGylation that has made it clinically useful and commercially successful is exactly the opposite of what is needed for promoting effective targeted drug therapy in diseases like AIDS. In other words, currently used PEGylation approaches that have been enormously successful for treating certain diseases like cancer may not appropriate for treating HIV infection in viral reservoirs or sanctuary sites such as macrophages, the central nervous system and testis. Our approach to functionalize PEG in order to shift the site of drug delivery from the blood to target cells is novel and counterintuitive given the current use of PEG. However, the general stealth property of the PEG moiety may reduce toxicity by reducing nanocarrier binding to cells not expressing FPR and FPRL1. Experimental studies on targeted drug delivery into cells have identified size as an important factor in cellular uptake of nanomaterials. It has been shown that particles with radii <50 nm exhibit significantly greater uptake compared with particles >50 nm (*206, 207*). Aoyama and coworkers (*208, 209*) reported on the effect of size on receptor-mediated endocytosis in glycoviral gene delivery by excluding potential complications arising from charge effects. They concluded that receptor-mediated endocytosis is strongly size-dependent and the optimal size is around 25 nm. In our study, increasing PEG size from 5K to 20K slightly enhanced nanocarrier uptake but uptake decreased when the size was further increased to 40K. The estimated molecular size of a 5 kDa PEG molecule is ~2 nm, while that of a 20 kDa PEG is 7 nm, and 10 nm for 40 kDa (*210*). The effective or apparent size of PEG nanocarriers is significantly increased by the binding of water to PEG, the hydrodynamic radius of the hydrated PEG nanocarrier is 3

to 9 times higher than predicted by their molecular weight (*210*). Therefore, a 20 kDa PEG-$(fMLF)_2$ has an effective molecular size of 20-60 nm. The optimal uptake of this nanocarrier and its size is consistent with the suggestions of Aoyama et al. On the other hand, 5 kDa and 40 kDa PEG-$(fMLF)_2$ showed less uptake because their effective sizes are either <25nm or >50 nm. Effective targeting to macrophages residing in tissues depends on multiple factors including plasma clearance, tissue distribution, receptor binding and cell uptake. The pharmacokinetics and biodistribution of nanocarriers relates to their size, charge, shape and rigidity and is primarily controlled by renal glomerular filtration and (*211*). The current results suggest that a delicate balance must be struck between maximizing the circulation half-life of nanocarriers in blood and their penetration into macrophage tissue compartments.

PEGylated systems made from commercially available multifunctional PEGs have a linear or forked shape. However they are limited for attachment of multiple copies of ligands. and limited capacity to conjugate functional groups, multiple copies, or drugs. These limitations have affected their potential as pharmaceutical drug carriers. Therefore we designed and synthesized a prototypical novel peptide-based PEG nanocarrier. The central component of the proposed nanocarriers is the peptide-based PEG scaffold that comprised the peptide backbone, Cys- $(\beta\text{-Ala-}\beta\text{-Ala-Lys-})_n$-amide (n=2, 4 or more), having 1 thiol group on the cysteine side chain and amino groups on lysine side chains. The flexibility of this peptide-based PEG nanocarrier is evident. For example, if a higher number of targeting agents is needed, a larger scaffold with more lysine moieties for PEG attachment can be utilized. Drugs can be attached by a disulfide (reversible) or thiosulfonyl [(non-reversible) via vinyl sulfone bond. The scaffold consisting of a peptide

backbone and PEG is the critical central feature of nanocarrier drug conjugates since: (1) it controls body and cellular disposition and uptake/retention, (2) it allows us to add functional groups (i.e., effectors) to target specific cell types and cause surface binding or uptake and (3) it allows us to attach exact numbers of multiple drugs or multiple targeting moieties using releasable or nonreleasable bonds. Furthermore, the molecular population of nanocarriers is monodisperse in its derivatization, a distinct advantage over other PEGylation carriers. Using these features we could potentially precisely control how, when and where anti-HIV drugs are able to exert their therapeutic effect.

5.5 Conclusions

The current results demonstrated that PEG nanocarriers with multiple copies of fMLF can specifically target human macrophage-like cells *in vitro* and that the number of fMLF copies attached determines extent of uptake. The results suggest that two fMLF residues are sufficient for achieving optimal targeting and improving uptake *in vitro*. We also demonstrated that 20 kDa (corresponding to 20-60 nm) may be the optimal PEG nanocarrier size for improved macrophage uptake. Since typical commercially available multifunctional PEGs limit the numbers of copies of drugs and targeting groups that may be attached to a nanocarrier, we designed an alternate carrier that retained the targeting and uptake properties of nonpeptide-based PEGs. However, the new nanocarrier allows for far greater flexibility in attaching multiple drugs, copies of drugs and/or targeting moieties. These results indicate great promise for improving targeted drug delivery to HIV-infected macrophages, which may eventually allow for better therapeutic regimens

by reducing dose, and improving tolerability and patient compliance with complicated regimens.

Table 5.1 Results of amino acid analysis of PEG-fMLF nanocarriers. The amino acids were normalized relative to phenylalanine.

Sample Name	Amino Acid Ratio (normalized by phenylalanine)				Concentration nM
	Met	Leu	Phe	Lys	(Expected 50 nM)
fMLF	0.90	1.20	1.00	1.00	36.00
PEG-(fMLF)	0.95	1.20	1.00	1.00	37.10
PEG-$(fMLF)_2$	0.97	1.23	1.00	0.95	37.87
PEG-$(fMLF)_4$	0.91	1.19	1.00	1.01	42.00
PB-PEG-$(fMLF)_2$	0.91	1.17	1.00	2.08	40.00
PB-PEG-$(fMLF)_4$	0.96	1.19	1.00	1.87	37.90

* PB: peptide-based

Scheme 5.1 Synthesis of PEG-fMLF nanocarriers with 1 copy (PEG_{5k}-fMLF, Scheme A), 2 copies (PEG_{5k}-$(fMLF)_2$, Scheme B) and 4 copies (PEG_{10k}-$(fMLF)_4$, Scheme C) copies of fMLF and fluorescein-labeled control PEG_{5k} without fMLF peptides (Scheme D).

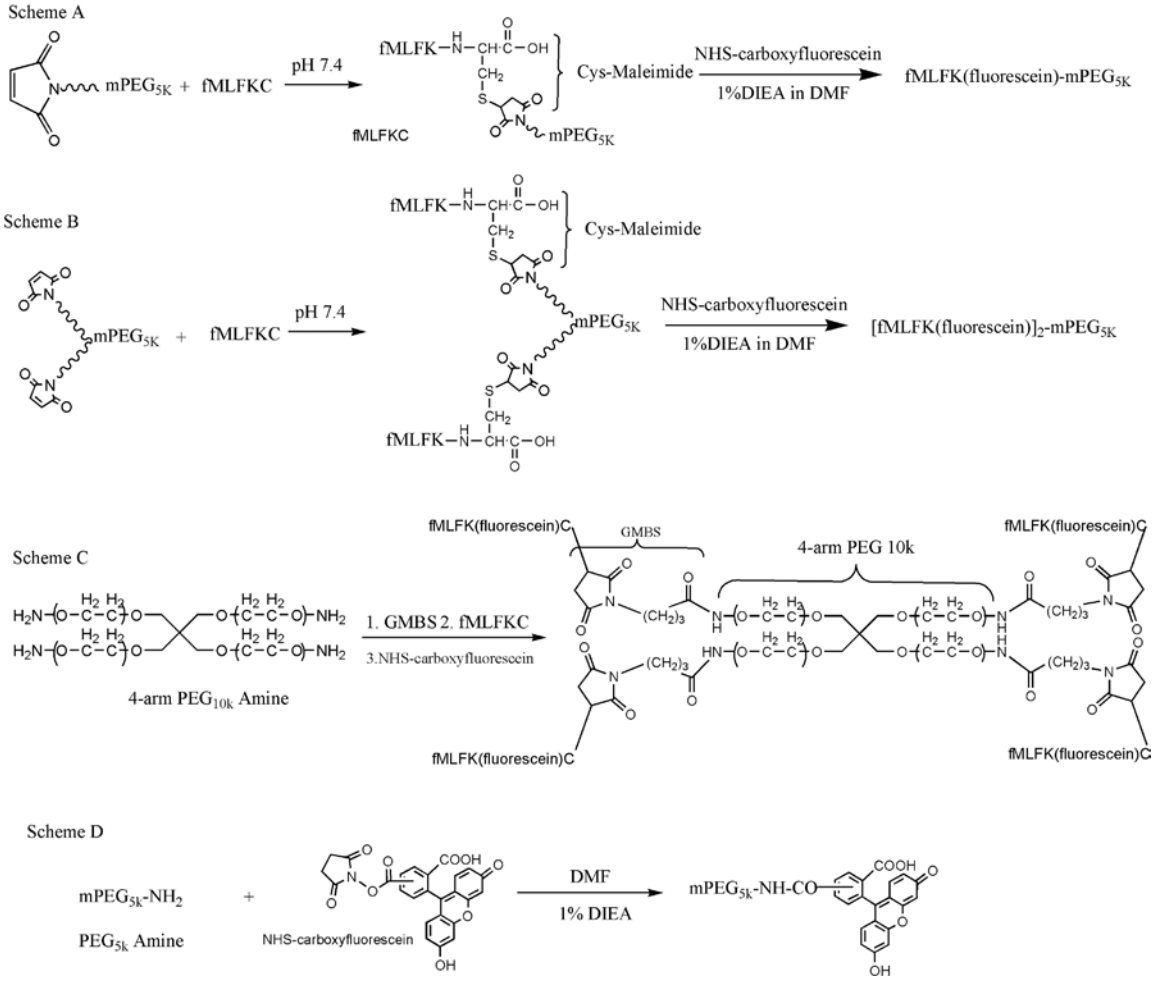

Scheme 5.2 Design of peptide-based PEG nanocarriers with 2 and 4 copies of fMLF peptides. The peptide acetyl-Cys-(β-Ala-β-Ala-Lys)n-amide (n=2, 4) are the backbone. NHS-PEG_{5k}-VS is the linker between peptide backbone and targeting groups fMLFKC, which form an amide bond with amine group on acetyl-Cys-(β-Ala-β-Ala-Lys)n-amide and a thioether bond with the thiol group on fMLFKC.

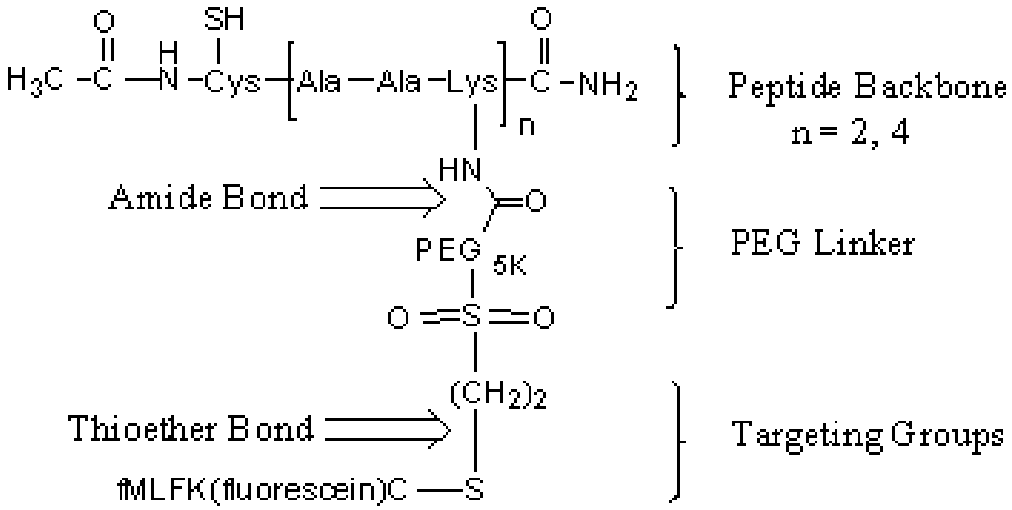

Figure 5.1 MALDI-TOF Spectra of PEG-fMLF nanocarriers. The starting material mPEG-MAL showed the poly-disperse peaks with average molecular weight at about 5518 Da. fMLFK(fluorescein)C-mPEG showed average peak at 6560 Da and [fMLFK(fluorescein)C]$_2$-mPEG showed average peak at 7604 Da.

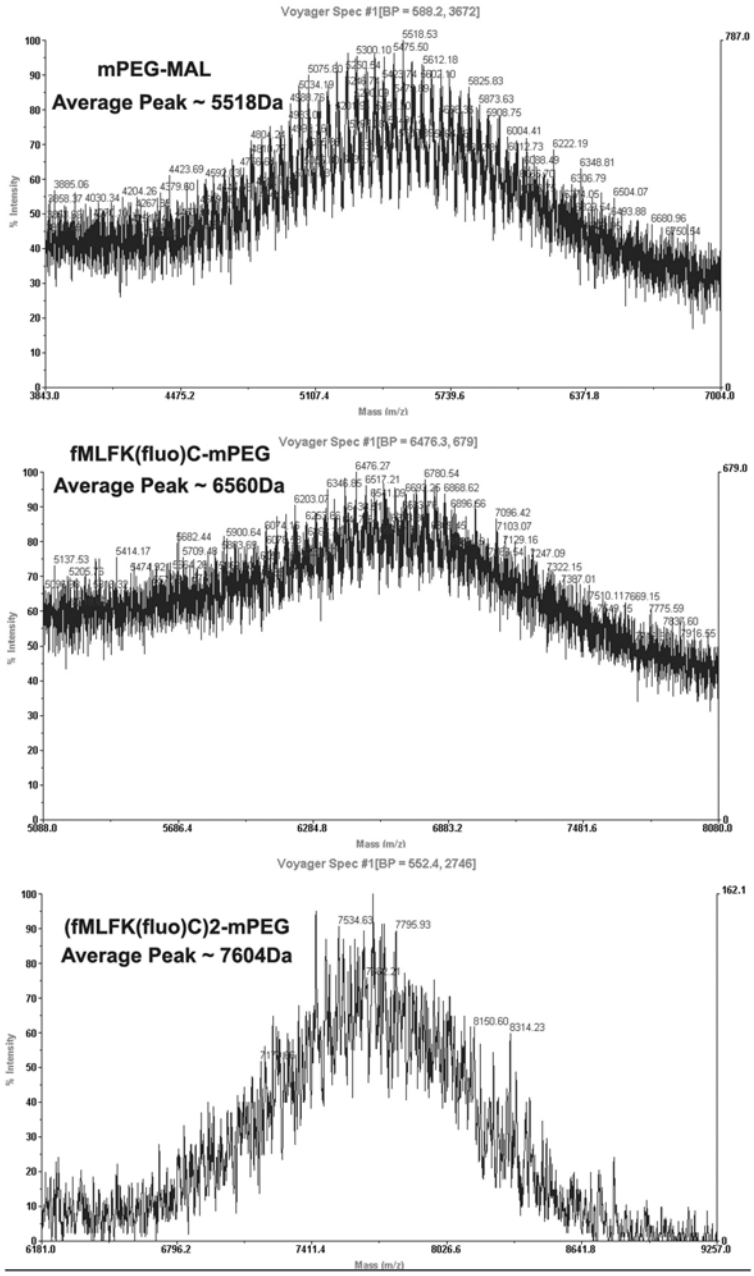

Figure 5.2 Expression of formyl peptide receptor (FPR) and formyl peptide receptor-like 1 (FPRL1) in undifferentiated and differentiated U937 by RT-PCR. Differentiated U937 cells expressed high level of transcripts for the formyl peptide receptor (FPR, 500 bp RT-PCR product) and formyl peptide receptor-like 1 (FPRL1, 1100 bp RT-PCR product), while undifferentiated U937 cells only expressed low levels of FRPL1 and no FPR.

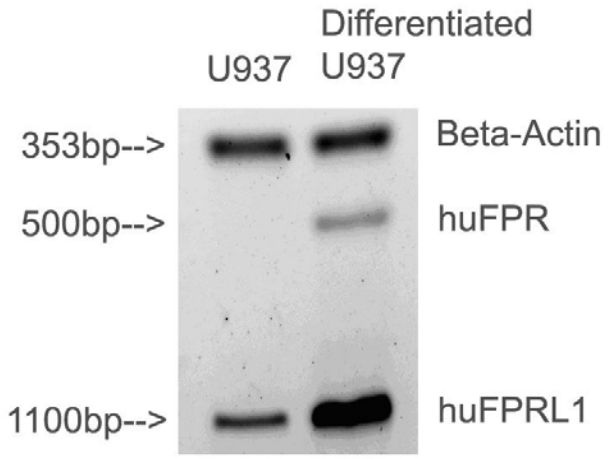

Figure 5.3 Time course of the uptake of fluorescein-labeled PEG-fMLF nanocarriers in differentiated U937 cells at 37ºC. Differentiated U937 cells were incubated for the indicated time period and plotted against nanocarrier uptake. Means ± S.D. for three observations are shown for each value. PEG_{5K}-fMLF enhanced macrophage uptake about 15-fold ($p<0.05$) after 4 hours of incubation at 37°C compared to the control PEG_{5k}. PEG_{5k}-$(fMLF)_2$ and PEG_{10k}-$(fMLF)_4$ uptake were about 45 and 60-fold higher than control PEG_{5k} uptake ($p<0.01$), respectively. (Statistically significant differences were observed between the PEG-fMLF nanocarriers and the control PEG_{5k}, * $p<0.01$, ** $p<0.05$).

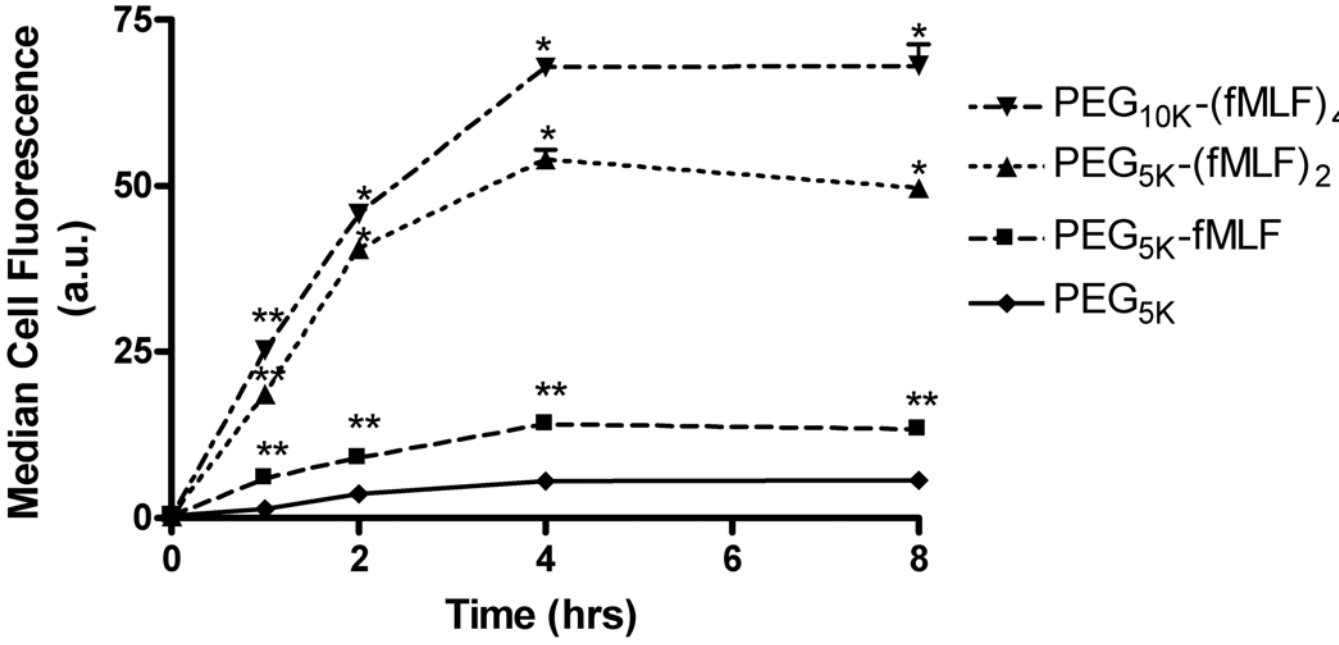

Figure 5.4 Uptake of fluorescein-labeled PEG-fMLF nanocarriers in U937 cells and differentiated U937 cells at 37ºC after 4 hours incubation. Means ± S.D. for three observations are shown for each value. (* Statistically significant difference between the U937 cells and differentiated U937 cells, $p<0.01$.)

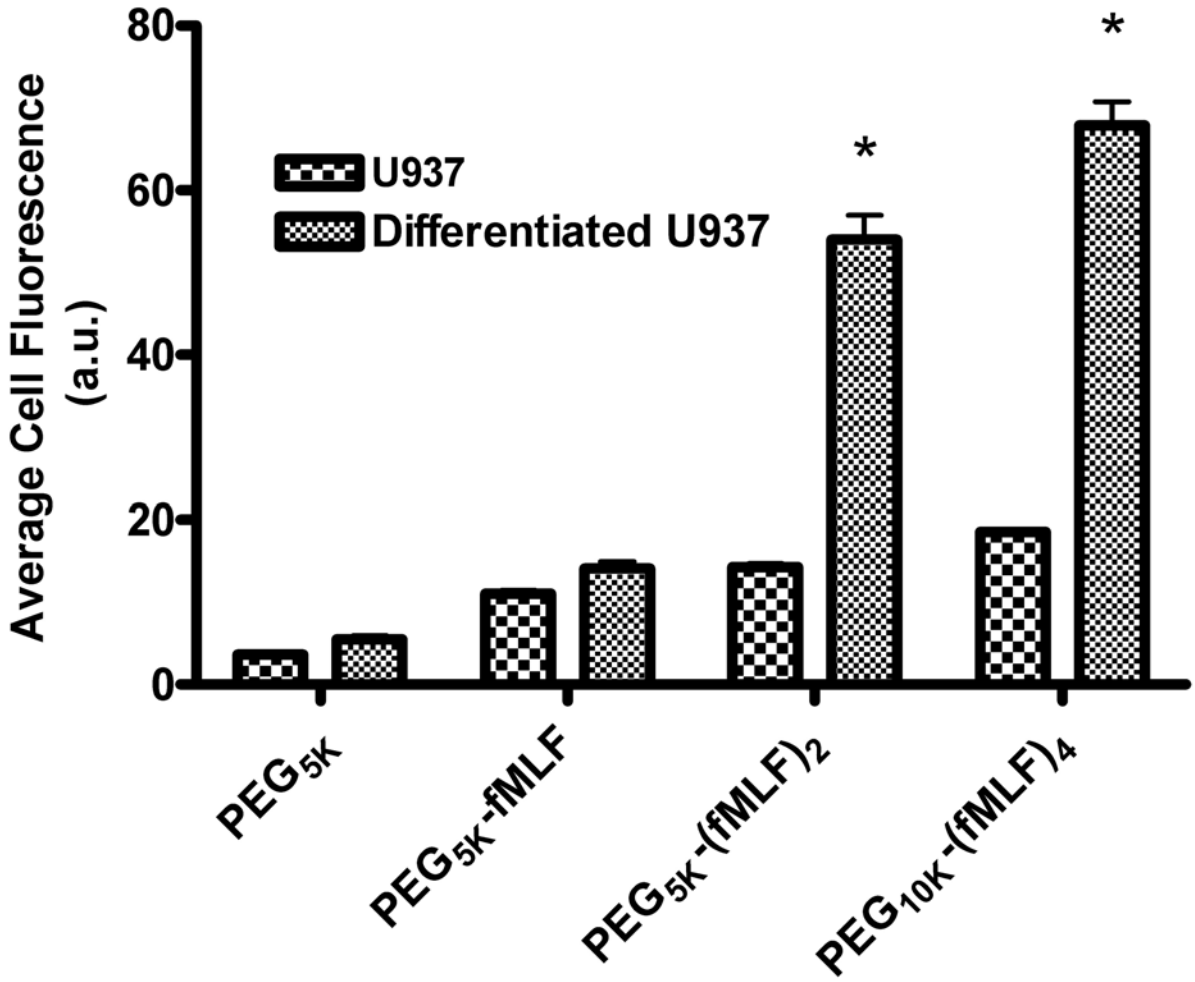

Figure 5.5 Uptake of fluorescein-labeled PEG-fMLF nanocarriers in differentiated U937 cells at 4 ºC and 37ºC after 4 hours incubation. Means ± S.D. for three observations are shown for each value. (* Statistically significant difference between 4 ºC and 37ºC treatments. $p<0.01$)

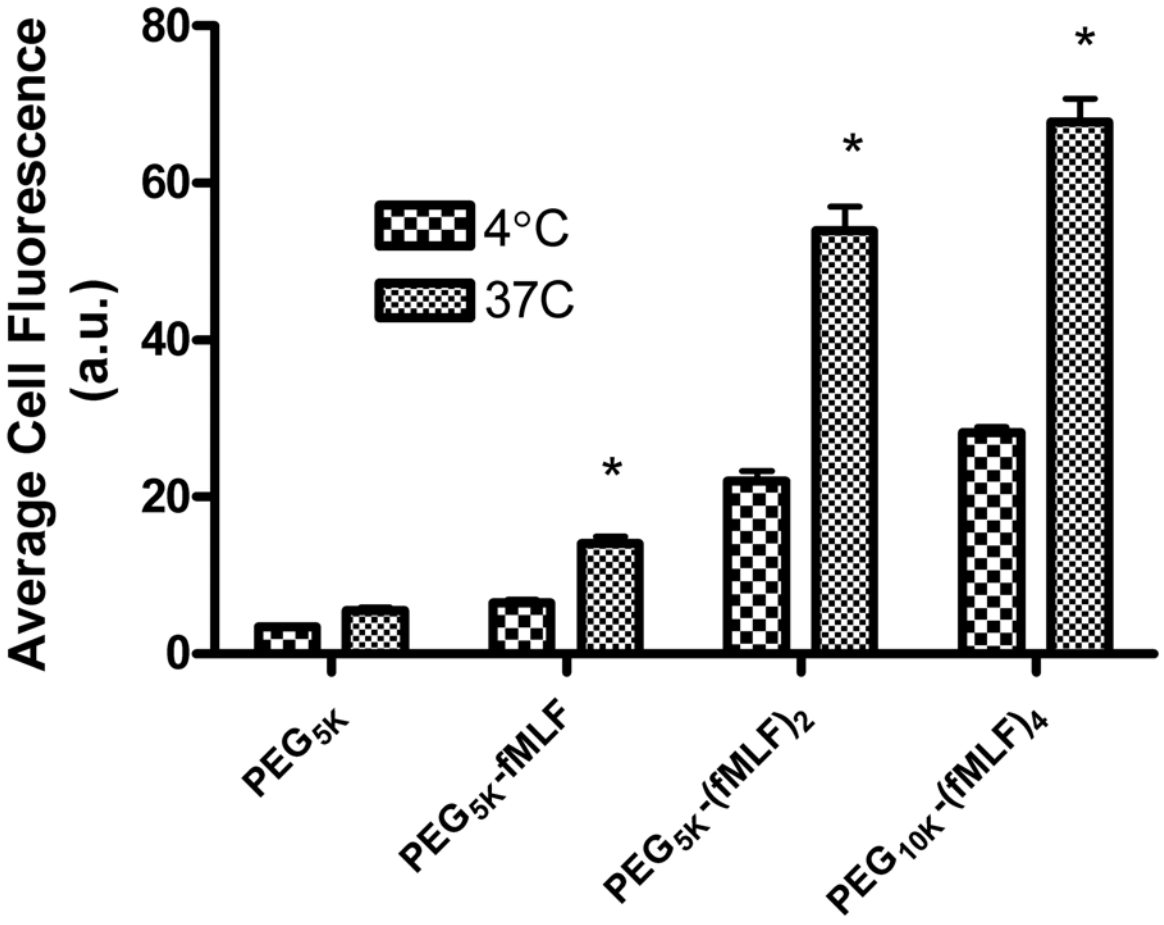

Figure 5.6 Uptake of fluorescein-labeled PEG-fMLF nanocarriers in differentiated U937 cells at 37ºC after 4 hours incubation in the absence and presence of 5 μM free fMLF. Means ± S.D. for three observations are shown for each value. (Statistically significant difference between the differentiated U937 cells incubated with and without 100× free fMLF * $p<0.01$, ** $p<0.05$)

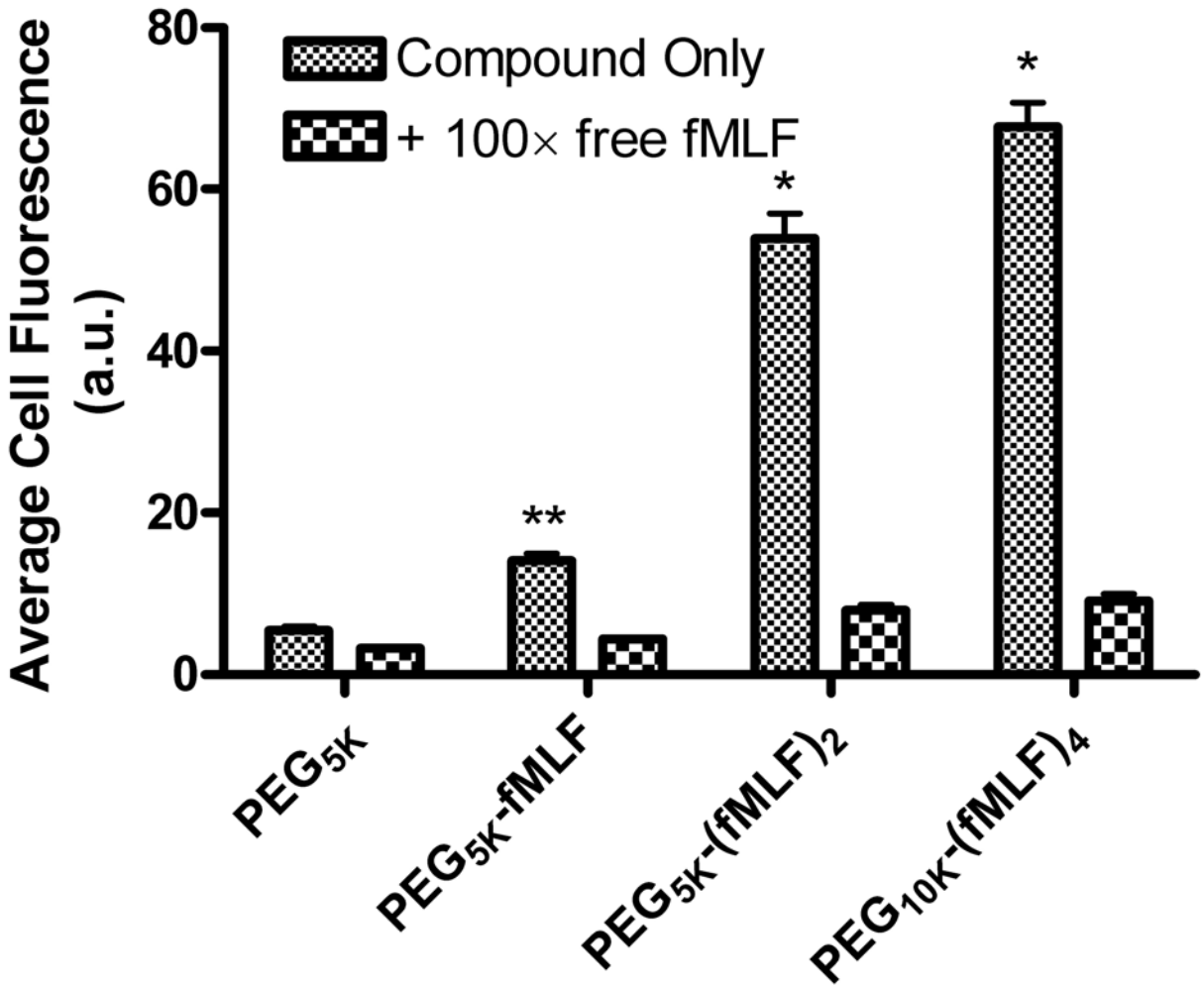

Figure 5.7 Uptake of fluorescein-labeled PEG-fMLF nanocarriers with different sizes in differentiated U937 cells after 4 hours incubation at 37ºC. Means ± S.D. for three observations are shown for each value. (* Statistically significant difference between the PEG_{5k} and the derivatized samples, $p<0.01$.)

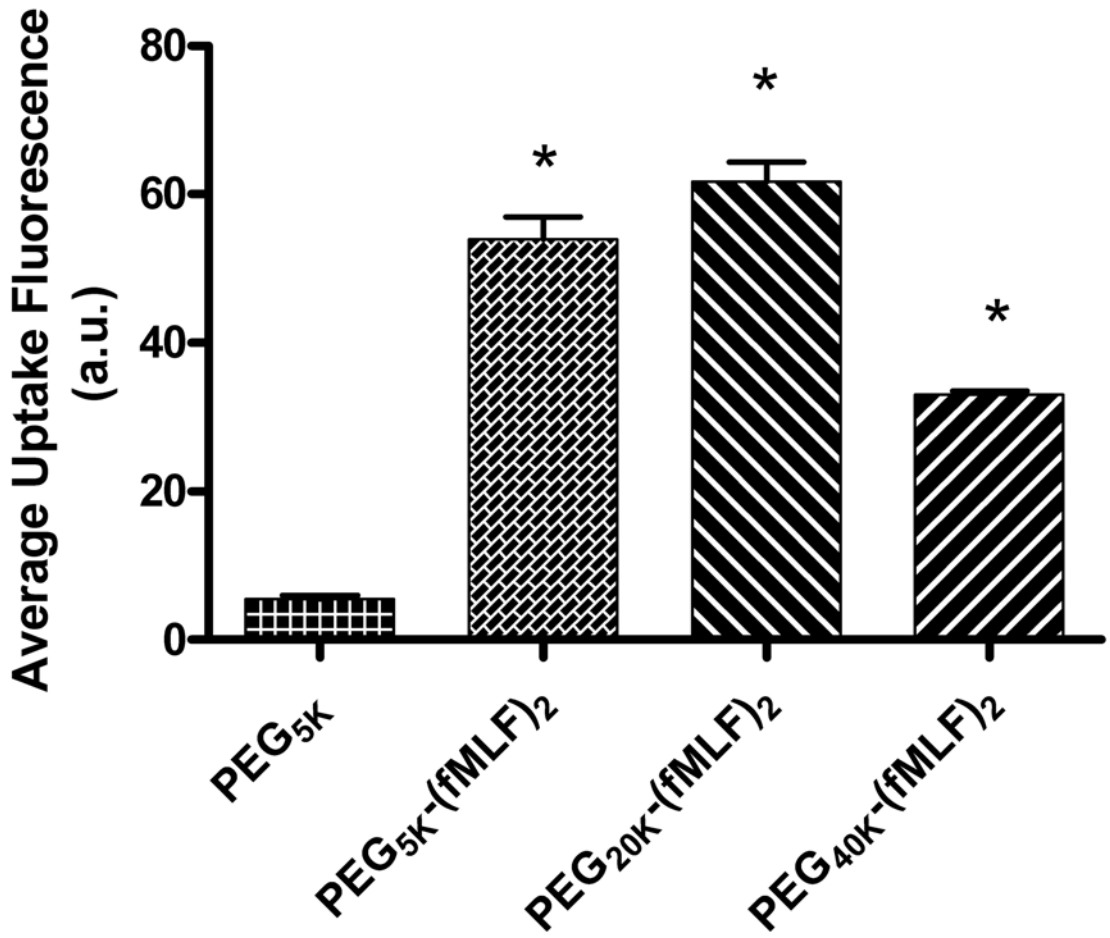

Figure 5.8 Uptake of fluorescein-labeled PEG-fMLF nanocarriers derived from Nektar PEGs or peptide-backbone (PB-)PEGs in differentiated U937 cells after 4 hours incubation at 37ºC. Means ± S.D. for three observations are shown for each value. (* Statistically significant difference between the control PEG_{5k} and PEG-fMLF nanocarriers, $p<0.01$)

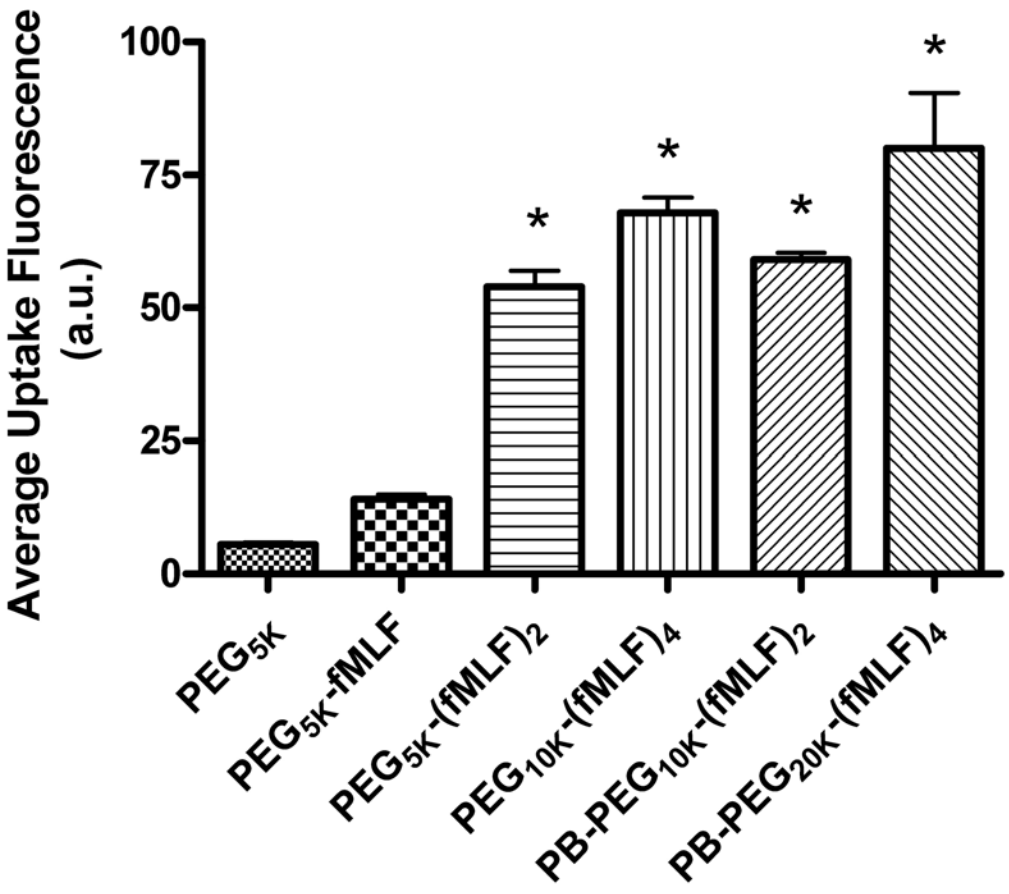

Figure 5.9 Fluorescence images of differentiated U937 cells incubated with fluorecein-labeled (A) PEG_{5k}, (B) PEG_{5k}-fMLF, (C) PEG_{5k}-$(fMLF)_2$, and (D) PEG_{10k}-$(fMLF)_4$. Representative histogram of flow cytometry results for PEG_{5k} (PEG), PEG_{5k}-fMLF (PF1), PEG_{5k}-$(fMLF)_2$ (PF2), and PEG_{10k}-$(fMLF)_4$ (PF4) was shown in Figure 5.9E.

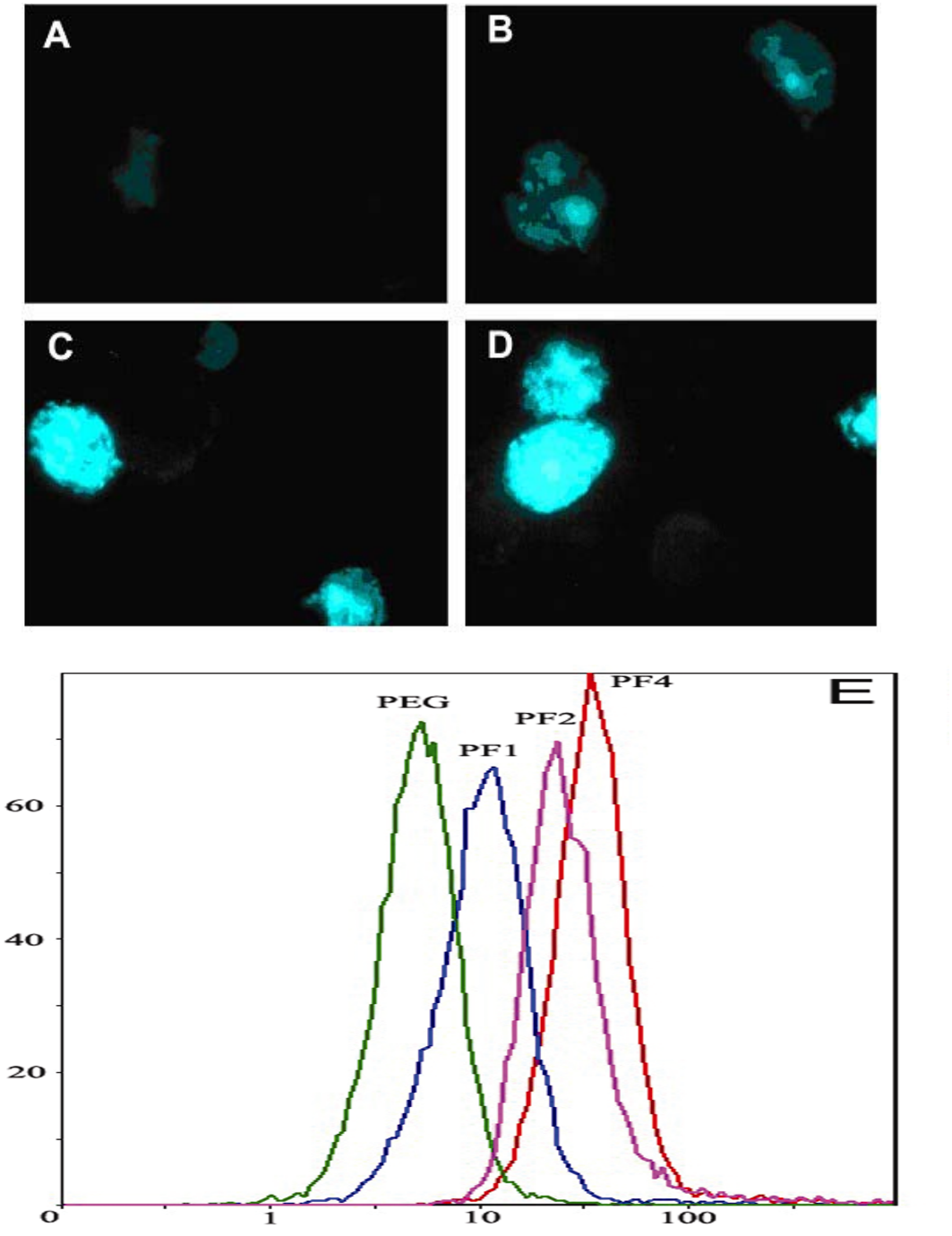

Figure 5.10 Calcium mobilization results of fMLF and PEG-fMLF nanocarriers. 100nM of each compound was tested in differentiated U937 loaded with calcium indicator Fluo-4 AM and the calcium flux was detected by fluorescence at Ex485 nm and Em530 nm for up to 400 seconds.

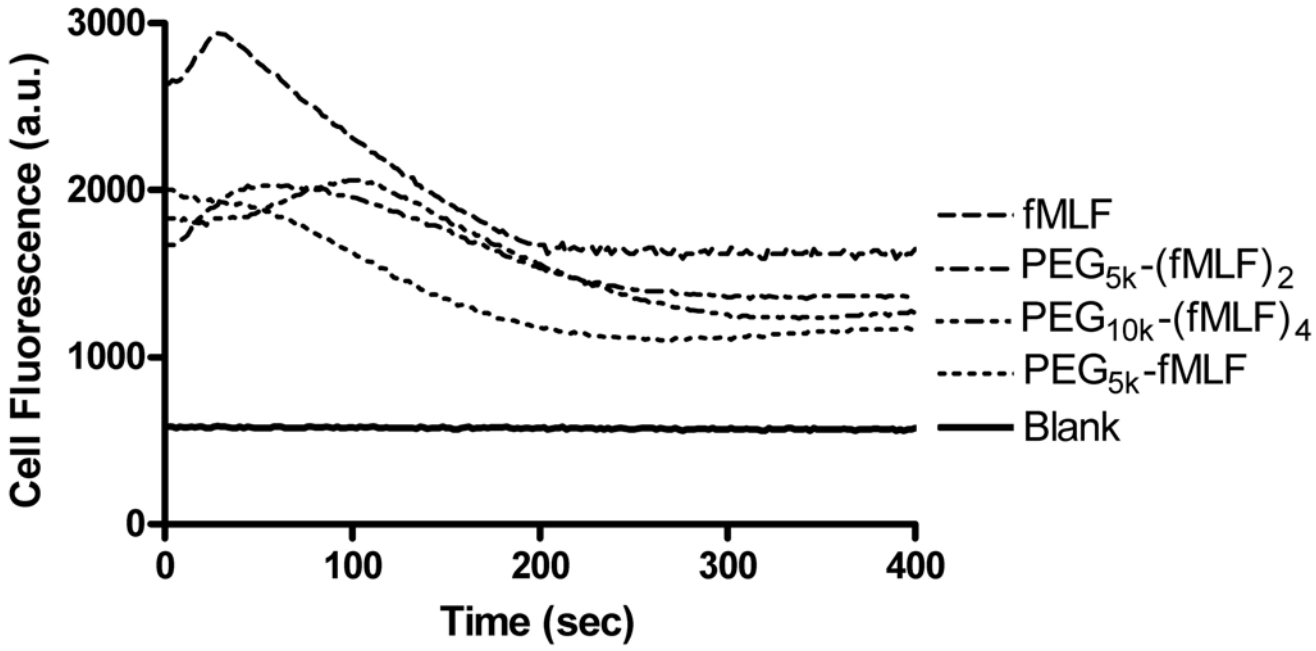

CHAPTER 6

DESIGN, SYNTHESIS AND EVALUATION OF MULTI-VALENT MACROPHAGE-TARGETED PEG-fMLF NANOCARRIERS II: PERITONEAL MACROPHAGE UPTAKE, PHARMACOKINETICS AND BIODISTRIBUTION OF MACROPHAGE-TARGETED PEG-fMLF (N-FORMYL-METHIONYL-LEUCYL-PHENYLALANINE) NANOCARRIERS

6.1 Introduction

Human immunodeficiency virus type 1 (HIV-1) infection is recognized as the major cause of the impairment of immune system functions that leads to the progression of the disease and the death in patients with acquired immunodeficiency syndrome (AIDS). Numerous advances in antiretroviral drug therapy have been made with the advent of highly active antiretroviral therapy (HAART) (*3*), a multiple drug treatment regimen. Despite these advances, curing HIV infection has remained an elusive goal due to many challenges including low and fluctuating drug concentrations due to poor drug absorption or patient non-adherence (*4*), the presence of viral reservoirs and sanctuary sites (*5*), and drug toxicity during chronic high dose therapy (*193*). Highly potent drugs already exist but inefficient *in vivo* delivery limits their usefulness and results in clinical "potency" viewed as only "on the threshold with little margin for error" (*193*). Among

the major causes of HIV treatment failure, insufficient drug exposure due to poor adherence to treatment regimens, inadequate and variable drug absorption and pharmacokinetics, or an inability of the agents to penetrate viral reservoirs is one of the areas where little progress has been made and efforts are generally lacking. This, combined with poor adherence to clinical regimens and the inability to eradicate HIV from tissue and cell compartments, strongly suggests an urgent need for targeted drug delivery approaches. The explosive growth of nanotechnology in the past decades offers great yet unfulfilled promise in the field of drug delivery. It is hypothesized that by using targeted nanoparticle drug delivery systems, anti-HIV drugs can accumulate in the HIV-infected tissues or cells selectively and quantitatively, while their concentration in non-infected tissues or cells should be much lower (*16-18*). Therefore, side effects are reduced, lower doses are needed and drug administration regimens are simplified (*17*). An ideal anti-HIV nanoparticle drug delivery system need to target specifically to the HIV infection sites, to balance well between the prolonged circulation in plasma and tissue penetration, and to be flexible enough in design to incorporate different combinations of targeting moieties and anti-HIV drugs.

Cells of the macrophage lineage play an important role in the initial stage of HIV-1 infection and continue to do so throughout the course of infection (*32*). Productively infected macrophages have been found in both untreated patients and those receiving HAART (*33*). HIV-1 infection of macrophages can be productive but noncytopathic, permitting macrophages to serve as long-lived sources of HIV production (*33*). More importantly they represent major viral reservoirs and are responsible for the relapse of the infection and resistance development on discontinuation of treatment. The tissue

distribution of macrophages defines the anatomical reservoirs of HIV. In the body, macrophages colonize the primary lymphoid organs such as fetal bone marrow, liver, thymus and secondary lymph organs such as spleen, adult bone marrow, lymph nodes, gut- and mucosal-associated lymphoid tissue (GALT and MALT), in addition to other major organs such as the brain, lungs, kidney (*34*). Throughout the course of HIV infection, macrophages have been implicated in carrying virus across the blood-brain barrier and establishing and maintaining HIV infection within the central nervous system (CNS), probably the most important anatomical HIV reservoir. *In situ* hybridization and immunohistochemical analyses revealed that tissue macrophage in the lymph nodes, spleen, gastrointestinal tract, liver, and kidney sustain high plasma virus loads in rhesus macaques after the depletion of $CD4^+$ T cells by a highly pathogenic simian immunodeficiency virus/HIV type 1 chimera (SHIV) (*212*). Viral particles have also been identified in kidney (*36*), brain (*37*) and the cerebrospinal fluid (*38*). There are many more HIV-1 infected cells in lymph nodes than in the blood, which in any case contains fewer than 2 percent of total body lymphocytes (*39*). Taken together, it is clear that macrophages are not only the primary target of HIV infection in patients but are an important source, in addition to $CD4^+$ T-lymphocytes, of HIV persistence during HAART (*40, 41*). Therefore, drug delivery to tissue macrophages represents a key challenge for eradicating HIV. Better drug delivery is needed to suppress viral replication inside macrophages in order to improve anti-HIV therapy.

For all of these reasons, therapeutic strategies aimed at delivering anti-HIV drugs specifically to macrophages to achieve sufficient concentrations and control of HIV replication have been explored by our group (*200*). Recently we showed that the

conjugation of multiple targeting fMLF peptides to a PEG polymer resulted in enhanced uptake into macrophages *in vitro* while the number of attached copies of fMLF determined extent of uptake (Bioconj Chem 2007, submitted). We also studied the relationship between the molecular features of PEG-fMLF nanocarriers (number of targeting peptide and PEG sizes) and cell uptake in order to optimize the design of the drug delivery system. The results suggested that appending only 2 copies of the ligand to the multifunctional nanocarrier is sufficient for optimal binding and the optimal size of the nanocarrier was about 20 kDa, which corresponds to a size of 20-60 nm. Furthermore, novel peptide-backbone PEG nanocarriers with flexible structural characteristics were designed and synthesized to probe nanocarrier structural requirements for optimal macrophage targeting and uptake. Peptide-backbone PEG-fMLF nanocarriers demonstrated their ability to targeting and be taken up by differentiated U937 cells, and in addition displayed other advantages over PEGylated systems derived from commercially available PEGs. However, effective targeting to macrophages residing in tissues requires a good balance between plasma clearance, tissue distribution, receptor binding and cell uptake. The pharmacokinetics and biodistribution of nanocarriers is primarily controlled by renal glomerular filtration and relates to their size, charge, shape and rigidity (*211*). A delicate balance must be struck between maximizing the circulation half-life of nanocarriers in blood and their penetration into macrophage tissue compartments. Therefore, it is imperative that the relationship between the *in vivo* tissue dispositional properties and/or cellular uptake and structural characteristics of nanocarriers be studied. In the present study, peritoneal macrophage uptake, pharmacokinetic and biodistribution of PEG-fMLF nanocarriers were investigated to

assess their potential of *in vivo* macrophage targeting. The results demonstrated the feasibility of using macrophage-targeted nanocarriers for enhancing drug uptake in macrophages residing in tissues.

6.2 Materials and Methods:

6.2.1 Materials

N-formyl-Met-Leu-Phe-Lys-Cys-amide and the backbone peptides acetyl-Cys(thiopyridine)-(β-Ala-β-Ala-Lys)$_4$-Amide were synthesized via FMoc Chemistry by the W.M. Keck Facility (New Haven, CT). NHS-PEG-VS (MW ~5 kDa), mPEG-MAL (MW ~5.5 kDa), mPEG-(MAL)$_2$ (MW ~5.5 kDa) and mPEG-NH_2 (MW ~5kDa) were obtained from Nektar Therapeutics (Huntsville, AL). N-succinnimidyl-[2, 3-^{3}H]-propionate was purchased from Amersham Bioscience (Piscataway, NJ). Propionic anhydride, DMF **(**dimethylformamide), DIEA (diisopropylethylamine), acetonitrile (ACN), trifluoroacetic acid (TFA), ether and other chemical reagents were purchased from Sigma-Aldrich (St. Louis, MO).

6.2.2 Synthesis of fluorescein-labeled PEG-fMLF Nanocarriers

2 mmole mPEG$_{5K}$-maleimide or mPEG$_{5K}$-(maleimide)$_2$ was dissolved in 1 mL phosphate-buffered saline (PBS, pH=7.4) at room temperature. To this were added 3 equivalents of fMLFKC (Scheme 6.1). The reaction was stirred overnight at room temperature. The excess solvent was removed under reduced pressure. The solid

PEGylated product was further reacted with 3 equivalents of NHS-carboxyfluorescein and 1% DIEA in 500 µL DMF. For control, 1mmole $mPEG_{5k}$-NH_2 were reacted with 3 equivalents of NHS-carboxyfluorescein and 1% DIEA in 500 µL DMF to yield $mPEG_{5k}$-fluorescein. The reaction was stirred for 3 hrs at room temperature. The final product was recrystallized from cold ether, washed thrice to remove impurities and dried under vacuum. Then the dried product was dissolved in ~5 mL ddH_2O and was dialyzed against ddH_2O for two days in the dark. The solution was dried under vacuum to yield the purified product.

To achieve a branched shape and multiple coupling sites, peptide-backbone PEG nanocarriers were designed and synthesized (Scheme 6.1C). For 4 copies fMLF PEG nanocarriers (Scheme 6.1C), 2 mmole of the backbone peptide acetyl-Cys(thiopyridine)-$[\beta$-Ala-β-Ala-Lys$]_4$-amide was reacted with 2 equivalents of NHS-PEG_{5k}-VS and 1% DIEA in 500 µL DMF. The reaction was carried out at room temperature for 3 hours. The product acetyl-Cys(thiopyridine)-$[\beta$-Ala-β-Ala- Lys(PEG_{5k}-VS)$]_4$-amide was purified by size exclusion chromatography with TSK Gel-3000PW column. The pooled fractions containing the product were dried under vacuum. Then this PEGylated intermediate was dissolved in 1 mL phosphate-buffered saline (PBS, pH=7.4) at room temperature. To this were added 3 equivalents of fMLFKC. The reaction was stirred overnight at room temperature. The excess solvent was removed under reduced pressure. The solid PEGylated product was further reacted with 3 equivalents of carboxyfluorescein-NHS and 1% DIEA in 500 µL DMF. The reaction was stirred for 3 hrs at room temperature. The product was then treated with 5 molar excess of dithiothreitol (DTT) for another 2

hours to remove the thiopyridine protection group on the peptide backbone. The final product was recrystallized from cold ether, washed thrice to remove impurities and dried under vacuum. Then the dried product was dissolved in ~5 mL ddH_2O and was dialyzed again ddH_2O for two days in the dark. The solution was dried under vacuum to yield the powder of purified product.

6.2.3 Synthesis of tritium-labeled PEG-fMLF nanocarriers

$mPEG_{5K}$-$(maleimide)_2$ (2 mmole) was dissolved in 1 mL phosphate-buffered saline (PBS, pH=7.4) at room temperature. To this were added 3 equivalents of fMLFKC. The reaction was stirred overnight at room temperature. The excess solvent was removed under reduced pressure. The solid PEGylated product was further reacted with N-succinnimidyl-[2, 3-^{3}H]-propionate and 1% DIEA in 1 mL DMF. The reaction was stirred for 3 hrs at room temperature and chased by 3 equivalents of cold propionic anhydride for 3 hrs. The final product was recrystallized from cold ether, washed thrice to remove impurities and dried under vacuum. The control $mPEG_{5K}$-NH_2 and PEG_{20k}-$(NH_2)_4$was directly reacted with N-succinnimidyl-[2, 3-^{3}H]-propionate and chased with 3 equivalents of cold propionic anhydride as described above.

The peptide-backbone nanocarrier acetyl-Cys(thiopyridine)-[β-Ala-β-Ala-Lys(PEG_{5k}-fMLFKC]$_4$-amide was synthesized as described above. The solid PEGylated product was reacted with 3 equivalents of N-succinnimidyl-[2, 3-^{3}H]-propionate and 1% DIEA in 1 mL DMF. The reaction was stirred for 3 hrs at room temperature and chased

by cold propionic anhydride for 3 hrs. The product was further treated with 5 molar excess of dithiothreitol (DTT) for another 2 hours to remove the thiopyridine protection group on the peptide backbone. The final product was recrystallized from cold ether, washed thrice to remove impurities and dried under vacuum.

6.2.4 In vitro Stability in PBS Buffer and Rabbit Plasma

The stability of the fluorescein-labeled PEG-fMLF nanocarriers was tested in 10 mM PBS (pH 7.4) and rabbit plasma at 37 °C for 24 hours. The PEG-nanocarriers were incubated separately in 10 mM PBS (pH 7.4) or spiked rabbit plasma at 37°C. Aliquots were withdrawn at different time points and centrifuged at 14,000x *g* for 90 min with a Microcon™ filter (molecular weight cut-off = 3,000 Da) (Amicon Inc., Beverly, MA). The free fMLF cleaved from the PEG nanocarrier during the incubation passes through the filter whereas the fMLF that remains linked is retained. The eluents and retentates resulting from the different incubation time points were withdrawn and subjected to fluorescence detection. Each measurement was done in triplicate.

The stability of the tritiated PEG-fMLF nanocarriers was tested in 10 mM phosphate buffered saline (pH 7.4) and rabbit plasma at 37 °C. One mL solutions of [fMLFK(^{3}H)C]$_2$-mPEG$_{5K}$ and acetyl-C[AAK(PEG$_{5K}$-fMLFK [^{3}H]C)]$_4$-amide were prepared in PBS (pH 7.4) and plasma to a final concentration of 1 μCi/mL. Aliquots (200μL) were withdrawn after 24 hours incubation. The proteins in plasma were precipitated using 800 μL acetonitrile followed by vortexing for 1 min and centrifuged for 5 min at 6000×*g*. Supernatant (50 μL) was directly injected into the HPLC (HP 1100)

equipped with and β-ram radioisotope detector. The column was TSK-GEL G3000PW HPLC column (Tosoh Corp., Japan). The mobile phase was 100% ddH_2O and the flow rate was maintained at 1 mL/min. The decrease in the area of the nanocarrier peak was monitored in triplicate to assess loss due to instability.

6.2.5 Animals

Male Sprague Dawley rats (jugular vein cannulated, weighing 250-300 g, 2-3 months of age) were purchased from Hilltop Lab Animals, Inc (Scottdale, PA). Female FVB mice, 5 or 6 weeks of age, were purchased from Taconic Farms (Germantown, PA). Animals were maintained on a 12-h light/dark cycle and received laboratory chow and water *ad libitum.* Animals were housed three or four per cage and were allowed to acclimatize to the animal facility for a minimum of 3 days prior to use. These investigations were carried out under established federal regulations and animal protocols approved by the Rutgers University Institutional Animal Care and Use Committee for the care and use of laboratory animals.

6.2.6 Uptake by Mouse Peritoneal Macrophages

Female FVB mice were injected with 5 μl fluorescent PEG-fMLF nanocarriers i.p. and incubated with the peritoneal macrophages for 4 h. Four hours after injection, the mice were killed by cervical dislocation, and each was peritoneally injected with 5 mL of saline. The peritoneum of the mouse was massaged for 1 min and the solution inside the

abdominal cavity was withdrawn to recover peritoneal macrophages. Macrophages were washed 3 times with 1 mL of phosphate buffer. The total cell-associated fluorescence was then analyzed by flow cytometry using a Coulter EPICS PROFILE equipped with a 25 mW argon laser. For each analysis, 10,000 to 20, 000 events were accumulated.

6.2.7 Pharmacokinetic and Biodistribution Studies

Male Sprague Dawley rats (jugular vein cannulated, weighing 250-300 g, 2-3 months of age) were used for PK and biodistribution studies. The animals were dosed intravenously via a tail vein injection with the nanocarriers to be tested (dosing volume: 0.5-1 mL/kg). After dose administration, blood samples (~0.2-0.3 mL/sample) were collected from the catheter at selected time points (0, 1, 5, 10, 15, 30 min and 1, 2, 4, 8 and 24 hrs) for up to 24 hrs post dose. After each sample was taken, the catheter is flushed with ~0.3 mL sterile heparinized saline (50 IU/mL) to compensate for blood loss and to prevent the catheter from clotting. Urine and feces were also collected for up to 24 h. At the end of the study, animals were euthanized by intravenous injection of pentobarbital at 100 mg/kg. Selected tissues, such as brain, heart, intestines, liver, lung, spleen, and kidneys were harvested, rinsed with PBS to wash away blood attached around the organs and weighed. Then ~0.1 g tissue specimens were digested in 1 mL of Solvable at 55 °C in a water bath for 2 hrs and cooled to room temperature. Three aliquots of 0.3 mL of 30 % hydrogen peroxide were added to samples for decolorization. Scintillation cocktail was added to the decolorized samples, samples were vortexed and the radioactivity of each sample was determined using a liquid scintillation analyzer

LSC-3100. Each dose regimen was tested in 3 rats to achieve adequate statistical power. Plasma concentration-time data are analyzed with 2-compartment model methods using WinNonlin (Pharsight Corporation, Mountain View, CA).

6.2.8 Pharmacokinetic Analysis

To determine the disposition of PEG nanocarriers, the plasma concentration-time profile was analyzed using a two-compartment model (WinNonlin v 4.1, Pharsight Corp., Apex, NC, USA). The model can be expressed by equation 1 and Figure 6.3:

$$C(T)=A*EXP(-\alpha*T)+B*EXP(-\beta*T) \quad (1)$$

The pharmacokinetic parameter, A, B, α, and β in equation 1 were calculated by WinNonlin. The first-order transfer rate constant from a central compartment (1) to a peripheral compartment (2), k12, the first-order transfer rate constant from a peripheral compartment (2) to a central compartment (1), k21, the elimination constant from the central compartment (1), k10, and the distribution volume of central compartment V1 were calculated by WinNonlin. The half-life at the β-phase of the plasma concentration-time curve was calculated using the parameter β.

6.2.9 Statistical Analysis

All statistical tests were performed using GraphPad Instat (GraphPad Software, Inc., San Diego, CA). A minimal p-value of 0.05 was used as the significance level for all

tests. One-way analysis of variance and Tukey test was performed on the uptake data. All data are reported as means ± S.D. of three observations, unless otherwise noted. The graphs were plotted using GraphPad Prism 4.01 (GraphPad Software, Inc., San Diego, CA).

6.3 Results:

6.3.1 Design and Synthesis of PEG-fMLF Nanocarriers

PEG-fMLF nanocarriers $mPEG_{5K}$-fMLF, $mPEG_{5K}$-$(fMLF)_2$, PEG_{10K}-$(fMLF)_4$ were prepared by coupling the fMLFKC to $mPEG_{5K}$ -MAL, $mPEG_{5K}$ -$(MAL)_2$ and PEG_{10K} -$(NH_2)_4$ according to the procedures described above (Scheme 6.1). The novel peptide-backbone nanocarriers were prepared by coupling the peptide backbone, acetyl-Cys(thiopyridine)-(β-Ala-β-Ala-Lys-)$_4$–amide to a heterobifunctional PEG, NHS-PEG-VS. The NHS moiety of NHS-PEG-VS reacts specifically with ε-amine groups on lysines of the backbone peptide and the VS group is used for attachment of PEG to the sulfhydryl (SH) moiety of the fMLFKC peptide. The resulting linkages formed are amide (for NHS) or thioether (for VS) bonds between fMLFKC and the peptide backbone. Both bonds are highly stable under physiological conditions. All the nanocarriers were purified from low molecular weight contaminants using 3 kDa dialysis bags against ddH_2O for 2 days. The purified products were confirmed by SEC using a TSK G3000PW column and concentrations were determined by amino acid analysis. Amino acid analysis also

confirmed the presence of methionine, leucine, phenylalanine, lysine and cysteine at the expected ratio in the final bioconjugate.

The selected PEG-fMLF nanocarriers (Scheme 6.2) were labeled by tritium by reaction with N-succinnimidyl-[2, 3-^{3}H]-propionate and chased with cold propionic anhydride. The final product was recrystallized from cold ether, washed thrice to remove impurities and dried under air. The purified products were confirmed by SEC using HP1100 HPLC equipped with a TSK G3000PW column and β-ram radio-detector (Figure 6.1).

6.3.2 Stability of PEG-fMLF Nanocarriers

The stability of the fluorescein-labeled and tritium-labeled PEG-fMLF nanocarriers were tested in 10 mM phosphate buffered saline (pH 7.4) and rabbit plasma at 37 °C for 24 hours. For [fMLFK(^{3}H)C]$_2$-mPEG$_{5K}$, thioether bonds linked fMLFKC and mPEG$_{5k}$-(MAL)2 and an amide linked fMLFKC and tritium-labeled propionate. For acetyl-C[AAK(PEG$_{5k}$-fMLFK(^{3}H)C)]$_4$ -amide, an amide bond (derived from NHS) or thioether bond (derived from VS) linked fMLFKC and the peptide backbone. All bonds are highly stable under physiological conditions. Both nanocarriers were very stable in PBS and only 3.2% degraded in rabbit plasma during 24-hour incubation.

6.3.3 Uptake by Mouse Peritoneal Macrophages

Injection of PEG-fMLF nanocarriers into the peritoneal cavity of FVB mice was used to determine the *in vivo* macrophage uptake (Figure 6.2). The mice in this study

were not injected with thioglycol, and, therefore, the macrophages in the peritoneal cavity were not activated. PEG-fMLF enhanced macrophage uptake only about 3.8-fold ($p<0.05$) after 4 hours incubation at 37°C compared to the control PEG_{5k}. On the other hand, PEG_{5k}-$(fMLF)_2$ and PEG_{20k}-$(fMLF)_4$ increased uptake 11.3 and 23.6-fold ($p<0.01$), respectively, compared to the control PEG_{5k}. These results were not surprising since we have shown the enhanced uptake by the attachment of multiple copies of fMLF in differentiated U937 cells (Bioconj Chem 2007, submitted), as was previously noted for neutrophil-like differentiated HL-60 cells (*200*). It should be noted that the difference in uptake between the nanocarriers with one and two copies of fMLF was less than what was observed *in vitro* but the difference between two and four copies was larger than in cultured cells. These results suggested bioconjugate uptake is enhanced by higher levels of fMLF ligand per PEG nanocarrier in the *in vivo* settings relative to results *in vitro*. However, an effect of PEG size cannot be excluded as explaining this result. The observation that binding to peritoneal macrophage was significantly enhanced even with just one copy of fMLF is in direct contrast to the lower binding of such conjugates *in vitro* (Bioconj Chem 2007, submitted, (*200*)). We cannot exclude the possibility that the increased effect of one copy of fMLF and increased effect on a higher copy number of 4 may partially be due to binding to other cell types present in the mouse peritoneum.

6.3.4 Pharmacokinetic Studies

The elimination profile of the tritium-labeled control PEG and PEG-fMLF nanocarriers in blood after IV administration is shown in Figure 6.4. The experimental data fit well to the theoretical curve, indicating that the injected PEG nanocarriers were

eliminated in accordance with a two-compartment model disposition behavior. Table 6.1 summarizes the pharmacokinetic parameters of each nanocarrier calculated using a two-compartment model. The elimination profiles and pharmacokinetic analysis reveals a clear difference between nanocarriers with different molecular weights and between nanocarriers with and without fMLF. Both PEG_{5K} and PEG_{5K} -$(fMLF)_2$ were eliminated rapidly from the blood circulation, with half-lives at 14.6 min and 44.9 min, respectively. In the contrast, PEG_{20K} and PEG_{20K} -$(fMLF)_4$ circulated much longer than 5 kDa PEG nanocarriers, with half-lives at 452.9 min and 177.1 min, respectively. It should be noted that the attachment of two fMLF peptides to PEG_{5K} increased the half-life about 3-fold and the area under curve (AUC) about 2.2-fold, respectively, indicating longer plasma residence due to the appended peptides. On the other hand, the attachment of four fMLF peptides to PEG_{20K} decreased the half-life of this longer-persisting PEG by about 60% and AUC by 57%, respectively.

6.3.5 Biodistribution Studies

The tissue distribution of PEG-fMLF nanocarriers are shown as accumulation per gram of tissue in Figure 6.5 and the distribution in macrophage containing tissues were shown as the percentage of total dose in Table 6.2. For PEG molecules without fMLF, radioactivity in the blood was 11% for PEG_{5K} and 42% for PEG_{20K}, consistent with the reduced radioactivity in the urine for the smaller PEG_{5K} (65%) and larger PEG_{20K} (32%). PEG_{5K}-$(fMLF)_2$ showed 2-fold higher accumulation than PEG_{5K} in blood, and 5% less recovery in urine with no significant differences observed in the accumulation in other tissues. PEG_{20K}-$(fMLF)_4$ showed higher accumulation than PEG_{20K} in blood (1.56-fold),

liver (1.48-fold) and kidney(1.42-fold) but about 5% less in blood (Table 6.2). The distribution in macrophage-containing tissues revealed significant differences between nanocarriers with and without targeting peptide fMLF. PEG_{5K} accumulated in the lung, kidneys, liver, and to a lesser extend, in the intestine, spleen, heart and brain. The attachment of two copies of fMLF to PEG_{5K} increased the accumulation in major macrophage-containing organs such as kidneys (3.2-fold, $p<0.05$), spleen (6.9-fold, $p<0.05$), lung (1.5-fold) and liver (1.5-fold) but did not significantly affect the accumulation in brain, heart and intestine. The peptide-backbone PEG nanocarrier acetyl-C-$[AAK(PEG)]_4$–amide has molecular weight about 20 kDa and accumulated in the lung, kidneys, liver, and to a lesser extent, in the intestine, spleen, heart and brain. The attachment of four copies of fMLF to acetyl-C-$[AAK(PEG)]_4$–amide increased the accumulation in major macrophage-containing organs such as kidneys (3.3-fold, $p<0.05$), spleen (3.8-fold, $p<0.05$), lung (2.7-fold) and liver (2.8-fold) but did not significantly affect the accumulation in brain, heart and intestine.

6.4 Discussion:

The clinical potential of anti-HIV agents has been limited by a variety of factors such as drug toxicity for uninfected cells and development of drug resistance, which leads to sub-therapeutic drug levels and the formation of viral reservoirs. Better drug delivery and targeting technologies are required to specifically increase target cell exposure to these potent therapeutic agents. Therefore, drug delivery systems specifically targeted to

macrophage cell surface receptors could potentially improve therapeutic efficacy and minimize systemic toxicity of anti-HIV drugs.

Macrophages are considered the first line of defense in the immune response to foreign invaders and have been found to play an important role during HIV-1 infection as both primary targets and major viral reservoirs. Macrophages possess various receptors such as formyl peptide, mannose and Fc receptors, which potentially offer a targeting enhancing option via receptor-mediated endocytosis. A previous report by Pooyan et. al. illustrated the potential of PEG nanocarrier bearing multiple copies of fMLF for improving *in vitro* macrophage targeting (*200*). Recently, we studied the effects of various molecular features of PEG-fMLF nanocarriers such as the number of targeting peptides and PEG sizes on cell uptake in human macrophage-like differentiated U937 cells. The results suggest that appending only 2 copies of the ligand to the multifunctional nanocarrier is sufficient for optimal binding and the optimal size of the nanocarrier for improved macrophage uptake *in vitro* was about 20 kDa, which corresponds to a size of 20-60 nm. However, effective pharmacological targeting to macrophages requires further *in vivo* study since the major delivery advantages of PEG nanocarriers can only be observed *in vivo*.

Effective targeting to macrophages residing in tissues requires a balance of plasma clearance, tissue distribution, receptor binding and cell uptake. Maximizing the circulation half-life of nanocarriers in blood but avoiding a reduction in their penetration into macrophage tissue compartments becomes a significant challenge. Indeed the polymeric portion, which often represents the major part of the construct, is more exposed than the drug to the biological environment and, therefore, can influence the

interaction with biological structures and dictate body targeting and disposition. Their chemical and physical characters usually dictate new properties and fate of the conjugate in the body. Therefore, the biopharmaceutical properties of the conjugates must be carefully investigated since slight differences in polymer structure may be reflected on different therapeutic performance of the conjugates. Thus, our goal in this study was to elucidate the relationship between the *in vivo* dispositional properties and structural characteristics of PEG-fMLF nanocarriers.

PEG was chosen as the pharmaceutical carrier for macrophage-targeted drug delivery system due to its ability to extend elimination half-life, increase stability and decrease immunogenicity of PEGylated pharmaceuticals, especially protein and peptide therapeutics (*19-25*). It is known that the biopharmaceutical properties of PEG nanocarriers depends strictly on the physicochemical and biological properties of the components of the constructs (which in our study are polymers and targeting moieties), as well as on the properties of the whole nanocarrier (*210*). The presence of PEG plays an important role in defining the *in vivo* fate of nanocarriers. In the present study, we have shown that increasing molecular weight of PEG-fMLF nanocarriers from 5 kDa to 20 kDa significantly increased the plasma residence. However, studies of PEG in solution showed that each ethylene glycol sub-unit is tightly associated with two or three water molecules. The binding of water to PEG makes PEGylated compounds function as though they are 3 to 9 times larger than a corresponding soluble protein of similar molecular weight (*204, 205*). Clinically used PEG polymers with associated water molecules act like a shield to protect the attached drug from enzymatic degradation, inhibit interactions with cell surface proteins and provide increased size to prevent rapid

renal filtration and clearance. These “stealth” properties of PEG have proven to be very valuable in prolonging drug blood levels. However, the reduction of interaction with cell-surfaces due to PEG limits its use as a biomaterial for cell-surface or intracellular drug delivery and targeting. Therefore, the very property of PEGylation that has made it clinically useful and commercially successful also limits its application for drug/nanocarrier targeting to HIV reservoirs or sanctuary sites such as macrophages, the central nervous system and testis. However, the current results showed that by covalent conjugation of macrophage targeting moiety fMLF to PEG, it is possible to achieve a higher accumulation in macrophages residing in tissues.

A 20 kDa peptide-backbone PEG nanocarrier acetyl-Cys-[β-Ala-β-Ala-Lys(PEG_{5k}-fMLFKC]$_4$-amide with branched shape and multiple coupling sites was shown to be the optimal structures tested for facilitating the delivery of PEG-fMLF nanocarriers to the macrophage-residing tissues and its ability to circulate for a long period of time in the blood. A branched PEG 'acts' as if it were much larger than a corresponding linear PEG of the same molecular mass. A linear PEG is distributed throughout the body with larger distribution volume while a branched PEG is distributed with a smaller distribution volume and early on delivered to the liver and spleen (*137*). The increase in the hydrodynamic size of F(ab′)$_2$ form of a humanized anti-interleukin-8 (anti-IL-8) antibody was about 7-fold by adding one 20 kDa PEG and about 11-fold by adding one branched 40 kDa (*138*). The F(ab′)2 conjugate obtained by linking a single branched 40 kDa PEG was found to possess an apparent size of 1600 kDa (protein equivalent), greatly over the kidney ultrafiltration limit, and an AUC after intravenous administration 15.7 higher than the unmodified protein (*138*). Branched PEGs are also better at cloaking the attached

polypeptide drug from the immune system and proteolytic enzymes, thereby reducing its antigenicity and likelihood of destruction (*139*). The binding of branched 10 kDa PEG to asparaginase reduced the antigenic character of the protein about 10-fold as compared to the counterpart obtained by modification with 5 kDa PEG (*134*). These results are attributable to the higher molecular weight and "umbrella like" structure of the branched polymer, which efficiently prevents the approach of anti-protein antibodies and immunocompetent cells.

Macrophages possess various receptors such as formyl peptide receptors, mannose receptors, Fc receptors, complement and many other receptors (*148-150*). These macrophage surface receptors determine the control of activities such as activation, recognition, endocytosis, secretion etc. A useful approach for promoting the uptake of drugs or drug delivery systems by macrophages is to incorporate into drug conjugates ligands capable of interacting with macrophage surface receptors. A number of natural ligands for macrophage targeting have been explored. It was shown by Muller and Schuber that mannose residue-conjugated liposomes were associated to peritoneal macrophages and Kupffer cells in about 2–4 times greater amount than were plain unconjugated liposomes (*154*). The acetylated low density lipoprotein (AcLDL), a ligand for macrophage scavenger receptors, was conjugated to AZT and showed 10-fold more uptake than AZT alone by a murine macrophage cell line J774.A and a human macrophage cell line U937 (*129*). In the present study, the peptide fMLF was chosen as the targeting moiety for formyl peptide receptor on macrophages because: (i) formyl peptide receptors are specifically expressed on phagocytic cells such as macrophages, dendritic cells and neutrophils; (ii) fMLF specifically binds to formyl peptide receptors

on macrophages with high affinity; (iii) down-regulation of CCR5 co-receptor by fMLF could potentially inhibit the viral entry into macrophages, which could result in additional therapeutic effects for anti-HIV drugs targeted to FPR. The attachment of two or four fMLF residues significantly increased uptake in peritoneal macrophages. The pharmacokinetic properties and tissue distribution revealed further differences between nanocarriers with and without targeting peptide fMLF. However, the impact was different among PEG nanocarriers with different molecular weights. The 3-fold increase of the half-life $t_{1/2}$ by attachment of two fMLF peptides to PEG_{5K} could be because two fMLF residues increased molecular weight of the nanocarrier by about 1450 Da. But we can't rule out the possibility of enhanced interaction of PEG_{5K}-$(fMLF)_2$ with monocytes, neutrophils or other cells in blood, which might also increase the plasma residence and decrease the renal clearance. On the other hand, the 40% decrease of the half-life $t_{1/2}$ by attachment of four fMLF peptides to PEG_{20K} is consistent with the observed enhanced accumulation in macrophage-rich tissues such as liver, kidneys and spleen, which indicated a non-renal mechanism of clearance from the circulation. The results demonstrated that the attachment of macrophage targeting moiety (fMLF) to 5 kDa and 20 kDa PEG increases accumulation of PEG nanocarriers in target macrophage-rich tissues. This targeting ability, combined with the prolonged plasma residence of 20 kDa PEG, makes the acetyl-C-$[AAK(PEG_{5K}$-fMLF$)]_4$–amide the most promising nanocarrier tested for improving macrophage targeting *in vivo*, which has a well balanced circulation half-life of nanocarriers in blood and the penetration into macrophages residing in tissues.

6.5 Conclusions

In conclusion, we have characterized the *in vivo* peritoneal uptake, pharmacokinetics and biodistribution of PEG-fMLF nanocarriers. These studies demonstrated the increased accumulation of the PEG nanocarriers with multiple copies of fMLF in peritoneal macrophages and macrophages residing in other tissues (e.g. liver, kidneys and spleen). This targeting ability, combined with the prolonged plasma residence of 20 kDa PEG, makes the acetyl-C-[AAK(PEG_{5K}-fMLF)]$_4$–amide the most promising nanocarrier tested for improving macrophage targeting *in vivo*, which has a well balanced circulation half-life of nanocarriers in blood and the penetration into macrophages residing in tissues. Furthermore, the peptide-backbone PEG nanocarrier designed and evaluated in this study contains not only increased accumulation in macrophages but also a flexible structure, which leaves ample room to incorporate the anti-HIV agents as well as the potential for modulating size and/or numbers of targeting moieties for optimal drug delivery and therapeutic efficacy.

This novel macrophage targeting system could specifically deliver the anti-HIV agents to the HIV infected tissues and therefore improve therapeutic efficacy, minimize systemic toxicity and simplify administration regimens. However the potential toxicity of the PEG-fMLF nanocarriers *in vivo* needs to be further investigated although the *in vitro* studies indicated the relative safety of the nanocarriers. We will continue to develop the drug delivery system based the PEG-fMLF nanocarriers in order to improve regimens for delivery of anti-HIV agents, and ultimately improve HIV therapy.

Table 6.1 Pharmacokinetic parameters of the control PEGs and PEG-fMLF nanocarriers carrying two or four fMLF moieties after i.v. injection in rats. The pharmacokinetic parameters of the control PEGs and PEG-fMLF nanocarriers were calculated using a two-compartment model by WinNonlin V4.1. Means ± S.D. for three rats are shown for each value.

Parameter	Units	PEG5K	PEG5K-(fMLF)2	PEG20K	PEG20K-(fMLF)4
AUC	min*ug/mL	1004.4+/-186.8	2267.1+/-308.2	55220.3+/-19890.5	24493.3+/-3194.4
k10_HL	min	2.1+/-0.1	7.8+/-2.6	194.0+/-34.3	107.5+/-4.0
Alpha	1/min	0.50+/-0.06	0.27+/-0.10	0.06+/-0.01	0.17+/-0.02
Beta	1/min	0.05+/-0.01	0.02+/-0.01	0.0015+/-0.0002	0.0039+/-0.0001
Alpha_HL	min	1.3+/-0.1	2.8+/-1.0	11.4+/-1.0	4.0+/-0.4
Beta_HL	min	14.6+/-3.0	44.9+/-22.7	452.9+/-59.2	177.1+/-3.5
A	ug/mL	307.2+/-41.7	182.8+/-31.1	113.7+/-22.3	63.2+/-6.0
B	ug/mL	20.2+/-3.8	26.8+/-11.1	80.5+/-22.6	94.6+/-13.4
Cmax	ug/mL	327.5+/-45.5	209.5+/-42.2	194.2+/-44.6	157.8+/-19.0
CL	mL/min	2.64+/-0.49	0.69+/-0.09	0.05+/-0.02	0.11+/-0.01
AUMC	min*min*ug/mL	10544.7+/-5329.7	106099.5+/-62796.8	35699901.3+/-15901671.8	6162927.3+/-775158.7
MRT	min	10.181+/-3.4	45.3+/-21.5	631.3+/-86.2	251.7+/-4.8
Vss	mL	26.1+/-4.0	30.2+/-10.6	31.6+/-7.6	27.1+/-3.6
V2	mL	18.0+/-5.1	22.7+/-9.1	17.8+/-4.9	10.4+/-1.7

Table 6.2 Tissue distribution of control PEGs and PEG-fMLF nanocarriers carrying two or four fMLF moieties after i.v. injection in rats. Means ± S.D. for three rats are shown for each value. Tissue distribution in macrophage containing tissues were shown as the percentage of total dose.

Tissues	Percent Distribution (%)			
	PEG_{5k}	PEG_{5k} -$(fMLF)_2$	PEG_{20k}	PEG_{20k}-$(fMLF)_4$
Brain	0.04+/-0.02	0.01+/-0.00	0.17+/-0.04	0.05+/-0.02
Heart	0.06+/-0.02	0.03+/-0.01	0.36+/-0.07	0.39+/-0.08
Intestine	0.24+/-0.07	0.13+/-0.07	1.47+/-0.32	1.12+/-0.33
Liver	0.76+/-0.09	0.70+/-0.02	4.38+/-0.41	6.47+/-1.45
Lung	0.19+/-0.11	0.20+/-0.18	2.13+/-0.92	2.30+/-0.84
Kidney	0.17+/-0.04	0.33+/-0.11	0.84+/-0.13	1.19+/-0.60
Spleen	0.02+/-0.01	0.07+/-0.02	0.15+/-0.01	0.30+/-0.11
Urine	65.48+/-9.04	60.38+/-7.19	32.00+/-4.35	50.27+/-5.25
Feces	0.22+/-0.07	0.40+/-0.03	0.06+/-0.01	0.42+/-0.04
Blood *	11.06+/-2.90	22.22+/-3.67	41.76+/-4.23	36.47+/-4.85
Remaining**	21.76	15.53	16.68	1.02

* Blood is the sum of radioactivity of blood samples taken at different time points.

** Remaining is the sum of radioactivity in uncollected blood, carcass and other tissues.

Scheme 6.1 Synthesis schemes of fluorescein–labeled PEG-fMLF nanocarriers with 1 (Scheme 6.1A), 2 (Scheme 6.1B) and 4 (Scheme 6.1C) copies of fMLF.

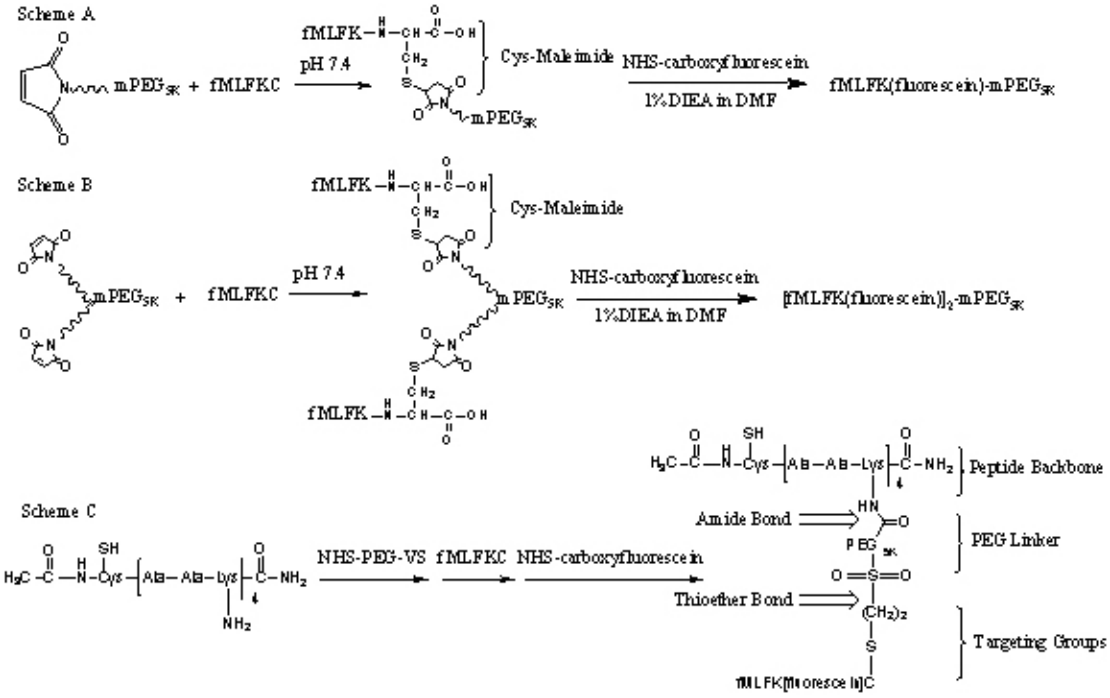

Scheme 6.2 Synthesis schemes of tritium-labeled PEG-fMLF nanocarriers with 2 (Scheme A) and 4 (Scheme B) copies of fMLF.

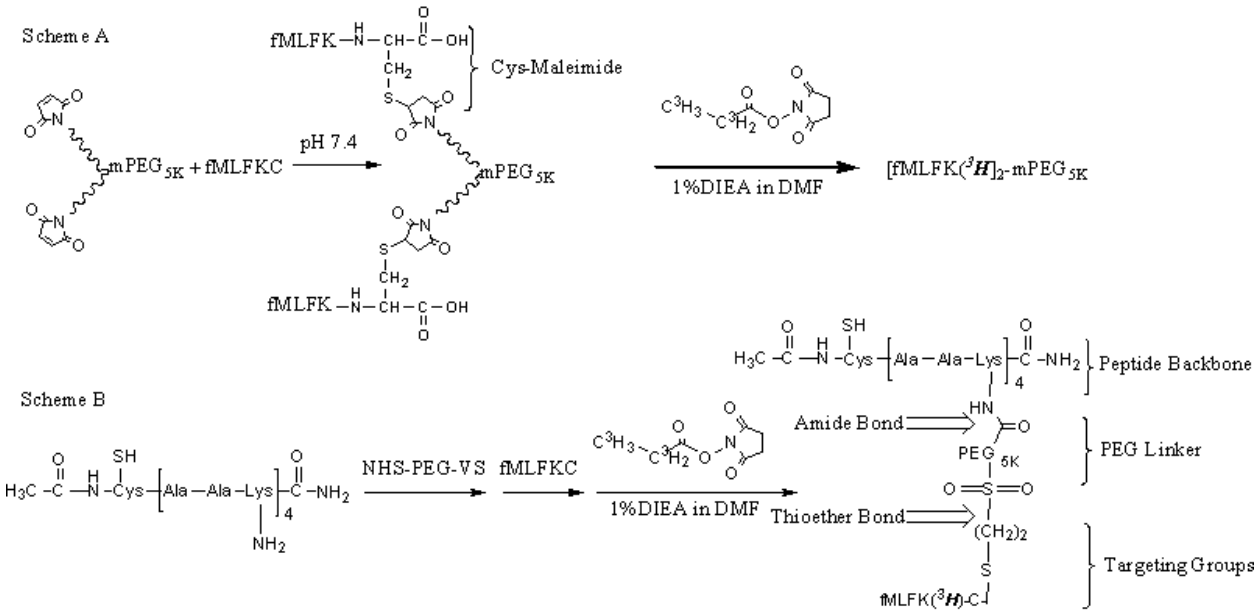

Figure 6.1 Size exclusion chromatography of tritium-labeled PEG-fMLF nanocarriers with 2(A) and 4 (Scheme B) copies of fMLF. The retention time was 14.9 min for [fMLFK(^{3}H)C]$_2$-mPEG$_{5K}$ and 13.9mins for acetyl-C[AAK(PEG$_{5K}$- fMLFK[^{3}H]C)]$_4$-amide.

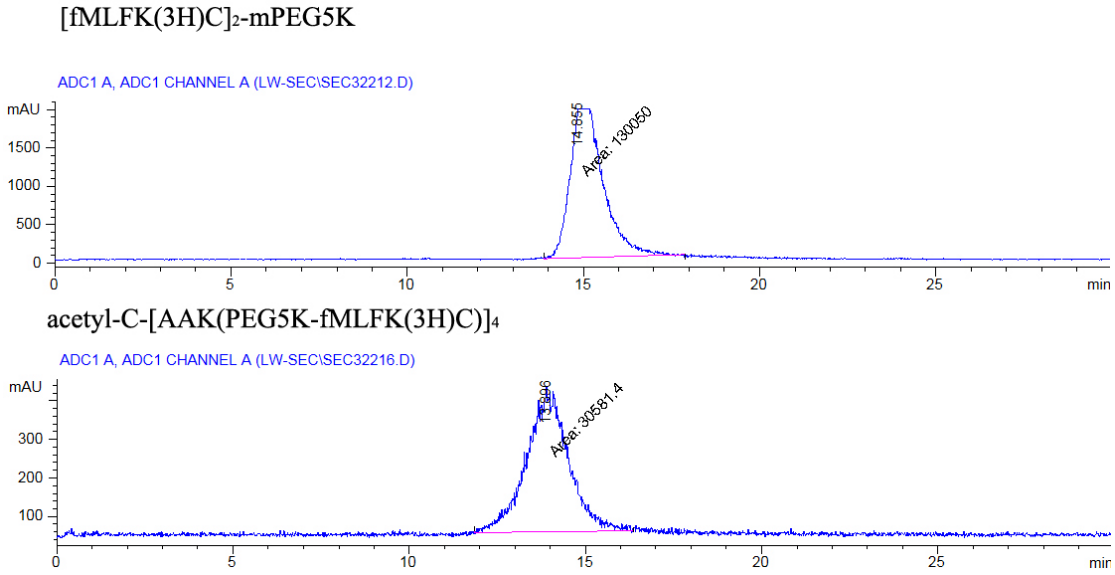

Figure 6.2 Uptake of PEG-fMLF nanocarriers in mice peritoneal macrophages at 37ºC after 4 hours incubation. Means ± S.D. for three experiments in mice are shown for each value. (* Statistically significant difference between the control PEG_{5K} and PEG-fMLF nanocarriers. $P<0.01$)

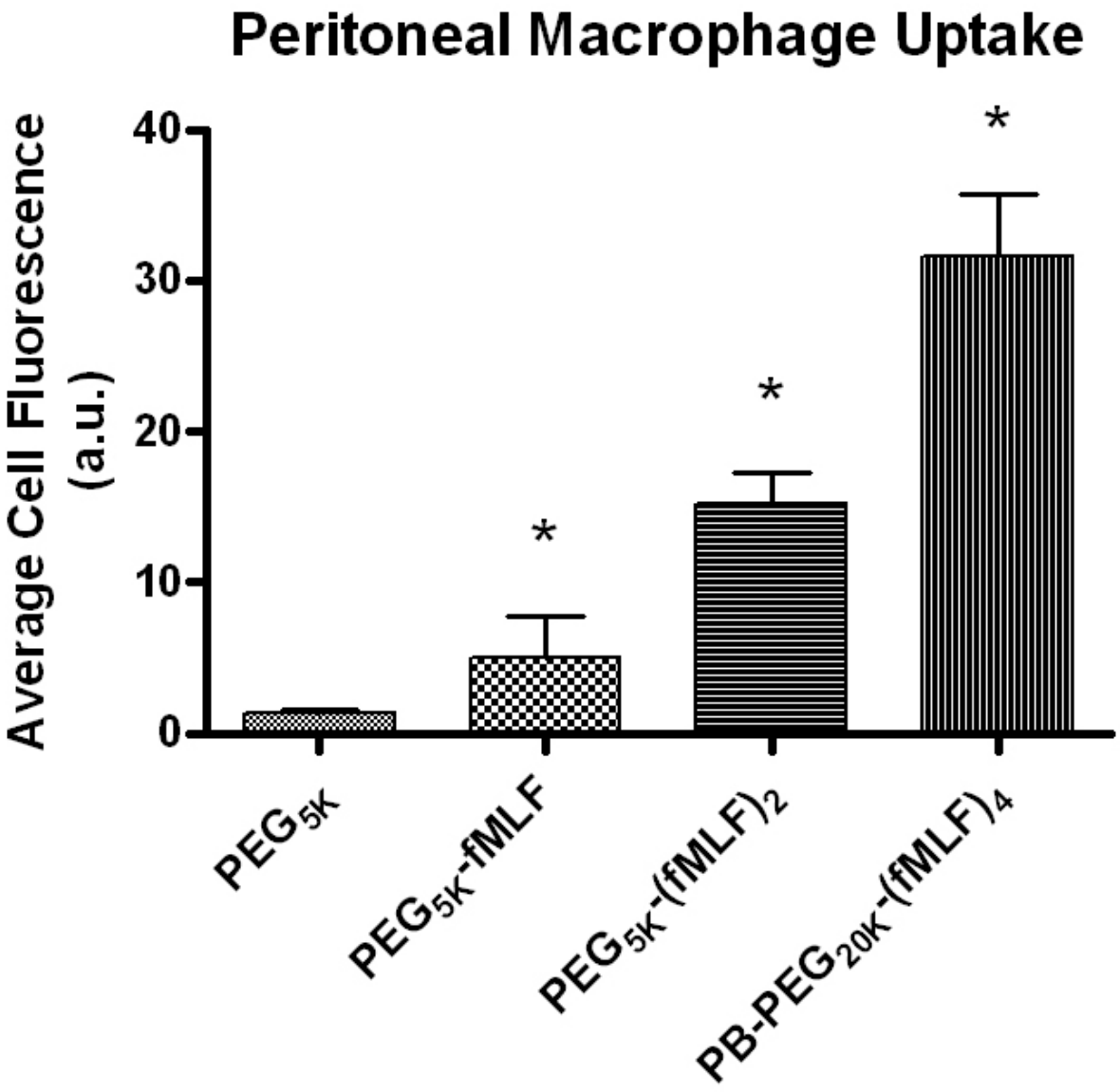

Figure 6.3 Two compartments model employed in the pharmacokinetic analysis of the blood concentration-time curve after i.v. injection by WinNonlin V4.1.

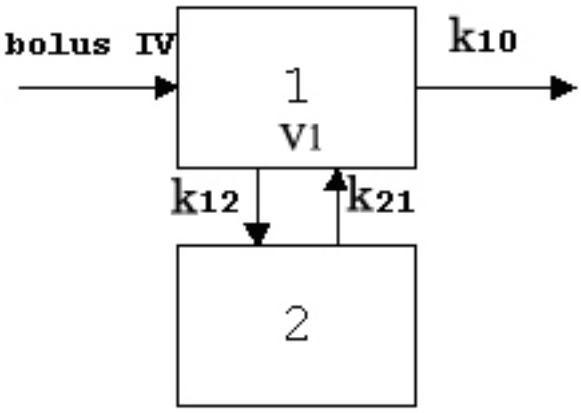

k12: The first-order transfer rate constant from a central compartment (1) to a peripheral compartment (2)

k21: the first-order transfer rate constant from a peripheral compartment (2) to a central compartment (1)

k10: the elimination constant from the central compartment (1)

V1 the distribution volume of central compartment

Figure 6.4 Plasma clearance of control PEGs and PEG-fMLF nanocarriers carrying two or four fMLF moieties in rats after i.v. injection. Means ± S.D. for rats are shown for each value.

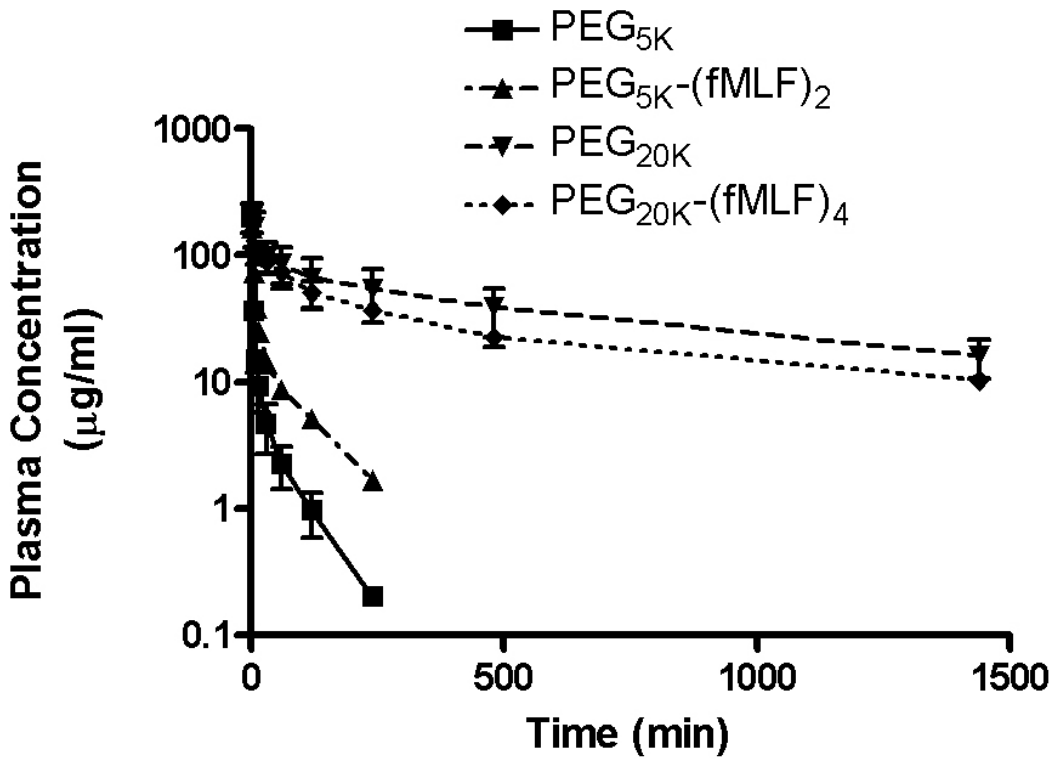

Figure 6.5 Tissue distribution of control PEGs and PEG-fMLF nanocarriers carrying two or four fMLF moieties in rats after i.v. injection. Means ± S.D. for three experiments in rats are shown for each value. (* $p<0.05$)

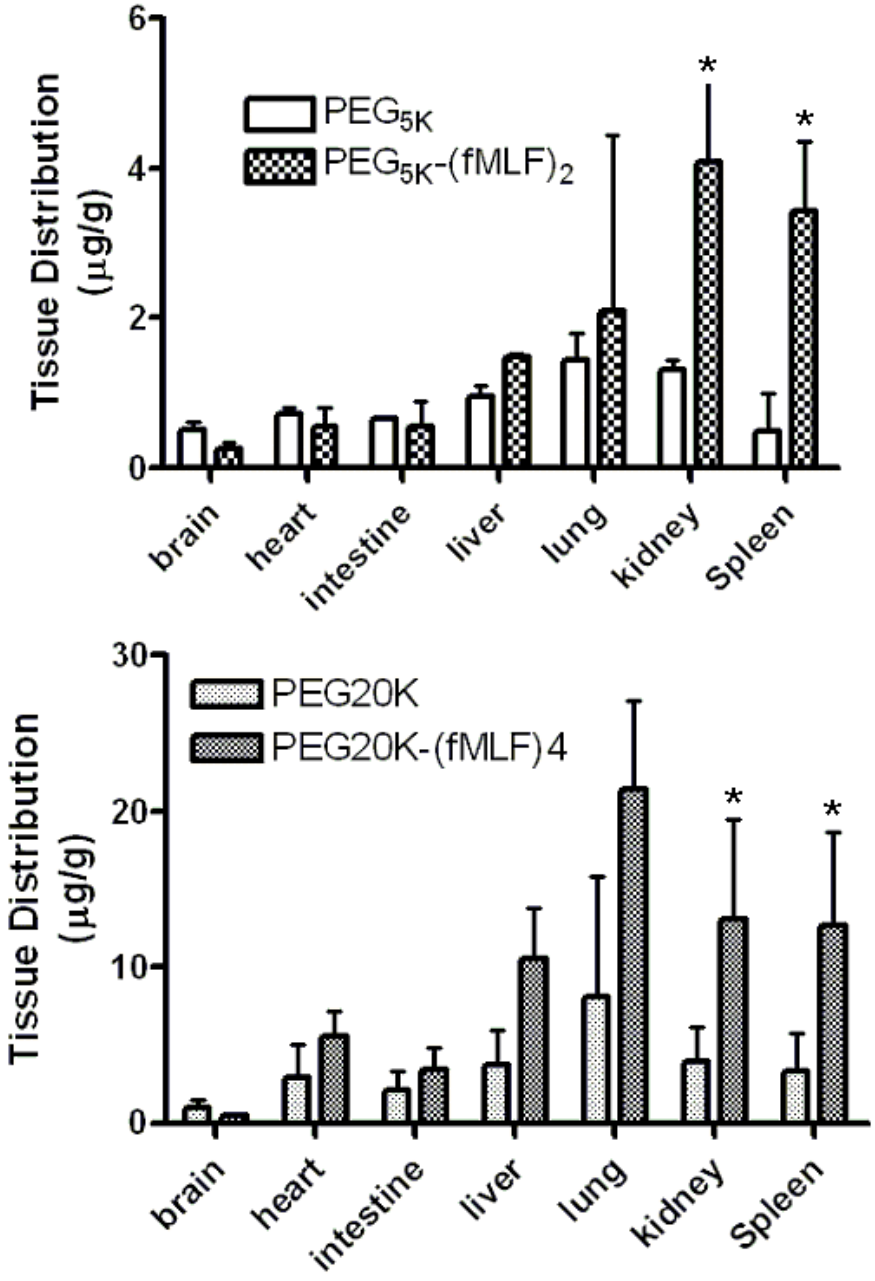

CHAPTER 7

SUMMARY AND CONCLUSIONS

Significant advances in antiretroviral drug therapy have been made with the advent of HAART (*3*), a multiple drug treatment regimen. Current anti-AIDS therapeutic agents and treatment regimens can provide a dramatically improved quality of life for HIV-positive people, many of whom have no detectable viral load for prolonged periods of time. Despite these advances, curing HIV infection has remained an elusive goal due to many challenges including low and fluctuating drug concentrations due to poor drug absorption or patient non-adherence (*4*), the presence of viral reservoirs and sanctuary sites (*5*), and drug toxicity due to the chronic therapy (*193*). Our long-term goal has been to develop nanotechnology-based drug delivery systems that can improve therapy by more precisely delivering effective drug concentrations to target cells including those in viral reservoirs and sanctuary sites. The theme of the current study is to investigate the value of combining AIDS drugs and modifiers of cellular uptake into macromolecular nanocarriers having novel pharmacological properties.

In Chapters 3 and 4, bioconjugates were prepared from different combinations of the approved drug, saquinavir, the antiviral and cell-penetrating moiety agent, R.I.CK-Tat9, the polymeric carrier, polyethylene glycol (PEG) and the cell uptake enhancer, biotin. Anti-HIV activities were measured in MT-2 cells, an HTLV-1-transformed human lymphoid cell line, infected with HIV-1 strain Vbu 3, while parallel studies were performed in uninfected cells to determine cellular toxicity. We showed that the retro-

inverso peptide R.I.CK-Tat9 was 60 times more potent than protease-sensitive L-Tat9, while the addition of biotin to R.I.CK-Tat9 resulted in an agent that was 2850 times more potent than L-Tat9. Flow cytometry and confocal microscopy studies suggest that effects on intracellular uptake and intracellular localization, as well as synergistic inhibitory effects of SQV and Tat peptides, contributed to substantial differences in antiviral activity. Our results demonstrate that highly potent nanoscale multi-drug nanocarriers with low non-specific toxicity can be produced by combining moieties with anti-HIV agents acting on different targets on macromolecules having improved delivery properties.

It is clear that macrophages are not only the primary target of HIV infection in patients but are an important source, in addition to $CD4^+$ T-lymphocytes, of HIV persistence during HAART. Therefore, drug delivery to tissue macrophages represents a key challenge for eradicating HIV. Better drug delivery is needed to suppress viral replication inside macrophages in order to improve anti-HIV therapy. Macrophages possess various receptors such as formyl peptide, mannose and Fc receptors, which potentially offer a targeting enhancing option via receptor-mediated endocytosis. In Chapter 5, we characterized the relationship between various molecular features of PEG-fMLF nanocarriers such as the number of targeting peptides and PEG sizes and cell uptake using human macrophage-like differentiated U937 cells. The results suggest that two fMLF residues are adequate for achieving optimal targeting and 20 kDa may be the optimal PEG size for improved macrophage uptake *in vitro*. Furthermore, novel peptide-backbone PEG nanocarriers with flexible structural characteristics were designed and synthesized to probe nanocarrier structural requirements for optimal macrophage

targeting and uptake. Peptide-backbone PEG-fMLF nanocarriers demonstrated their ability of targeting and be taken up by differentiated U937 cells, and in addition displayed other advantages over PEGylated systems derived from commercially available PEGs. However, effective pharmacological targeting to macrophages requires further *in vivo* study since the major delivery advantages of PEG nanocarriers can only be observed *in vivo*.

In Chapter 6, *in vivo* peritoneal macrophage uptake, pharmacokinetic and biodistribution were further investigated. FVB mice were injected i.p. with different fluorescein-labeled PEG-fMLF nanocarriers and recovered peritoneal macrophages revealed that the attachment of two and four copies of fMLF significantly enhanced the uptake compared to control PEG and PEG with one copy of fMLF. These results demonstrated that PEG-fMLF nanocarriers could be utilized to enhance delivery to peritoneal macrophages. The pharmacokinetic properties and tissue distribution revealed further differences between nanocarriers with and without targeting peptide fMLF. However, the impact was different among PEG nanocarriers with different molecular weights. The 3-fold increase of the half-life $t_{1/2}$ by attachment of two fMLF peptides to PEG_{5K} could be because two fMLF residues increased molecular weight of the nanocarrier by about 1450 Da. But we can't rule out the possibility of enhanced interaction of PEG_{5K}-$(fMLF)_2$ with monocytes, neutrophils or other cells in blood, which might also increase the plasma residence and decrease the renal clearance. On the other hand, the 40% decrease of the half-life $t_{1/2}$ by attachment of four fMLF peptides to PEG_{20K} is consistent with the observed enhanced accumulation in macrophage-rich tissues such as liver, kidneys and spleen, which indicated a non-renal mechanism of

clearance from the circulation. The results demonstrated that the attachment of macrophage targeting moiety (fMLF) to 5 kDa and 20 kDa PEG increases accumulation of PEG nanocarriers in target macrophage-rich tissues. This targeting ability, combined with the prolonged plasma residence of 20 kDa PEG, makes the acetyl-C-[AAK(PEG_{5K}-fMLF)]$_4$–amide the most promising nanocarrier tested for improving macrophage targeting *in vivo*, which has a well balanced circulation half-life of nanocarriers in blood and the penetration into macrophages residing in tissues.

In summary, macrophage-targeted PEG-fMLF nanocarriers were successfully designed, synthesized and evaluated *in vivo*. The attachment of multiple copies of fMLF led to increased peritoneal macrophage uptake and accumulation in macrophage-rich tissues. The current studies demonstrated the feasibility of using macrophage-targeted nanocarriers for enhancing specific drug uptake in macrophages. This novel macrophage targeting system could sepecifically deliver the anti-HIV agents to the HIV infected tissues and therefore improve therapeutic efficacy, minimize systemic toxicity and simplify administration regimens. However the potential toxicity of the PEG-fMLF nanocarriers *in vivo* needs to be further investigated although the *in vitro* studies indicated the relative safety of the nanocarriers. We will continue to develop the drug delivery system based the PEG-fMLF nanocarriers in order to improve regimens for delivery of anti-HIV agents, and ultimately improve HIV therapy.

8. Bibliography

(1) Autran, B., Carcelain, G., Li, T. S., Blanc, C., Mathez, D., Tubiana, R., Katlama, C., Debre, P., and Leibowitch, J. (1997) Positive effects of combined antiretroviral therapy on CD4+ T cell homeostasis and function in advanced HIV disease. *Science 277*, 112-6.

(2) Ferrando, S., van Gorp, W., McElhiney, M., Goggin, K., Sewell, M., and Rabkin, J. (1998) Highly active antiretroviral treatment in HIV infection: benefits for neuropsychological function. *Aids 12*, F65-70.

(3) Vandamme, A. M., Van Vaerenbergh, K., and De Clercq, E. (1998) Anti-human immunodeficiency virus drug combination strategies. *Antivir Chem Chemother 9*, 187-203.

(4) Bangsberg, D. R., Hecht, F. M., Charlebois, E. D., Zolopa, A. R., Holodniy, M., Sheiner, L., Bamberger, J. D., Chesney, M. A., and Moss, A. (2000) Adherence to protease inhibitors, HIV-1 viral load, and development of drug resistance in an indigent population. *AIDS 14*, 357-66.

(5) Schrager, L. K., and D'Souza, M. P. (1998) Cellular and anatomical reservoirs of HIV-1 in patients receiving potent antiretroviral combination therapy. *Jama 280*, 67-71.

(6) Carr, A., Samaras, K., Burton, S., Law, M., Freund, J., Chisholm, D. J., and Cooper, D. A. (1998) A syndrome of peripheral lipodystrophy, hyperlipidaemia and insulin resistance in patients receiving HIV protease inhibitors. *Aids 12*, F51-8.

(7) Safrin, S., and Grunfeld, C. (1999) Fat distribution and metabolic changes in patients with HIV infection. *Aids 13*, 2493-505.

(8) Chun, T. W., Stuyver, L., Mizell, S. B., Ehler, L. A., Mican, J. A., Baseler, M., Lloyd, A. L., Nowak, M. A., and Fauci, A. S. (1997) Presence of an inducible HIV-1 latent reservoir during highly active antiretroviral therapy. *Proc.Natl.Acad.Sci.U.S.A 94*, 13193.

(9) Flexner, C. (1998) HIV-protease inhibitors. *N Engl J Med 338*, 1281-92.

(10) Gartner, S., Markovits, P., Markovitz, D. M., Kaplan, M. H., Gallo, R. C., and Popovic, M. (1986) The role of mononuclear phagocytes in HTLV-III/LAV infection. *Science 233*, 215-9.

(11) Ho, D. D., Rota, T. R., and Hirsch, M. S. (1986) Infection of monocyte/macrophages by human T lymphotropic virus type III. *J Clin Invest 77*, 1712-5.

(12) Koenig, S., Gendelman, H. E., Orenstein, J. M., Dal Canto, M. C., Pezeshkpour, G. H., Yungbluth, M., Janotta, F., Aksamit, A., Martin, M. A., and Fauci, A. S. (1986) Detection of AIDS virus in macrophages in brain tissue from AIDS patients with encephalopathy. *Science 233*, 1089.

(13) Meltzer, M. S., Nakamura, M., Hansen, B. D., Turpin, J. A., Kalter, D. C., and Gendelman, H. E. (1990) Macrophages as susceptible targets for HIV infection, persistent viral reservoirs in tissue, and key immunoregulatory cells that control levels of virus replication and extent of disease. *AIDS Res. Hum. Retroviruses 6*, 967-71.

(14) Perno, C. F., Newcomb, F. M., Davis, D. A., Aquaro, S., Humphrey, R. W., Calio, R., and Yarchoan, R. (1998) Relative potency of protease inhibitors in monocytes/macrophages acutely and chronically infected with human immunodeficiency virus. *J Infect Dis 178*, 413-22.

(15) Kim, R. B., Fromm, M. F., Wandel, C., Leake, B., Wood, A. J., Roden, D. M., and Wilkinson, G. R. (1998) The drug transporter P-glycoprotein limits oral absorption and brain entry of HIV-1 protease inhibitors. *J Clin Invest 101*, 289-94.

(16) Langer, R. (1998) Drug delivery and targeting. *Nature 392*, 5-10.

(17) Langer, R. (2001) Drug delivery. Drugs on target. *Science 293*, 58-9.

(18) Torchilin, V. P. (2000) Drug targeting. *Eur J Pharm Sci 11 Suppl 2*, S81-91.

(19) Kozlowski, A., and Harris, J. M. (2001) Improvements in protein PEGylation: pegylated interferons for treatment of hepatitis C. *J Control Release 72*, 217-24.

(20) Harris, J. M., Martin, N. E., and Modi, M. (2001) Pegylation: a novel process for modifying pharmacokinetics. *Clin Pharmacokinet 40*, 539-51.

(21) Kozlowski, A., Charles, S. A., and Harris, J. M. (2001) Development of pegylated interferons for the treatment of chronic hepatitis C. *BioDrugs 15*, 419-29.

(22) Conover, C. D., Greenwald, R. B., Pendri, A., Gilbert, C. W., and Shum, K. L. (1998) Camptothecin delivery systems: enhanced efficacy and tumor accumulation of camptothecin following its conjugation to polyethylene glycol via a glycine linker. *Cancer Chemother Pharmacol 42*, 407-14.

(23) Greenwald, R. B. (2001) PEG drugs: an overview. *J Control Release 74*, 159-71.

(24) Greenwald, R. B., Choe, Y. H., McGuire, J., and Conover, C. D. (2003) Effective drug delivery by PEGylated drug conjugates. *Adv Drug Deliv Rev 55*, 217-50.

(25) Roberts, M. J., Bentley, M. D., and Harris, J. M. (2002) Chemistry for peptide and protein PEGylation. *Adv Drug Deliv Rev 54*, 459-76.

(26) UNAIDS. (2006) in *Report on the global AIDS epidemic*

(27) Organization, J. U. N. P. o. H. A. a. W. H. (2000) (UNAIDS/WHO, Ed.), Geneva, 2000.

(28) Barre-Sinoussi, F., Chermann, J. C., Rey, F., Nugeyre, M. T., Chamaret, S., Gruest, J., Dauguet, C., Axler-Blin, C., Vezinet-Brun, F., Rouzioux, C., Rozenbaum, W., and Montagnier, L. (1983) Isolation of a T-lymphotropic retrovirus from a patient at risk for acquired immune deficiency syndrome (AIDS). *Science 220*, 868-71.

(29) Gallo, R. C., Sarin, P. S., Gelmann, E. P., Robert-Guroff, M., Richardson, E., Kalyanaraman, V. S., Mann, D., Sidhu, G. D., Stahl, R. E., Zolla-Pazner, S., Leibowitch, J., and Popovic, M. (1983) Isolation of human T-cell leukemia virus in acquired immune deficiency syndrome (AIDS). *Science 220*, 865-7.

(30) Dalgleish, A. G., Beverley, P. C., Clapham, P. R., Crawford, D. H., Greaves, M. F., and Weiss, R. A. (1984) The CD4 (T4) antigen is an essential component of the receptor for the AIDS retrovirus. *Nature 312*, 763.

(31) Doranz, B. J., Berson, J. F., Rucker, J., and Doms, R. W. (1997) Chemokine receptors as fusion cofactors for human immunodeficiency virus type 1 (HIV-1). *Immunol Res 16*, 15-28.

(32) Schuitemaker, H., Kootstra, N. A., de Goede, R. E., de Wolf, F., Miedema, F., and Tersmette, M. (1991) Monocytotropic human immunodeficiency virus type 1 (HIV-1) variants detectable in all stages of HIV-1 infection lack T-cell line tropism and syncytium-inducing ability in primary T-cell culture. *J Virol 65*, 356-63.

(33) Aquaro, S., Calio, R., Balzarini, J., Bellocchi, M. C., Garaci, E., and Perno, C. F. (2002) Macrophages and HIV infection: therapeutical approaches toward this strategic virus reservoir. *Antiviral Res. 55*, 209.

(34) Ahsan, F., Rivas, I. P., Khan, M. A., and Torres Suarez, A. I. (2002) Targeting to macrophages: role of physicochemical properties of particulate carriers--liposomes and microspheres--on the phagocytosis by macrophages. *J Control Release 79*, 29-40.

(35) Igarashi, T., Brown, C. R., Endo, Y., Buckler-White, A., Plishka, R., Bischofberger, N., Hirsch, V., and Martin, M. A. (2001) Macrophage are the principal reservoir and sustain high virus loads in rhesus macaques after the depletion of CD4+ T cells by a highly pathogenic simian immunodeficiency virus/HIV type 1 chimera (SHIV): Implications for HIV-1 infections of humans. *Proc Natl Acad Sci U S A 98*, 658-63.

(36) Marras, D., Bruggeman, L. A., Gao, F., Tanji, N., Mansukhani, M. M., Cara, A., Ross, M. D., Gusella, G. L., Benson, G., D'Agati, V. D., Hahn, B. H., Klotman, M. E., and Klotman, P. E. (2002) Replication and compartmentalization of HIV-1 in kidney epithelium of patients with HIV-associated nephropathy. *Nat Med 8*, 522-6.

(37) Price, R. W., Brew, B., Sidtis, J., Rosenblum, M., Scheck, A. C., and Cleary, P. (1988) The brain in AIDS: central nervous system HIV-1 infection and AIDS dementia complex. *Science 239*, 586-92.

(38) Ho, D. D., Rota, T. R., Schooley, R. T., Kaplan, J. C., Allan, J. D., Groopman, J. E., Resnick, L., Felsenstein, D., Andrews, C. A., and Hirsch, M. S. (1985) Isolation of HTLV-III from cerebrospinal fluid and neural tissues of patients with neurologic syndromes related to the acquired immunodeficiency syndrome. *N Engl J Med 313*, 1493-7.

(39) Stebbing, J., Gazzard, B., and Douek, D. C. (2004) Where does HIV live? *N Engl J Med 350*, 1872-80.

(40) Crowe, S. M., and Sonza, S. (2000) HIV-1 can be recovered from a variety of cells including peripheral blood monocytes of patients receiving highly active antiretroviral therapy: a further obstacle to eradication. *J Leukoc Biol 68*, 345-50.

(41) Sonza, S., Mutimer, H. P., Oelrichs, R., Jardine, D., Harvey, K., Dunne, A., Purcell, D. F., Birch, C., and Crowe, S. M. (2001) Monocytes harbour replication-competent, non-latent HIV-1 in patients on highly active antiretroviral therapy. *AIDS 15*, 17-22.

(42) Detels, R., Munoz, A., McFarlane, G., Kingsley, L. A., Margolick, J. B., Giorgi, J., Schrager, L. K., and Phair, J. P. (1998) Effectiveness of potent antiretroviral therapy on time to AIDS and death in men with known HIV infection duration. Multicenter AIDS Cohort Study Investigators. *Jama 280*, 1497-503.

(43) Gulick, R. M., Mellors, J. W., Havlir, D., Eron, J. J., Gonzalez, C., McMahon, D., Richman, D. D., Valentine, F. T., Jonas, L., Meibohm, A., Emini, E. A., and Chodakewitz, J. A. (1997) Treatment with indinavir, zidovudine, and lamivudine in adults with human immunodeficiency virus infection and prior antiretroviral therapy. *N Engl J Med 337*, 734-9.

(44) Hammer, S. M., Squires, K. E., Hughes, M. D., Grimes, J. M., Demeter, L. M., Currier, J. S., Eron, J. J., Jr., Feinberg, J. E., Balfour, H. H., Jr., Deyton, L. R., Chodakewitz, J. A., and Fischl, M. A. (1997) A controlled trial of two nucleoside analogues plus indinavir in persons with human immunodeficiency virus infection and CD4 cell counts of 200 per cubic millimeter or less. AIDS Clinical Trials Group 320 Study Team. *N Engl J Med 337*, 725-33.

(45) Palella, F. J., Jr., Delaney, K. M., Moorman, A. C., Loveless, M. O., Fuhrer, J., Satten, G. A., Aschman, D. J., and Holmberg, S. D. (1998) Declining morbidity and mortality among patients with advanced human immunodeficiency virus infection. HIV Outpatient Study Investigators. *N Engl J Med 338*, 853-60.

(46) Vittinghoff, E., Scheer, S., O'Malley, P., Colfax, G., Holmberg, S. D., and Buchbinder, S. P. (1999) Combination antiretroviral therapy and recent declines in AIDS incidence and mortality. *J Infect Dis 179*, 717-20.

(47) Dore, G. J., Brown, T., Tarantola, D., and Kaldor, J. M. (1998) HIV and AIDS in the Asia-Pacific region: an epidemiological overview. *AIDS 12 Suppl B*, S1-10.

(48) Miller, V., Mocroft, A., Reiss, P., Katlama, C., Papadopoulos, A. I., Katzenstein, T., van Lunzen, J., Antunes, F., Phillips, A. N., and Lundgren, J. D. (1999) Relations among CD4 lymphocyte count nadir, antiretroviral therapy, and HIV-1 disease progression: results from the EuroSIDA study. *Ann Intern Med 130*, 570-7.

(49) Lin, J. H. (1997) Human immunodeficiency virus protease inhibitors. From drug design to clinical studies. *Adv Drug Deliv Rev 27*, 215-233.

(50) Debouck, C. (1992) The HIV-1 protease as a therapeutic target for AIDS. *AIDS Res.Hum.Retroviruses 8*, 153.

(51) Roberts, N. A., Martin, J. A., Kinchington, D., Broadhurst, A. V., Craig, J. C., Duncan, I. B., Galpin, S. A., Handa, B. K., Kay, J., and Krohn, A. (1990) Rational design of peptide-based HIV proteinase inhibitors. *Science 248*, 358.

(52) Aungst, B. J. (1999) P-glycoprotein, secretory transport, and other barriers to the oral delivery of anti-HIV drugs. *Adv Drug Deliv Rev 39*, 105-116.

(53) Sinko, P. J., Kunta, J. R., Usansky, H. H., and Perry, B. A. (2004) Differentiation of gut and hepatic first pass metabolism and secretion of saquinavir in ported rabbits. *J Pharmacol Exp Ther 310*, 359-66.

(54) Sawchuk, R. J., and Yang, Z. (1999) Investigation of distribution, transport and uptake of anti-HIV drugs to the central nervous system. *Adv Drug Deliv Rev 39*, 5-31.

(55) Williams, G. C., Liu, A., Knipp, G., and Sinko, P. J. (2002) Direct evidence that saquinavir is transported by multidrug resistance-associated protein (MRP1) and canalicular multispecific organic anion transporter (MRP2). *Antimicrob.Agents Chemother. 46*, 3456-3462.

(56) Jones, K., Bray, P. G., Khoo, S. H., Davey, R. A., Meaden, E. R., Ward, S. A., and Back, D. J. (2001) P-Glycoprotein and transporter MRP1 reduce HIV protease inhibitor uptake in CD4 cells: potential for accelerated viral drug resistance? *Aids 15*, 1353-8.

(57) Doranz, B. J., Grovit-Ferbas, K., Sharron, M. P., Mao, S. H., Goetz, M. B., Daar, E. S., Doms, R. W., and O'Brien, W. A. (1997) A small-molecule inhibitor

directed against the chemokine receptor CXCR4 prevents its use as an HIV-1 coreceptor. *J Exp Med 186*, 1395-400.

(58) O'Brien, W. A., Sumner-Smith, M., Mao, S. H., Sadeghi, S., Zhao, J. Q., and Chen, I. S. (1996) Anti-human immunodeficiency virus type 1 activity of an oligocationic compound mediated via gp120 V3 interactions. *J Virol 70*, 2825-31.

(59) Baba, M., Nishimura, O., Kanzaki, N., Okamoto, M., Sawada, H., Iizawa, Y., Shiraishi, M., Aramaki, Y., Okonogi, K., Ogawa, Y., Meguro, K., and Fujino, M. (1999) A small-molecule, nonpeptide CCR5 antagonist with highly potent and selective anti-HIV-1 activity. *Proc Natl Acad Sci U S A 96*, 5698-703.

(60) Kilby, J. M., Hopkins, S., Venetta, T. M., DiMassimo, B., Cloud, G. A., Lee, J. Y., Alldredge, L., Hunter, E., Lambert, D., Bolognesi, D., Matthews, T., Johnson, M. R., Nowak, M. A., Shaw, G. M., and Saag, M. S. (1998) Potent suppression of HIV-1 replication in humans by T-20, a peptide inhibitor of gp41-mediated virus entry. *Nat Med 4*, 1302-7.

(61) Wild, C. T., Shugars, D. C., Greenwell, T. K., McDanal, C. B., and Matthews, T. J. (1994) Peptides corresponding to a predictive alpha-helical domain of human immunodeficiency virus type 1 gp41 are potent inhibitors of virus infection. *Proc Natl Acad Sci U S A 91*, 9770-4.

(62) Castagna, A., Biswas, P., Beretta, A., and Lazzarin, A. (2005) The appealing story of HIV entry inhibitors : from discovery of biological mechanisms to drug development. *Drugs 65*, 879-904.

(63) Perno, C. F., Santoro, N., Balestra, E., Aquaro, S., Cenci, A., Lazzarino, G., Di Pierro, D., Tavazzi, B., Balzarini, J., Garaci, E., Grimaldi, S., and Calio, R. (1997) Red blood cells mediated delivery of 9-(2-phosphonylmethoxyethyl)adenine to primary macrophages: efficiency metabolism and activity against human immunodeficiency virus or herpes simplex virus. *Antiviral Res. 33*, 153.

(64) Choudhury, I., Wang, J., Rabson, A. B., Stein, S., Pooyan, S., Stein, S., and Leibowitz, M. J. (1998) Inhibition of HIV-1 replication by a Tat RNA-binding domain peptide analog. *J.Acquir.Immune.Defic.Syndr.Hum.Retrovirol. 17*, 104.

(65) Hamy, F., Brondani, V., Florsheimer, A., Stark, W., Blommers, M. J., and Klimkait, T. (1998) A new class of HIV-1 Tat antagonist acting through Tat-TAR inhibition. *Biochemistry 37*, 5086-95.

(66) Meltzer, M. S., Nakamura, M., Hansen, B. D., Turpin, J. A., Kalter, D. C., and Gendelman, H. E. (1990) Macrophages as susceptible targets for HIV infection, persistent viral reservoirs in tissue, and key immunoregulatory cells that control levels of virus replication and extent of disease. *AIDS Res Hum Retroviruses 6*, 967-71.

(67) Jeang, K. T., Xiao, H., and Rich, E. A. (1999) Multifaceted activities of the HIV-1 transactivator of transcription, Tat. *J.Biol.Chem. 274*, 28837.

(68) Kaushik, N., Basu, A., Palumbo, P., Myers, R. L., and Pandey, V. N. (2002) Anti-TAR polyamide nucleotide analog conjugated with a membrane-permeating peptide inhibits human immunodeficiency virus type 1 production. *J.Virol. 76*, 3881.

(69) Richter, S. N., and Palu, G. (2006) Inhibitors of HIV-1 Tat-mediated transactivation. *Curr Med Chem 13*, 1305-15.

(70) Hauber, J., Malim, M. H., and Cullen, B. R. (1989) Mutational analysis of the conserved basic domain of human immunodeficiency virus tat protein. *J.Virol. 63*, 1181.

(71) Ruben, S., Perkins, A., Purcell, R., Joung, K., Sia, R., Burghoff, R., Haseltine, W. A., and Rosen, C. A. (1989) Structural and functional characterization of human immunodeficiency virus tat protein. *J.Virol. 63*, 1.

(72) Madore, S. J., and Cullen, B. R. (1993) Genetic analysis of the cofactor requirement for human immunodeficiency virus type 1 Tat function. *J.Virol. 67*, 3703.

(73) Lohr, M., Kibler, K. V., Zachary, I., Jeang, K. T., and Selwood, D. L. (2003) Small HIV-1-Tat peptides inhibit HIV replication in cultured T-cells. *Biochem.Biophys.Res.Commun. 300*, 609.

(74) Ghezzi, S., Noonan, D. M., Aluigi, M. G., Vallanti, G., Cota, M., Benelli, R., Morini, M., Reeves, J. D., Vicenzi, E., Poli, G., and Albini, A. (2000) Inhibition of CXCR4-dependent HIV-1 infection by extracellular HIV-1 Tat. *Biochem.Biophys.Res.Commun. 270*, 992.

(75) Xiao, H., Neuveut, C., Tiffany, H. L., Benkirane, M., Rich, E. A., Murphy, P. M., and Jeang, K. T. (2000) Selective CXCR4 antagonism by Tat: implications for in vivo expansion of coreceptor use by HIV-1. *Proc.Natl.Acad.Sci.U.S.A 97*, 11466.

(76) Choudhury, I., Wang, J., Stein, S., Rabson, A., and Leibowitz, M. J. (1999) Translational effects of peptide antagonists of Tat protein of human immunodeficiency virus type 1. *J Gen Virol 80 (Pt 3)*, 777-82.

(77) Lee, H. J., and Pardridge, W. M. (2001) Pharmacokinetics and delivery of tat and tat-protein conjugates to tissues in vivo. *Bioconjug Chem 12*, 995-9.

(78) Wang, J. (1997) in *Graduate Program in Chemistry* pp 125, Rutgers University, Piscataway.

(79) M.J., A., and Ross, J. A. (1992) *The Natural Immune System: The Macropahge*, Oxford University Press, New York.

(80) van't Wout, A. B., Kootstra, N. A., Mulder-Kampinga, G. A., Albrecht-van Lent, N., Scherpbier, H. J., Veenstra, J., Boer, K., Coutinho, R. A., Miedema, F., and Schuitemaker, H. (1994) Macrophage-tropic variants initiate human immunodeficiency virus type 1 infection after sexual, parenteral, and vertical transmission. *J Clin Invest 94*, 2060-7.

(81) Zhu, T., Mo, H., Wang, N., Nam, D. S., Cao, Y., Koup, R. A., and Ho, D. D. (1993) Genotypic and phenotypic characterization of HIV-1 patients with primary infection. *Science 261*, 1179-81.

(82) Lewin, S. R., Lambert, P., Deacon, N. J., Mills, J., and Crowe, S. M. (1997) Constitutive expression of p50 homodimer in freshly isolated human monocytes decreases with in vitro and in vivo differentiation: a possible mechanism influencing human immunodeficiency virus replication in monocytes and mature macrophages. *J Virol 71*, 2114-9.

(83) Naif, H. M., Li, S., Alali, M., Sloane, A., Wu, L., Kelly, M., Lynch, G., Lloyd, A., and Cunningham, A. L. (1998) CCR5 expression correlates with susceptibility of maturing monocytes to human immunodeficiency virus type 1 infection. *J Virol 72*, 830-6.

(84) Rich, E. A., Chen, I. S., Zack, J. A., Leonard, M. L., and O'Brien, W. A. (1992) Increased susceptibility of differentiated mononuclear phagocytes to productive

infection with human immunodeficiency virus-1 (HIV-1). *J Clin Invest 89*, 176-83.

(85) Sonza, S., Maerz, A., Deacon, N., Meanger, J., Mills, J., and Crowe, S. (1996) Human immunodeficiency virus type 1 replication is blocked prior to reverse transcription and integration in freshly isolated peripheral blood monocytes. *J Virol 70*, 3863-9.

(86) Jordan, C. A., Watkins, B. A., Kufta, C., and Dubois-Dalcq, M. (1991) Infection of brain microglial cells by human immunodeficiency virus type 1 is CD4 dependent. *J Virol 65*, 736-42.

(87) Lewin, S. R., Sonza, S., Irving, L. B., McDonald, C. F., Mills, J., and Crowe, S. M. (1996) Surface CD4 is critical to in vitro HIV infection of human alveolar macrophages. *AIDS Res. Hum. Retroviruses 12*, 877-83.

(88) Olafsson, K., Smith, M. S., Marshburn, P., Carter, S. G., and Haskill, S. (1991) Variation of HIV infectibility of macrophages as a function of donor, stage of differentiation, and site of origin. *J Acquir Immune Defic Syndr 4*, 154-64.

(89) Embretson, J., Zupancic, M., Ribas, J. L., Burke, A., Racz, P., Tenner-Racz, K., and Haase, A. T. (1993) Massive covert infection of helper T lymphocytes and macrophages by HIV during the incubation period of AIDS. *Nature 362*, 359-62.

(90) Hufert, F. T., Schmitz, J., Schreiber, M., Schmitz, H., Racz, P., and von Laer, D. D. (1993) Human Kupffer cells infected with HIV-1 in vivo. *J Acquir Immune Defic Syndr 6*, 772-7.

(91) Lewin, S. R., Kirihara, J., Sonza, S., Irving, L., Mills, J., and Crowe, S. M. (1998) HIV-1 DNA and mRNA concentrations are similar in peripheral blood monocytes and alveolar macrophages in HIV-1-infected individuals. *AIDS 12*, 719-27.

(92) McIlroy, D., Autran, B., Cheynier, R., Clauvel, J. P., Oksenhendler, E., Debre, P., and Hosmalin, A. (1996) Low infection frequency of macrophages in the spleens of HIV+ patients. *Res Virol 147*, 115-21.

(93) Orenstein, J. M., Fox, C., and Wahl, S. M. (1997) Macrophages as a source of HIV during opportunistic infections. *Science 276*, 1857-61.

(94) Plata, F., Garcia-Pons, F., Ryter, A., Lebargy, F., Goodenow, M. M., Dat, M. H., Autran, B., and Mayaud, C. (1990) HIV-1 infection of lung alveolar fibroblasts and macrophages in humans. *AIDS Res. Hum. Retroviruses 6*, 979-86.

(95) Crowe, S., Mills, J., and McGrath, M. S. (1987) Quantitative immunocytofluorographic analysis of CD4 surface antigen expression and HIV infection of human peripheral blood monocyte/macrophages. *AIDS Res. Hum. Retroviruses 3*, 135-45.

(96) Pelchen-Matthews, A., Kramer, B., and Marsh, M. (2003) Infectious HIV-1 assembles in late endosomes in primary macrophages. *J Cell Biol 162*, 443-55.

(97) Raposo, G., Moore, M., Innes, D., Leijendekker, R., Leigh-Brown, A., Benaroch, P., and Geuze, H. (2002) Human macrophages accumulate HIV-1 particles in MHC II compartments. *Traffic 3*, 718-29.

(98) Gould, S. J., Booth, A. M., and Hildreth, J. E. (2003) The Trojan exosome hypothesis. *Proc Natl Acad Sci U S A 100*, 10592-7.

(99) Blankson, J. N., Persaud, D., and Siliciano, R. F. (2002) The challenge of viral reservoirs in HIV-1 infection. *Annu Rev Med 53*, 557-93.

(100) Chun, T. W., and Fauci, A. S. (1999) Latent reservoirs of HIV: obstacles to the eradication of virus. *Proc Natl Acad Sci U S A 96*, 10958-61.

(101) Finzi, D., and Siliciano, R. F. (1998) Viral dynamics in HIV-1 infection. *Cell 93*, 665-71.

(102) Chun, T. W., Davey, R. T., Jr., Ostrowski, M., Shawn, J. J., Engel, D., Mullins, J. I., and Fauci, A. S. (2000) Relationship between pre-existing viral reservoirs and the re-emergence of plasma viremia after discontinuation of highly active anti-retroviral therapy. *Nat.Med. 6*, 757.

(103) Zhang, L., Chung, C., Hu, B. S., He, T., Guo, Y., Kim, A. J., Skulsky, E., Jin, X., Hurley, A., Ramratnam, B., Markowitz, M., and Ho, D. D. (2000) Genetic characterization of rebounding HIV-1 after cessation of highly active antiretroviral therapy. *J.Clin.Invest 106*, 839.

(104) Lambotte, O., Taoufik, Y., de Goer, M. G., Wallon, C., Goujard, C., and Delfraissy, J. F. (2000) Detection of infectious HIV in circulating monocytes from patients on prolonged highly active antiretroviral therapy. *J.Acquir.Immune.Defic.Syndr. 23*, 114.

(105) Sharkey, M. E., Teo, I., Greenough, T., Sharova, N., Luzuriaga, K., Sullivan, J. L., Bucy, R. P., Kostrikis, L. G., Haase, A., Veryard, C., Davaro, R. E., Cheeseman, S. H., Daly, J. S., Bova, C., Ellison, R. T., III, Mady, B., Lai, K. K., Moyle, G., Nelson, M., Gazzard, B., Shaunak, S., and Stevenson, M. (2000) Persistence of episomal HIV-1 infection intermediates in patients on highly active anti-retroviral therapy. *Nat.Med. 6*, 76.

(106) Tschachler, E., Groh, V., Popovic, M., Mann, D. L., Konrad, K., Safai, B., Eron, L., diMarzo, V. F., Wolff, K., and Stingl, G. (1987) Epidermal Langerhans cells--a target for HTLV-III/LAV infection. *J.Invest Dermatol. 88*, 233.

(107) Perelson, A. S., Essunger, P., and Ho, D. D. (1997) Dynamics of HIV-1 and CD4+ lymphocytes in vivo. *AIDS 11 Suppl A*, S17-24.

(108) Gendelman, H. E., Orenstein, J. M., Martin, M. A., Ferrua, C., Mitra, R., Phipps, T., Wahl, L. A., Lane, H. C., Fauci, A. S., Burke, D. S., and et al. (1988) Efficient isolation and propagation of human immunodeficiency virus on recombinant colony-stimulating factor 1-treated monocytes. *J Exp Med 167*, 1428-41.

(109) Orenstein, J. M., Meltzer, M. S., Phipps, T., and Gendelman, H. E. (1988) Cytoplasmic assembly and accumulation of human immunodeficiency virus types 1 and 2 in recombinant human colony-stimulating factor-1-treated human monocytes: an ultrastructural study. *J Virol 62*, 2578-86.

(110) Perelson, A. S., Essunger, P., Cao, Y., Vesanen, M., Hurley, A., Saksela, K., Markowitz, M., and Ho, D. D. (1997) Decay characteristics of HIV-1-infected compartments during combination therapy. *Nature 387*, 188-91.

(111) Crowe, S. M., Mills, J., Kirihara, J., Boothman, J., Marshall, J. A., and McGrath, M. S. (1990) Full-length recombinant CD4 and recombinant gp120 inhibit fusion between HIV infected macrophages and uninfected CD4-expressing T-lymphoblastoid cells. *AIDS Res. Hum. Retroviruses 6*, 1031.

(112) Mastino, A., Grelli, S., Piacentini, M., Oliverio, S., Favalli, C., Perno, C. F., and Garci, E. (1993) Correlation between induction of lymphocyte apoptosis and

prostaglandin E2 production by macrophages infected with HIV. *Cell Immunol. 152*, 120.

(113) Aquaro, S., Panti, S., Caroleo, M. C., Balestra, E., Cenci, A., Forbici, F., Ippolito, G., Mastino, A., Testi, R., Mollace, V., Calio, R., and Perno, C. F. (2000) Primary macrophages infected by human immunodeficiency virus trigger CD95-mediated apoptosis of uninfected astrocytes. *J.Leukoc.Biol. 68*, 429.

(114) Nieuwkerk, P. T., Sprangers, M. A., Burger, D. M., Hoetelmans, R. M., Hugen, P. W., Danner, S. A., van Der Ende, M. E., Schneider, M. M., Schrey, G., Meenhorst, P. L., Sprenger, H. G., Kauffmann, R. H., Jambroes, M., Chesney, M. A., de Wolf, F., and Lange, J. M. (2001) Limited patient adherence to highly active antiretroviral therapy for HIV-1 infection in an observational cohort study. *Arch Intern Med 161*, 1962-8.

(115) Paterson, D. L., Swindells, S., Mohr, J., Brester, M., Vergis, E. N., Squier, C., Wagener, M. M., and Singh, N. (2000) Adherence to protease inhibitor therapy and outcomes in patients with HIV infection. *Ann Intern Med 133*, 21-30.

(116) Williams, G. C., and Sinko, P. J. (1999) Oral absorption of the HIV protease inhibitors: a current update. *Adv Drug Deliv Rev 39*, 211-238.

(117) Aquaro, S., Bagnarelli, P., Guenci, T., De Luca, A., Clementi, M., Balestra, E., Calio, R., and Perno, C. F. (2002) Long-term survival and virus production in human primary macrophages infected by human immunodeficiency virus. *J Med Virol 68*, 479-88.

(118) Aquaro, S., Guenci, T., Santo, F. D., Francesconi, M., Calio, R., and Perno, C. F. (2004) Potent antiviral activity of amprenavir in primary macrophages infected by human immunodeficiency virus. *Antiviral Res. 61*, 133.

(119) Brigger, I., Dubernet, C., and Couvreur, P. (2002) Nanoparticles in cancer therapy and diagnosis. *Adv Drug Deliv Rev 54*, 631-51.

(120) Schafer, V., von Briesen, H., Andreesen, R., Steffan, A. M., Royer, C., Troster, S., Kreuter, J., and Rubsamen-Waigmann, H. (1992) Phagocytosis of nanoparticles by human immunodeficiency virus (HIV)-infected macrophages: a possibility for antiviral drug targeting. *Pharm Res 9*, 541-6.

(121) Couvreur, P., and Vauthier, C. (2006) Nanotechnology: intelligent design to treat complex disease. *Pharm Res 23*, 1417-50.

(122) Pandey, R., and Khuller, G. K. (2006) Nanotechnology based drug delivery system(s) for the management of tuberculosis. *Indian J Exp Biol 44*, 357-66.

(123) Rotomskis, R., Streckyte, G., and Karabanovas, V. (2006) [Nanoparticles in diagnostics and therapy: towards nanomedicine]. *Medicina (Kaunas) 42*, 542-58.

(124) Duzgunes, N., Pretzer, E., Simoes, S., Slepushkin, V., Konopka, K., Flasher, D., and de Lima, M. C. (1999) Liposome-mediated delivery of antiviral agents to human immunodeficiency virus-infected cells. *Mol Membr Biol 16*, 111-8.

(125) Bender, A., Schfer, V., Steffan, A. M., Royer, C., Kreuter, J., Rubsamen-Waigmann, H., and von Briesen, H. (1994) Inhibition of HIV in vitro by antiviral drug-targeting using nanoparticles. *Res Virol 145*, 215-20.

(126) Bender, A. R., von Briesen, H., Kreuter, J., Duncan, I. B., and Rubsamen-Waigmann, H. (1996) Efficiency of nanoparticles as a carrier system for antiviral agents in human immunodeficiency virus-infected human monocytes/macrophages in vitro. *Antimicrob Agents Chemother 40*, 1467-71.

(127) Lobenberg, R., Araujo, L., von Briesen, H., Rodgers, E., and Kreuter, J. (1998) Body distribution of azidothymidine bound to hexyl-cyanoacrylate nanoparticles after i.v. injection to rats. *J Control Release 50*, 21-30.

(128) Fridkin, M., Tsubery, H., Tzehoval, E., Vonsover, A., Biondi, L., Filira, F., and Rocchi, R. (2005) Tuftsin-AZT conjugate: potential macrophage targeting for AIDS therapy. *J Pept Sci 11*, 37-44.

(129) Hu, J., Liu, H., and Wang, L. (2000) Enhanced delivery of AZT to macrophages via acetylated LDL. *J Control Release 69*, 327-35.

(130) Classen, D. C., Pestotnik, S. L., Evans, R. S., Lloyd, J. F., and Burke, J. P. (1997) Adverse drug events in hospitalized patients. Excess length of stay, extra costs, and attributable mortality. *Jama 277*, 301-6.

(131) Cramer, M. P., and Saks, S. R. (1994) Translating safety, efficacy and compliance into economic value for controlled release dosage forms. *Pharmacoeconomics 5*, 482-504.

(132) McKenney, J. M., and Harrison, W. L. (1976) Drug-related hospital admissions. *Am J Hosp Pharm 33*, 792-5.

(133) Davis, S., Abuchowski, A., Park, Y. K., and Davis, F. F. (1981) Alteration of the circulating life and antigenic properties of bovine adenosine deaminase in mice by attachment of polyethylene glycol. *Clin Exp Immunol 46*, 649-52.

(134) Monfardini, C., Schiavon, O., Caliceti, P., Morpurgo, M., Harris, J. M., and Veronese, F. M. (1995) A branched monomethoxypoly(ethylene glycol) for protein modification. *Bioconjug Chem 6*, 62-9.

(135) Dust, J. M., Fang, Z. H., and Harris, J. M. (1990) Proton NMR characterization of poly(ethylene glycols) and derivatives *Macromolecules 23*, 3742-6.

(136) Liang, W. W., Shi, X., Deshpande, D., Malanga, C. J., and Rojanasakul, Y. (1996) Oligonucleotide targeting to alveolar macrophages by mannose receptor-mediated endocytosis. *Biochim.Biophys.Acta 1279*, 227.

(137) Caliceti, P., Schiavon, O., and Veronese, F. M. (1999) Biopharmaceutical properties of uricase conjugated to neutral and amphiphilic polymers. *Bioconjug Chem 10*, 638-46.

(138) Koumenis, I. L., Shahrokh, Z., Leong, S., Hsei, V., Deforge, L., and Zapata, G. (2000) Modulating pharmacokinetics of an anti-interleukin-8 F(ab')(2) by amine-specific PEGylation with preserved bioactivity. *Int J Pharm 198*, 83-95.

(139) Veronese, F. M., Caliceti, P., and Schiavon, O. (1997) Branched and linear poly(ethylene glycol): Influence of the polymer structure on enzymological, pharmacokinetic, and immunological properties of protein conjugates. *Journal of Bioactive and Compatible Polymers 12*, 196-207.

(140) Bailon, P., Palleroni, A., Schaffer, C. A., Spence, C. L., Fung, W. J., Porter, J. E., Ehrlich, G. K., Pan, W., Xu, Z. X., Modi, M. W., Farid, A., and Berthold, W. (2001) Rational design of a potent, long-lasting form of interferon: A 40 kDa branched polyethylene glycol-conjugated interferon alpha-2a for the treatment of hepatitis C. *Bioconjugate Chemistry 12*, 195-202.

(141) Algranati, N. E., Sy, S., and Modi, M. (1999) A branched methoxy 40 KDA polyethylene glycol (PEG) moiety optimizes the pharmacokinetics (PK) of peginter-feron alpha-2A (PEG-IFN) and may explain its enhanced efficacy in chronic hepatitis C (CHC). *Hepatology 30*, 190A-190A.

(142) Esslinger, H. U., Haas, S., Maurer, R., Lassmann, A., Dubbers, K., and Muller-Peltzer, H. (1997) Pharmacodynamic and safety results of PEG-Hirudin in healthy volunteers. *Thromb Haemost 77*, 911-9.

(143) Yoo, S. D., Jun, H., Shin, B. S., Lee, H. S., Park, M. O., Deluca, P. P., and Lee, K. C. (2000) Pharmacokinetic disposition of polyethylene glycol-modified salmon calcitonins in rats. *Chem Pharm Bull (Tokyo) 48*, 1921-4.

(144) Paranjpe, P. V., Chen, Y., Kholodovych, V., Welsh, W., Stein, S., and Sinko, P. J. (2004) Tumor-targeted bioconjugate based delivery of camptothecin: design, synthesis and in vitro evaluation. *J Control Release 100*, 275-92.

(145) Greenwald, R. B., Gilbert, C. W., Pendri, A., Conover, C. D., Xia, J., and Martinez, A. (1996) Drug delivery systems: water soluble taxol 2'-poly(ethylene glycol) ester prodrugs-design and in vivo effectiveness. *J Med Chem 39*, 424-31.

(146) Rouquayrol, M., Gaucher, B., Roche, D., Greiner, J., and Vierling, P. (2002) Transepithelial transport of prodrugs of the HIV protease inhibitors saquinavir, indinavir, and nelfinavir across Caco-2 cell monolayers. *Pharm Res 19*, 1704-12.

(147) Lewis, C. E., and McGee, J. O. D. (1992) *The Macrophage*, IRL Press at Oxford University Press, Oxford ; New York.

(148) Prossnitz, E. R., and Ye, R. D. (1997) The N-formyl peptide receptor: a model for the study of chemoattractant receptor structure and function. *Pharmacol Ther 74*, 73-102.

(149) Burke, B., and Lewis, C. E. (2002) *The macrophage*, 2nd ed., Oxford University Press, Oxford ; New York.

(150) Vernon-Roberts, B. (1972) *The macrophage*, University Press, Cambridge [Eng.].

(151) Derksen, J. T., Morselt, H. W., Kalicharan, D., Hulstaert, C. E., and Scherphof, G. L. (1987) Interaction of immunoglobulin-coupled liposomes with rat liver macrophages in vitro. *Exp Cell Res 168*, 105-15.

(152) Derksen, J. T., Morselt, H. W., and Scherphof, G. L. (1988) Uptake and processing of immunoglobulin-coated liposomes by subpopulations of rat liver macrophages. *Biochim Biophys Acta 971*, 127-36.

(153) Morikawa, K., Nayar, R., and Fidler, I. J. (1988) In vitro activation of tumoricidal properties in mouse macrophages using the chemotactic peptide N-formyl-methionyl-leucyl-phenylalanine (FMLP) incorporated in liposomes. *Cancer Immunol Immunother 27*, 1-6.

(154) Crowe, S., Zhu, T., and Muller, W. A. (2003) The contribution of monocyte infection and trafficking to viral persistence, and maintenance of the viral reservoir in HIV infection. *J.Leukoc.Biol. 74*, 635.

(155) Nayar, R., Morikawa, K., and Fidler, I. J. (1987) Characterization of liposomes containing the chemotactic peptide N-formyl-methionyl-leucyl-phenylalanine (FMLP) and their interaction with mouse macrophages. *Cancer Drug Deliv 4*, 233-44.

(156) Marasco, W. A., Phan, S. H., Krutzsch, H., Showell, H. J., Feltner, D. E., Nairn, R., Becker, E. L., and Ward, P. A. (1984) Purification and identification of formyl-methionyl-leucyl-phenylalanine as the major peptide neutrophil chemotactic factor produced by Escherichia coli. *J Biol Chem 259*, 5430-9.

(157) Schiffmann, E., Corcoran, B. A., and Wahl, S. M. (1975) N-formylmethionyl peptides as chemoattractants for leucocytes. *Proc Natl Acad Sci U S A 72*, 1059-62.

(158) Quehenberger, O., Prossnitz, E. R., Cavanagh, S. L., Cochrane, C. G., and Ye, R. D. (1993) Multiple domains of the N-formyl peptide receptor are required for high-affinity ligand binding. Construction and analysis of chimeric N-formyl peptide receptors. *J Biol Chem 268*, 18167-75.

(159) Ye, R. D., Cavanagh, S. L., Quehenberger, O., Prossnitz, E. R., and Cochrane, C. G. (1992) Isolation of a cDNA that encodes a novel granulocyte N-formyl peptide receptor. *Biochem Biophys Res Commun 184*, 582-9.

(160) Murphy, P. M. (1996) *The N-formyl peptide chemotactic receptors.*, CRC Press, Boca Raton, FL.

(161) Le, Y., Wetzel, M. A., Shen, W., Gong, W., Rogers, T. J., Henderson, E. E., and Wang, J. M. (2001) Desensitization of chemokine receptor CCR5 in dendritic cells at the early stage of differentiation by activation of formyl peptide receptors. *Clin Immunol 99*, 365-72.

(162) Li, B. Q., Wetzel, M. A., Mikovits, J. A., Henderson, E. E., Rogers, T. J., Gong, W., Le, Y., Ruscetti, F. W., and Wang, J. M. (2001) The synthetic peptide WKYMVm attenuates the function of the chemokine receptors CCR5 and CXCR4 through activation of formyl peptide receptor-like 1. *Blood 97*, 2941-7.

(163) Shen, W., Li, B., Wetzel, M. A., Rogers, T. J., Henderson, E. E., Su, S. B., Gong, W., Le, Y., Sargeant, R., Dimitrov, D. S., Oppenheim, J. J., and Wang, J. M. (2000) Down-regulation of the chemokine receptor CCR5 by activation of chemotactic formyl peptide receptor in human monocytes. *Blood 96*, 2887-94.

(164) Shen, W., Proost, P., Li, B., Gong, W., Le, Y., Sargeant, R., Murphy, P. M., Van Damme, J., and Wang, J. M. (2000) Activation of the chemotactic peptide receptor FPRL1 in monocytes phosphorylates the chemokine receptor CCR5 and attenuates cell responses to selected chemokines. *Biochem Biophys Res Commun 272*, 276-83.

(165) Ezekowitz, R. A., Sastry, K., Bailly, P., and Warner, A. (1990) Molecular characterization of the human macrophage mannose receptor: demonstration of multiple carbohydrate recognition-like domains and phagocytosis of yeasts in Cos-1 cells. *J Exp Med 172*, 1785-94.

(166) Taylor, M. E., Conary, J. T., Lennartz, M. R., Stahl, P. D., and Drickamer, K. (1990) Primary structure of the mannose receptor contains multiple motifs resembling carbohydrate-recognition domains. *J Biol Chem 265*, 12156-62.

(167) Drickamer, K., and Taylor, M. E. (1993) Biology of animal lectins. *Annu Rev Cell Biol 9*, 237-64.

(168) Taylor, M. E., Bezouska, K., and Drickamer, K. (1992) Contribution to ligand binding by multiple carbohydrate-recognition domains in the macrophage mannose receptor. *J Biol Chem 267*, 1719-26.

(169) Ezekowitz, R. A., and Stahl, P. D. (1988) The structure and function of vertebrate mannose lectin-like proteins. *J Cell Sci Suppl 9*, 121-33.

(170) Stahl, P. D. (1990) The macrophage mannose receptor: current status. *Am J Respir Cell Mol Biol 2*, 317-8.

(171) Larder, B. A. (1995) Viral resistance and the selection of antiretroviral combinations. *J.Acquir.Immune.Defic.Syndr.Hum.Retrovirol. 10 Suppl 1*, S28.

(172) Opravil, M., Hirschel, B., Lazzarin, A., Furrer, H., Chave, J. P., Yerly, S., Bisset, L. R., Fischer, M., Vernazza, P., Bernasconi, E., Battegay, M., Ledergerber, B., Gunthard, H., Howe, C., Weber, R., and Perrin, L. (2002) A randomized trial of simplified maintenance therapy with abacavir, lamivudine, and zidovudine in human immunodeficiency virus infection. *J Infect Dis 185*, 1251-60.

(173) Cole, S. P., Bhardwaj, G., Gerlach, J. H., Mackie, J. E., Grant, C. E., Almquist, K. C., Stewart, A. J., Kurz, E. U., Duncan, A. M., and Deeley, R. G. (1992) Overexpression of a transporter gene in a multidrug-resistant human lung cancer cell line. *Science 258*, 1650-4.

(174) Goldie, J. H., and Coldman, A. J. (1984) The genetic origin of drug resistance in neoplasms: implications for systemic therapy. *Cancer Res 44*, 3643-53.

(175) Jeang, K. T., Xiao, H., and Rich, E. A. (1999) Multifaceted activities of the HIV-1 transactivator of transcription, Tat. *J.Biol.Chem. 274*, 28837-28840.

(176) Frankel, A. D., and Pabo, C. O. (1988) Cellular uptake of the tat protein from human immunodeficiency virus. *Cell 55*, 1189-93.

(177) Zhang, X., Wan, L., Pooyan, S., Su, Y., Gardner, C. R., Leibowitz, M. J., Stein, S., and Sinko, P. J. (2004) Quantitative assessment of the cell penetrating properties of RI-Tat-9: evidence for a cell type-specific barrier at the plasma membrane of epithelial cells. *Mol Pharm 1*, 145-55.

(178) Nori, A., Jensen, K. D., Tijerina, M., Kopeckova, P., and Kopecek, J. (2003) Tat-conjugated synthetic macromolecules facilitate cytoplasmic drug delivery to human ovarian carcinoma cells. *Bioconjug Chem 14*, 44-50.

(179) Harris, J. M., and Chess, R. B. (2003) Effect of pegylation on pharmaceuticals. *Nat Rev Drug Discov 2*, 214-21.

(180) Jones, K., Bray, P. G., Khoo, S. H., Davey, R. A., Meaden, E. R., Ward, S. A., and Back, D. J. (2001) P-Glycoprotein and transporter MRP1 reduce HIV protease inhibitor uptake in CD4 cells: potential for accelerated viral drug resistance? *AIDS 15*, 1353-1358.

(181) Gunaseelan, S., Debrah, O., Wan, L., Leibowitz, M. J., Rabson, A. B., Stein, S., and Sinko, P. J. (2004) Synthesis of poly(ethylene glycol)-based saquinavir prodrug conjugates and assessment of release and anti-HIV-1 bioactivity using a novel protease inhibition assay. *Bioconjug Chem 15*, 1322-33.

(182) Chen, L. L., Frankel, A. D., Harder, J. L., Fawell, S., Barsoum, J., and Pepinsky, B. (1995) Increased cellular uptake of the human immunodeficiency virus-1 Tat protein after modification with biotin. *Anal Biochem 227*, 168-75.

(183) Chorev, M., and Goodman, M. (1995) Recent developments in retro peptides and proteins--an ongoing topochemical exploration. *Trends Biotechnol. 13*, 438-445.

(184) Fromme, B., Eftekhari, P., Van Regenmortel, M., Hoebeke, J., Katz, A., and Millar, R. (2003) A novel retro-inverso gonadotropin-releasing hormone (GnRH) immunogen elicits antibodies that neutralize the activity of native GnRH. *Endocrinology 144*, 3262-3269.

(185) Wender, P. A., Mitchell, D. J., Pattabiraman, K., Pelkey, E. T., Steinman, L., and Rothbard, J. B. (2000) The design, synthesis, and evaluation of molecules that enable or enhance cellular uptake: peptoid molecular transporters. *Proc Natl Acad Sci USA 97*, 13003-8.

(186) Foroutan, S. M., and Watson, D. G. (1999) The in vitro evaluation of polyethylene glycol esters of hydrocortisone 21-succinate as ocular prodrugs. *Int.J.Pharm. 182*, 79-92.

(187) Lewin, S. R., Sonza, S., Irving, L. B., McDonald, C. F., Mills, J., and Crowe, S. M. (1996) Surface CD4 is critical to in vitro HIV infection of human alveolar macrophages. *AIDS Res Hum Retroviruses 12*, 877-83.

(188) Choudhury, I., Wang, J., Rabson, A. B., Stein, S., Pooyan, S., Stein, S., and Leibowitz, M. J. (1998) Inhibition of HIV-1 replication by a Tat RNA-binding domain peptide analog. *J Acquir Immune Defic Syndr Hum Retrovirol 17*, 104-11.

(189) Wan, L., Zhang, X., Gunaseelan, S., Pooyan, S., Debrah, O., Leibowitz, M. J., Rabson, A. B., Stein, S., and Sinko, P. J. (2006) Novel multi-component nanopharmaceuticals derived from poly(ethylene) glycol, retro-inverso-Tat nonapeptide and saquinavir demonstrate combined anti-HIV effects. *AIDS Res. Ther. 3*, 12.

(190) Nori, A., Jensen, K. D., Tijerina, M., Kopeckova, P., and Kopecek, J. (2003) Tat-conjugated synthetic macromolecules facilitate cytoplasmic drug delivery to human ovarian carcinoma cells. *Bioconjug.Chem. 14*, 44.

(191) Xiaoping, Z., Li, W., Shahriar, P., Carol, R. G., Michael, J. L., Stanley, S., and Patrick, J. S. (2004) in *Molecular Pharmaceutics* pp 145.

(192) Conover, C. D., Pendri, A., Lee, C., Gilbert, C. W., Shum, K. L., and Greenwald, R. B. (1997) Camptothecin delivery systems: the antitumor activity of a camptothecin-20-0-polyethylene glycol ester transport form. *Anticancer Res. 17*, 3361-3368.

(193) Richman, D. D. (2001) HIV chemotherapy. *Nature 410*, 995-1001.

(194) Roos, M. T., Lange, J. M., de Goede, R. E., Coutinho, R. A., Schellekens, P. T., Miedema, F., and Tersmette, M. (1992) Viral phenotype and immune response in primary human immunodeficiency virus type 1 infection. *J Infect Dis 165*, 427-32.

(195) Connor, R. I., Paxton, W. A., Sheridan, K. E., and Koup, R. A. (1996) Macrophages and CD4+ T lymphocytes from two multiply exposed, uninfected individuals resist infection with primary non-syncytium-inducing isolates of human immunodeficiency virus type 1. *J Virol 70*, 8758-64.

(196) Liu, R., Paxton, W. A., Choe, S., Ceradini, D., Martin, S. R., Horuk, R., MacDonald, M. E., Stuhlmann, H., Koup, R. A., and Landau, N. R. (1996) Homozygous defect in HIV-1 coreceptor accounts for resistance of some multiply-exposed individuals to HIV-1 infection. *Cell 86*, 367-77.

(197) Le, Y., Yang, Y., Cui, Y., Yazawa, H., Gong, W., Qiu, C., and Wang, J. M. (2002) Receptors for chemotactic formyl peptides as pharmacological targets. *Int Immunopharmacol 2*, 1-13.

(198) Niedel, J. E., Kahane, I., and Cuatrecasas, P. (1979) Receptor-mediated internalization of fluorescent chemotactic peptide by human neutrophils. *Science 205*, 1412-4.

(199) van Eerd, J. E., Boerman, O. C., Corstens, F. H., and Oyen, W. J. (2003) Radiolabeled chemotactic cytokines: new agents for scintigraphic imaging of infection and inflammation. *Q J Nucl Med 47*, 246-55.

(200) Pooyan, S., Qiu, B., Chan, M. M., Fong, D., Sinko, P. J., Leibowitz, M. J., and Stein, S. (2002) Conjugates bearing multiple formyl-methionyl peptides display enhanced binding to but not activation of phagocytic cells. *Bioconjug Chem 13*, 216-23.

(201) Fischer, D. G., Pike, M. C., Koren, H. S., and Snyderman, R. (1980) Chemotactically responsive and nonresposive forms of a continuous human monocyte cell line. *J Immunol 125*, 463-5.

(202) Pike, M. C., Fischer, D. G., Koren, H. S., and Snyderman, R. (1980) Development of specific receptors for N-formylated chemotactic peptides in a human monocyte cell line stimulated with lymphokines. *J Exp Med 152*, 31-40.

(203) Wan, L., Zhang, X., Gunaseelan, S., Pooyan, S., Debrah, O., Leibowitz, M. J., Rabson, A. B., Stein, S., and Sinko, P. J. (2006) Novel Multi-component Nanopharmaceuticals Derived from Poly(ethylene) Glycol, Retro-inverso-Tat Nonapeptide and Saquinavir Demonstrate Combined Anti-HIV Effects. *AIDS Research and Therapy*.

(204) Harris, J. M. (1991) *Poly(Ethylene Glycol) Chemistry: Biotechnical and Biomedical Applications*, Plenum Press, New York

(205) Sherman, M. R., Williams, L. D., Saifer, M. C. P., French, J. A., Kwak, L. W., and Oppenheim, J. J. (1997) *Conjugation of high, molecular weight poly(ethylene glycol) to cytokines: granulocyte-macrophage colony stimulating factors as model substrates.* , ACS, Washington, DC

(206) Desai, M. P., Labhasetwar, V., Walter, E., Levy, R. J., and Amidon, G. L. (1997) The mechanism of uptake of biodegradable microparticles in Caco-2 cells is size dependent. *Pharm Res 14*, 1568-73.

(207) Prabha, S., Zhou, W. Z., Panyam, J., and Labhasetwar, V. (2002) Size-dependency of nanoparticle-mediated gene transfection: studies with fractionated nanoparticles. *Int J Pharm 244*, 105-15.

(208) Nakai, T., Kanamori, T., Sando, S., and Aoyama, Y. (2003) Remarkably size-regulated cell invasion by artificial viruses. Saccharide-dependent self-aggregation of glycoviruses and its consequences in glycoviral gene delivery. *J Am Chem Soc 125*, 8465-75.

(209) Osaki, F., Kanamori, T., Sando, S., Sera, T., and Aoyama, Y. (2004) A quantum dot conjugated sugar ball and its cellular uptake. On the size effects of endocytosis in the subviral region. *J Am Chem Soc 126*, 6520-1.

(210) Caliceti, P., and Veronese, F. M. (2003) Pharmacokinetic and biodistribution properties of poly(ethylene glycol)-protein conjugates. *Adv Drug Deliv Rev 55*, 1261-77.

(211) Arendshorst, W. J., and Navar, L. G. (1988) *Renal circulation and glomerular hemodynamics*, Brown, Boston, MA.

(212) Igarashi, T., Brown, C. R., Endo, Y., Buckler-White, A., Plishka, R., Bischofberger, N., Hirsch, V., and Martin, M. A. (2001) Macrophage are the principal reservoir and sustain high virus loads in rhesus macaques after the depletion of CD4+ T cells by a highly pathogenic simian immunodeficiency virus/HIV type 1 chimera (SHIV): Implications for HIV-1 infections of humans. *Proc.Natl.Acad.Sci.U.S.A 98*, 658.

CURRICULUM VITA

Li Wan

Education

Sep 2000 - May 2007	Ph.D., Pharmaceutics	Rutgers University, Piscataway, NJ
Sep 1996 - Jun 1999	M.S., Biopharmaceutics	Nanjing University, Nanjing, China
Sep 1992 - Jun 1996	B.S., Biology	Nanjing University, Nanjing, China

Experience

Apr 2006 – Present	Senior Research Scientist	Wyeth, Pearl River, NY 10965
Jun 2003 – Aug 2003	Formulation Scientist	GlaxoSmithKline, Parsippany, NJ 07054
Jun 2001 – Aug 2001	Analytical Scientist	Enzon Inc., Piscataway, NJ 08854

Publications

Wan, L. , Pooyan, S., Palombo, MS, Zhang, X, Leibowitz, MJ, Stein, S., and Sinko, P.J. Optimizing size and copy number for PEG-fMLF (n-formyl-methionyl-leucylphenylalanine) nanocarrier uptake by macrophages. **Bioconjugate Chem.** 2007 (Submitted)

Wan, L., Gunaseelan, S., Debrah O., Leibowitz M.J., Rabson A.B., Stein S. and Sinko P.J., Novel multi-component nanopharmaceuticals derived from poly(ethylene) glycol, retro-inverso-Tat nonapeptide and saquinavir demonstrate combined anti-HIV effects. **AIDS Research and Therapy.** 2006 Apr 24; 3:12.

Gunaseelan, S., Debrah, O., **Wan, L.,** Leibowitz, M.J., Rabson, A.B., Stein, S., Sinko, P.J., Synthesis of Poly(ethylene glycol)-Based Saquinavir Prodrug Conjugates and Assessment of Release and Anti-HIV-1 Bioactivity Using a Novel Protease Inhibition Assay. **Bioconjugate Chem.** 2004; *15*(6); 1322-1333.

Zhang, X., **Wan, L.,** Pooyan, S., Su, Y., Gardner, C. R., Leibowitz, M.J., Stein, S., Sinko, P.J., Quantitative Assessment of the Cell Penetrating Properties of RI-Tat-9: Evidence for a Cell Type-Specific Barrier at the Plasma Membrane of Epithelial Cells. **Molecular Pharmaceutics** 2004; 1(2); 145-155.